공학박사학위논문

Simulation and Experiment for a Design of a Solid Oxide Fuel Cell – Homogeneous Charge Compression Ignition Engine Hybrid System

SOFC – HCCI 엔진 하이브리드 시스템 설계를 위한 시뮬레이션 및 실험적 연구

2018 년 2 월

서울대학교 대학원

기계항공공학부

최 원 재

Simulation and Experiment for a Design of a Solid Oxide Fuel Cell – Homogeneous Charge Compression Ignition Engine Hybrid System

A DISSERTATION SUBMITTED TO THE SCHOOL OF MECHANICAL AND AEROSPACE ENGINEERING OF SEOUL NATIONAL UNIVERSITY IN PARTIAL FULFILLMENT OF THE REQUIREMENTS FOR THE DEGREE OF DOCTOR OF PHILOSOPHY

Wonjae Choi

Feb 2018

Abstract

Simulation and Experiment for a Design of a Solid Oxide Fuel Cell – Homogeneous Charge Compression Ignition Engine Hybrid System

Wonjae Choi
School of Mechanical Engineering
The Graduate School
Seoul National University

A solid oxide fuel cell (SOFC) hybrid system is a system that combines an SOFC with an additional power generation device to increase the efficiency of the system. Thus far, the SOFC–gas turbine hybrid system has been primarily investigated for SOFC hybrid systems. However, the current power generation capacity of an SOFC is less than several MWs; for this generation capacity, an internal combustion engine (ICE) is generally more efficient and economical than a gas turbine. Focusing on this point, recently, the concept of an SOFC–ICE hybrid system was proposed. To successfully combust the SOFC anode off-gas, which includes a large amount of diluents (H_2O and CO_2), the homogeneous charge compression ignition (HCCI) method was selected instead of spark ignition as the combustion strategy of the ICE in the hybrid system.

Although the concept of an SOFC–HCCI engine hybrid system has been proposed, the researches on this hybrid system have been very limited. Therefore, this dissertation aims to fully investigate the operation characteristics of the SOFC–HCCI engine hybrid system by conducting experiments and simulations.

In the first step of the investigation of the hybrid system, an experimental study of HCCI engine operation fuelled by SOFC anode off-gas was conducted. For the HCCI engine experiments, a single-cylinder HCCI engine and experimental equipment for emulating SOFC anode off-gas were constructed. Various HCCI engine experiments were performed while varying several control parameters, e.g., the fuel utilization factor of an SOFC, which primarily affects the composition and flow rate of the engine intake gas. The experiments indicated that the HCCI combustion was achieved even with highly diluted gas when the intake temperature was sufficient. In addition, the results indicated that HCCI engine operation fuelled by SOFC anode off-gas yields a significant amount of power (w/ 25-30% gross indicated efficiency) and produces significantly low NO_x emissions (< 5 ppm @ O_2 15%) under stable HCCI combustion (< 5% COV $IMEP_g$, which is the coefficient of variance of the gross indicated mean effective pressure). Considering that the experiment was performed using a small single-cylinder engine, these experimental results reveal that the use of an HCCI engine as the bottoming cycle in an SOFC hybrid system is feasible. However, HCCI engine operation was not always stable in all experimental conditions. Engine operation with an exceedingly low engine load ($IMEP_g$ < 1.8 bar) should be avoided as it decreases the stability of engine operation. In addition, an engine intake gas with excessive dilution (fuel molar fraction < 0.125) should be avoided to decrease the amount of unburned CO emission and maintain a CO

combustion efficiency higher than 90%.

In the second step of the investigation of the hybrid system, the operation of the SOFC and the entire hybrid system was analysed. The impacts of the HCCI engine operation on the system, especially on the SOFC, were investigated by integrating the experimental results of the HCCI engine with simulation models of the other system components. Steady-state simulation models were constructed by utilizing MATLAB from Mathworks together with the Cantera thermodynamic tool box and GRI 3.0 mechanism. A direct internal reforming planar-type SOFC was selected for the SOFC in the hybrid system, and the SOFC was modelled using a one-dimensional model to investigate the coupling effects of direct internal reforming and electrochemical reactions. The system analysis indicated that the SOFC in the SOFC–HCCI engine hybrid system utilized SOFC anode inlet gas at a low temperature (e.g., 750 ~ 800 K) and low reforming rate (e.g., 30 ~ 40%). Therefore, the operating temperature at the entrance part of the SOFC is relatively low (e.g., 900 K); thus, an anode-supported-type SOFC that can reduce the ohmic loss of the electrolyte at this relatively low temperature is preferable for the SOFC in the hybrid system. An analysis of the entire system was conducted while varying several control parameters, e.g., the fuel utilization factor of the SOFC. The design point of the operation was determined by considering not only the performance but also the stability of operation. At the design point, the SOFC generates 4.97 kW of power, and the HCCI engine generates 0.93 kW of power while emitting ~ 1 ppm NO_x and ~ 1300 ppm CO. The system efficiency was calculated as 58.5% at this design point.

In the third step of the investigation of the hybrid system, an experimental study of the entire SOFC–HCCI engine hybrid system was conducted to directly verify the

feasibility of system operation by an experiment. The experiment of the first 200-hour continuous operation of the SOFC-HCCI engine hybrid system was conducted. The operating point of the 200-hour continuous operation was determined based on the previously mentioned system analysis. The experiment verified the feasibility of the hybrid system. Particularly, the experiment indicated that the pressure oscillation caused by the HCCI engine did not significantly affect the SOFC as it was cancelled a lot when it reaches the SOFC anode due to the flow path between the engine intake and the SOFC. However, in the experiment, electric heaters and a burner were utilized to increase the temperature of the anode and cathode inlet gas for the stability of SOFC operation due to the over-expected amount of heat loss from the system. Therefore, from the experiment of entire system, it was also confirmed that reducing the heat loss is essential for achieving more successful operation of the system.

In the fourth step of the investigation of the hybrid system, methods to resolve major three problems of the system operation (CO emissions, a large amount of heat loss, and the limitation of increasing fuel utilization factor of the SOFC), which were confirmed from previously mentioned investigations, were studied. For this, simulations of the entire system were performed. Three methods resolving these problems (additional catalytic oxidizer, heat recovery from the engine coolant, and increasing the compression ratio of the engine) were introduced; the effects of each method were analysed. Based on these analyses, the optimized design of the SOFC–HCCI engine hybrid system was determined. With the optimized system design, the system efficiency was estimated as ~ 63.8%, and the pollutant emissions are expected to be maintained at near-zero for the 5-kW class power generation system. Considering that the size of the system is relatively small, these results can be

regarded as very promising.

In the last step of the research on the hybrid system, simulation study on the system performance was conducted while increasing the system size whereas maintaining the determined design of system. For scaling up the system, the number of modularized SOFC stacks was increased, and the size of a cylinder of HCCI engine was enlarged. Simulations indicated that as the system size increased, the surface to volume ratio decreased and the engine heat loss decreased; thus, the efficiencies of HCCI engine, SOFC, and the entire system were increased. Therefore, it was confirmed that the scale-up of the system helps to increase the system efficiency. Especially, it was estimated that when the system is scaled up to 100-kW, the efficiency of ~ 67.4% can be achieved. This result can be regarded as a very promising result that shows the possibility of the SOFC-HCCI engine hybrid system being used as ultra-high efficiency power generation systems.

Keywords: solid oxide fuel cell (SOFC), SOFC–internal combustion engine hybrid system, homogeneous charge compression ignition (HCCI) engine, highly diluted gas combustion, anode-supported intermediate-temperature solid oxide fuel cell, direct internal reforming, design-point of system operation, optimization of system design.

***Identification Number*: 2013-20723**

Table of Contents

List of Figures

List of Tables

Chapter 1
Introduction to SOFC–HCCI engine hybrid system

1.1. Introduction to SOFC hybrid systems

The use of solid oxide fuel cells (SOFCs) in future power generation systems is attracting significant attention due to their advantages, including high efficiency, fuel flexibility, and the ability to operate without an expensive catalyst, such as Pt.[1] To achieve the full commercialization of SOFCs, studies are being actively conducted to increase the efficiency of SOFCs. Research on SOFC hybrid systems, which improve the power generation efficiency by combining an SOFC with an additional power generation device, has revealed that a hybrid system can be a powerful tool for increasing efficiency. An SOFC typically consumes only 80% or less of the incoming fuel with more than 20% of the fuel being emitted as anode off-gas. As shown in figure 1.1, an SOFC hybrid system uses this remaining fuel in the additional power generating device, which is also referred to as the bottoming cycle of an SOFC, to produce additional power and increase efficiency.

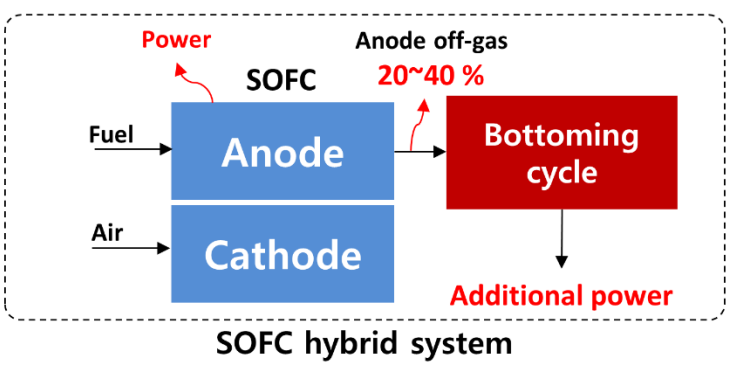

Figure 1.1. Concept of SOFC hybrid system

1.2. Previous studies of SOFC–gas turbine hybrid system

The SOFC–gas turbine (GT) hybrid system has been primarily investigated for the SOFC hybrid system. The SOFC–GT hybrid system has been explored using various approaches, such as numerical simulations, experiments, hardware-based simulations, and thermos-economic analyses.[2] These studies have analysed the various aspects of an SOFC–GT hybrid system, such as system configuration, operation characteristics, full and part-load operation, fuel flexibility, and the control of the system.[2-18] The experimental studies directly verified the actual feasibility of system operation.[13-17] Siemens Power Corporation has developed a 220 kW-class pressurized SOFC–GT hybrid system, which has operated for approximately 2900 hours and achieves an efficiency of 53%.[17] Mitsubishi Heavy Industries has also developed a 220 kW-class pressurized SOFC–GT hybrid system and has reported an operating time of more than 3000 hours and an achieved efficiency of 52%.[16] Figures 1.2 and 1.3 display pictures of the SOFC–gas turbine hybrid systems developed by these two power generation device companies.

Figure 1.2. SOFC – GT hybrid system developed by Siemens Power Corporation

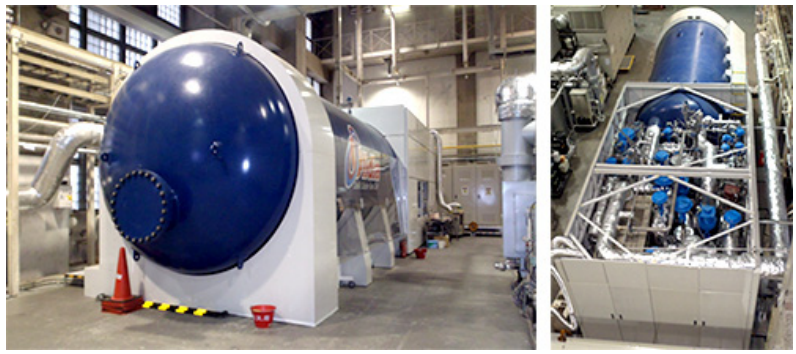

Figure 1.3. SOFC – GT hybrid system developed by Mitsubishi Heavy Industries

1.3. Proposal of SOFC–internal combustion engine hybrid system

The current power generation capacity of an SOFC is typically below several MWs; for this generation capacity, internal combustion engines (ICEs) are more frequently employed than GTs as ICEs are generally more efficient and economical than GTs at this generation capacity.[19, 20] Therefore, the use of an ICEs may have the potential to be used as a bottoming cycle of an SOFC. Focusing on this point, recently, the concept of an SOFC–ICE hybrid system was proposed and registered for US and Korean patents.[21]

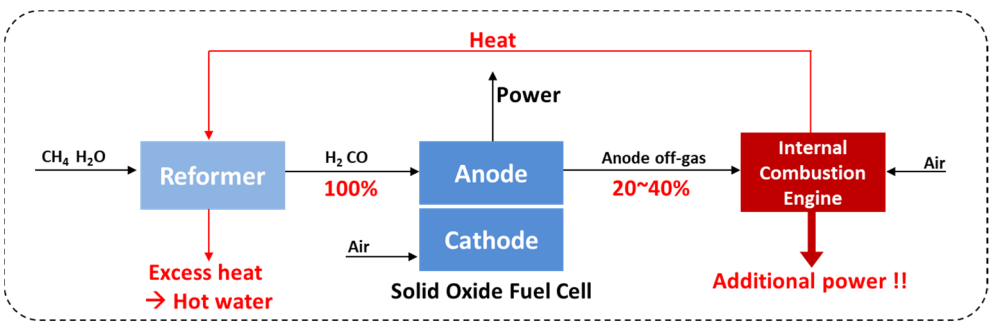

Figure 1.4. Concept of SOFC–internal combustion engine hybrid system

Figure 1.4 shows the concept of an SOFC–internal combustion engine hybrid system. As shown in the figure, the SOFC anode off-gas is transferred to the internal combustion engine to be combusted in the engine to produce additional power. Different from a gas turbine, the combustion inside an internal combustion engine is discontinuous and should occur in every engine cycle. Therefore, the combustion of the SOFC anode off-gas is expected to be more difficult and selecting the proper combustion strategies is important. The exhaust gas of the engine is transferred to the reformer to provide the heat for external reforming.

1.4. HCCI as the combustion strategy of internal combustion engine in the hybrid system

The patented concept has additional significance: it proposes the application of homogeneous charge compression ignition (HCCI) as the combustion strategy of the ICE in an SOFC–ICE hybrid system. The inventors claimed that spark ignition, which is the combustion strategy extensively employed in ICEs fuelled by gaseous fuels, is not appropriate for the ICE of an SOFC–ICE hybrid system due to the high dilution level of the fuel of an ICE, i.e., the SOFC anode off-gas. In the presence of a large amount of diluent in the fuel of an ICE, the flame propagation speed, which is an important parameter of the spark ignition method, is significantly reduced, and proper combustion is unlikely to occur unless additional fuel is provided for the ICE.[22, 23] For reference, an exemplary composition of SOFC anode off-gas in a typical SOFC operating condition with natural gas is shown in table 1.1. As shown in the table, the amount of diluent is approximately four times the amount of fuel. For this reason, the HCCI combustion strategy, which is known to be capable of adequately combusting highly diluted gas, achieving high efficiency, and producing low NO_x emissions, is proposed as the combustion strategy for the ICE in the SOFC–ICE hybrid system.

Table 1.1. Composition of SOFC anode off-gas

(for SOFC fuel utilization factor of 70% and steam-to-carbon ratio of 2.5)

H_2	18.2%	Fuel	21.5%
CO	3.3%		
H_2O	63.4%	Diluent	78.5%
CO_2	15.1%		

For reference, an HCCI engine was originally developed for use in vehicles. Despite their excellent efficiency and good pollutant emission characteristics, the HCCI engine

has not been extensively employed. One of the major difficulties of the HCCI engine is control of the combustion, as the HCCI combustion strategy is a method that employs auto-ignition caused by compressing a premixed mixture of air and fuel. Unlike the spark ignition engine, which uses a spark to trigger combustion, and the compression ignition engine, which uses fuel injection to trigger combustion, the HCCI engine only uses chemical reactions to cause combustion. As a result, controlling the combustion of an HCCI engine is difficult.

However, unlike the case of usage in vehicles, where the operating point of the engine continuously changes, the control of an HCCI engine in an electric power generation system is relatively easy due to the constancy of the operating point of the power generation system. For this reason, the researches on using HCCI engine for power generation have been also conducted.[24-26]

1.5. Previous studies of SOFC–HCCI engine hybrid system

Researches on SOFC – HCCI engine hybrid system have also been conducted.[27-30] For example, Park et al. conducted a thermos-economics analysis to compare the SOFC–HCCI engine hybrid system with the SOFC–GT hybrid system in terms of energy efficiency, total cost, and environmental impacts.[28] The analysis revealed that, for 100 kW-class system, the SOFC–HCCI engine hybrid system is considered to be superior to the SOFC–GT hybrid system in terms of not only energy efficiency but also economic aspects. Lee et al. similarly compared the SOFC–HCCI engine hybrid system with SOFC–GT hybrid system in terms by conducting exergoeconomic evaluation and a similar conclusion was reached.[30] Kang et al. constructed a dynamic model of an SOFC–ICE hybrid system and analysed the transient behaviour of the SOFC–ICE hybrid system during the increase of load.[27] The study showed the first research work on the transient behaviour of SOFC–HCCI engine hybrid system and the model developed in the study can be utilized for developing control strategies of the system.

Table 1.2. Comparison of SOFC–HCCI engine hybrid system with SOFC stand-alone system and SOFC–gas turbine hybrid system [28]

	SOFC stand-alone	SOFC–gas turbine	SOFC–HCCI engine
Fuel input (kW) (LHV)	174.0	174.0	174.0
Net power production (kW)	89.6	100.3	104.5
Net efficiency (%)	51.5	57.6	60.1
LCOE ($/kWh)*	0.3491	0.3202	0.3111

* SOFC stack life time is five years

However, unlike the case of the SOFC–GT hybrid system, the studies of the SOFC–HCCI engine hybrid system are limited; the studies have been performed using only simulation and thermos-economics analysis. Therefore, it is necessary to fully investigate the operation characteristics by conducting experiments as well as simulations.

1.6. Objectives of this dissertation

This dissertation aims to fully investigate the SOFC - HCCI engine hybrid system by conducting simulations and experiments. This dissertation has three objectives, which are summarized as follows:

The first objective is to verify the feasibility of the system operation via experiments. This objective is achieved by experimentally investigating the feasibility of HCCI engine operation fuelled by SOFC anode off-gas and the feasibility of entire system operation.

The second objective is to understand the operation characteristics of the system and determine the design point of operation that achieves not only the best performance but also the stability of operation. Achieving this objective requires understanding how the SOFC and HCCI engine operate when control parameters change. In this system, the SOFC and the HCCI engine are connected and continuously affect each other. Therefore, the effect of HCCI engine operation on the SOFC and the effect of SOFC operation on the HCCI engine are explored.

The third objective is to determine the system design to achieve the best performance and stable operation. As this system has not been developed yet, the optimized design of the system has not been decided. Therefore, this dissertation aims to propose the optimized system design of the SOFC–HCCI engine hybrid system.

1.7. Guiding questions

To achieve the objectives of this dissertation, various analyses have been performed via experiments and simulations. When conducting these analyses, I was trying to answer the following four guiding questions:

1. **Does an HCCI engine fuelled by SOFC anode off-gas successfully operate?**

   The first question pertains to whether an HCCI engine fuelled by SOFC anode off-gas can operate with successful combustion and satisfactory performance. The operation of an HCCI engine should be confirmed while varying the system operating conditions because the research on the HCCI engine operation in SOFC – HCCI engine hybrid system is lacking.

2. **Can an SOFC successfully operate under a combined operation with an HCCI engine?**

   The second question pertains to whether an SOFC can successfully operate in ta hybrid system with an HCCI engine. In an SOFC stand-alone system, heat is generated by oxidizing SOFC anode off-gas and is primarily utilized for reforming. On the other hand, in an SOFC-HCCI engine hybrid system, since the power is extracted from the SOFC anode off-gas, the amount of heat supplied to the external reformer is reduced. Therefore, whether the SOFC can be successfully operated in this situation must be confirmed. Additionally, as the anode side of the SOFC is directly connected to the HCCI engine, it is necessary to confirm whether the pressure oscillation caused by the operation of the HCCI engine has an adverse effect on the SOFC.

3. **What is the best approach to controlling the system for achieving the best performance and a stable operation?**

   The third question is to identify the necessary system control for achieving the best performance as well as the stability of operation. In this system, both devices are constantly affecting each other. Thus, a change in one device operation inevitably changes the operation of another device. In this constantly influential situation, it is necessary to determine how to control the system for ensuring stable and good operation of both devices.

4. **What is the best design of the system to maximize the system performance?**

   The fourth question pertains to determine the design of an SOFC–HCCI engine hybrid system to maximize the system performance. As this system remains in the concept stage, the detailed design of the system needs to be determined.

1.8. Organization of the dissertation

This dissertation consists of the analyses to answer the guiding questions. Figure 1.5 shows the outline of the dissertation. It indicates how each guiding question is handled in the dissertation and how each chapter is linked to each other.

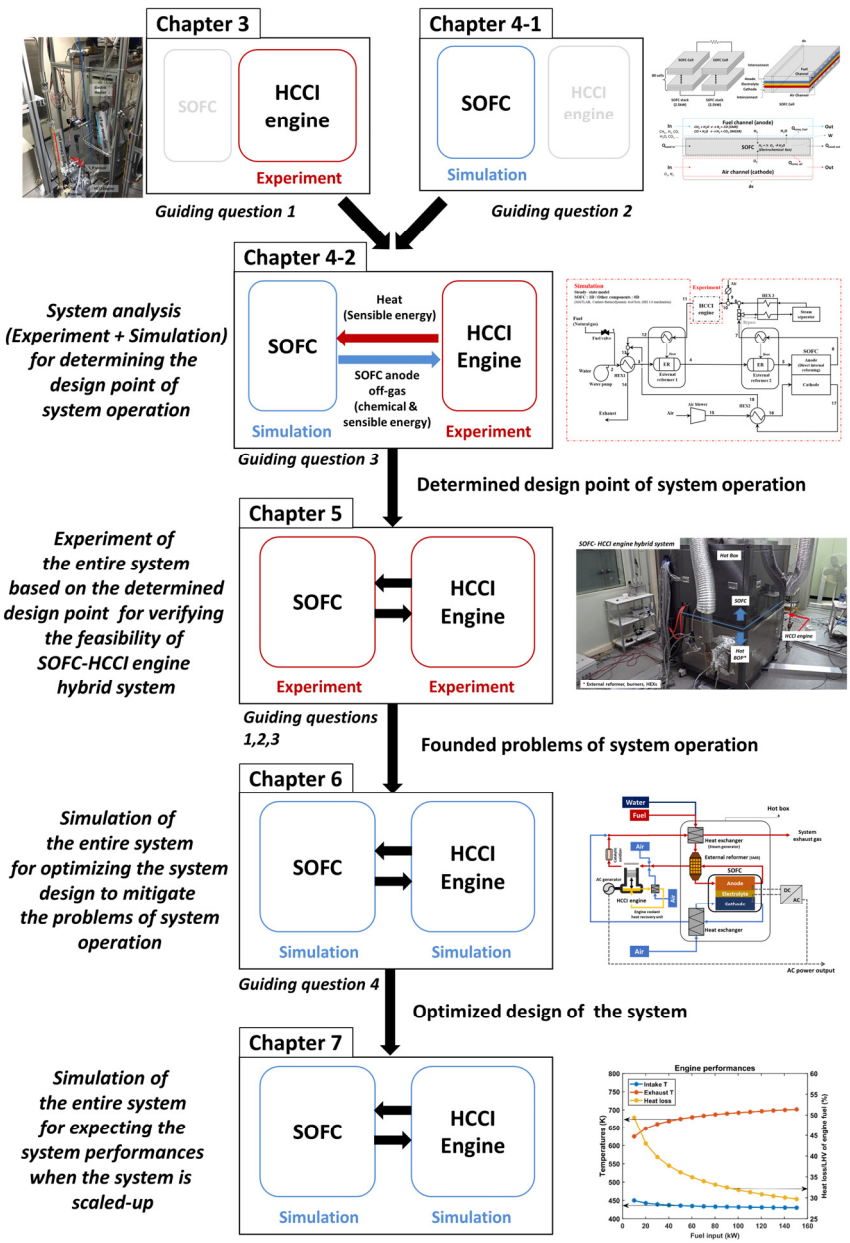

Figure 1.5. Outline of the dissertation

First, in chapter 2, the system proposed and analysed in this dissertation is outlined.

The operation of the system and its control parameters are described in chapter 2.

In chapter 3, guiding question 1, which pertains to the feasibility of the HCCI engine operation fuelled by SOFC anode off-gas, is answered. Chapter 3 experimentally proves that the HCCI engine operation in the hybrid system is feasible. The required controls to achieve successful HCCI engine operation are also determined in this chapter.

In chapter 4, guiding questions 2 and 3 are answered by conducting a system analysis. A system analysis is performed by integrating the experimental results of the HCCI engine and the simulation models of other system components, including the SOFC. The operating characteristics of the SOFC in the hybrid system were identified in this chapter. Additionally, the feedback effect of the SOFC and HCCI engine is understood in this chapter. Based on these understandings, the design point of the system operation is determined, considering not only the system performance but also the stability of operation.

In chapter 5, guiding questions 1 to 3 were answered again via experiments of the entire SOFC–HCCI engine hybrid system. The experiments were conducted near the determined design point of operation from chapter 4. By these experiments, the feasibility of the system was directly verified. From the results of the experiments, the issues of the system operation to be resolved for improving the system performance are also identified.

In chapter 6, guiding question 4 is answered via simulation of the entire system. Three modifications to system design for resolving the issues of the system operation are introduced in this chapter. Additionally, the performance of the optimized system is introduced in this chapter.

In chapter 7, the performance of the system was predicted via simulations when the size of the system was scaled-up from 5 kW-class to 100 kW-class, whereas the design

of the system was fixed to the optimized design determine in chapter 6. The performance of 100 kW-class SOFC–HCCI engine hybrid system is estimated in this chapter.

Chapter 2
SOFC-HCCI engine hybrid system in this dissertation

2.1. Description of SOFC–HCCI engine hybrid system

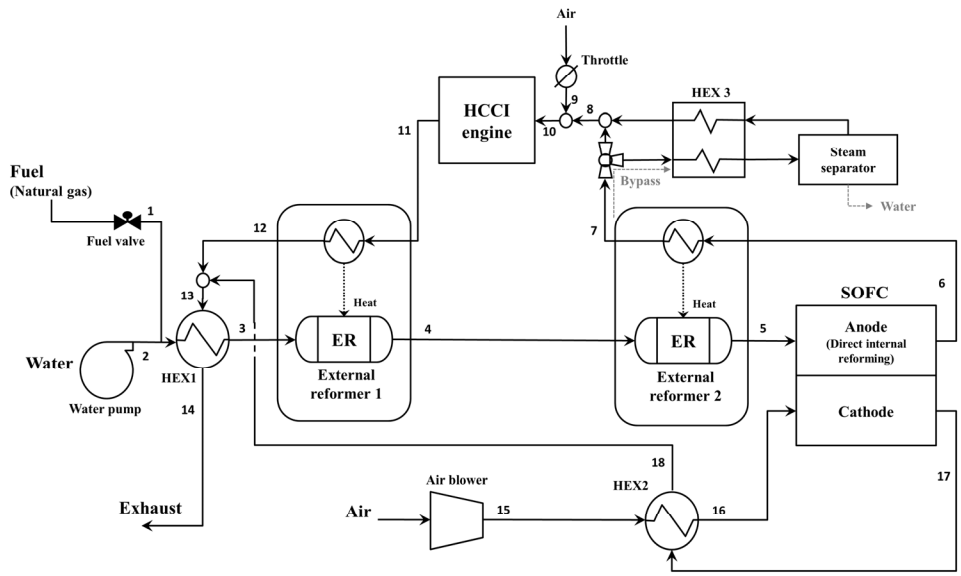

Figure 2.1. Schematic of the SOFC-HCCI engine hybrid system

Figure 2.1 shows the schematic of the SOFC–HCCI engine hybrid system proposed in this dissertation. The main components of this system are the SOFC, HCCI engine, and external reformers. In this system, these three components are connected and continuously affect each other.

First, the fuel of the system, i.e., natural gas, enters the system together with water and is reformed in external reformer 1. The reforming is conducted through a steam–methane reforming reaction. The heat required for the reforming reaction is supplied by the exhaust gas of the HCCI engine. Partially reformed gas is then further reformed in external reformer 2. The heat required for the reforming in external reformer 2 is supplied by the remaining heat of the SOFC anode off-gas. Since the SOFC anode off-gas is at a high temperature of 700 to 1000 °C, external reformer 2 delivers the excess

heat of the SOFC anode off-gas to the partially reformed gas to help the reforming process while lowering the temperature of the engine intake gas to an appropriate level for HCCI engine operation. The outlet gas of external reformer 2, which is partially reformed gas, is input into the SOFC. The remainder of the reforming is achieved by direct internal reforming inside the SOFC. Therefore, in the SOFC, the electrochemical reaction and the internal reforming reaction occur simultaneously. The heat generated by the electrochemical reaction is used for internal reforming, and the reformed gas is used again in the electrochemical reaction. The SOFC anode off-gas emitted from the SOFC is input into the HCCI engine after going through the system components controlling the quantity of the steam and air in the engine intake gas. The components controlling the engine intake gas consist of a bypass flow path, steam separator, and throttle. The HCCI engine combusts the SOFC anode off-gas and produces additional power. The exhaust gas of the HCCI engine again provides the heat required for reforming in the external reformer. Meanwhile, air is supplied to the cathode side of the SOFC through a blower. If ambient-temperature air were to be supplied to the SOFC, the large temperature difference inside the SOFC would destroy the SOFC cell. Therefore, the temperature of the air supplied to the SOFC is increased via heat exchange with the SOFC cathode off-gas.

2.2. Control parameters of the system

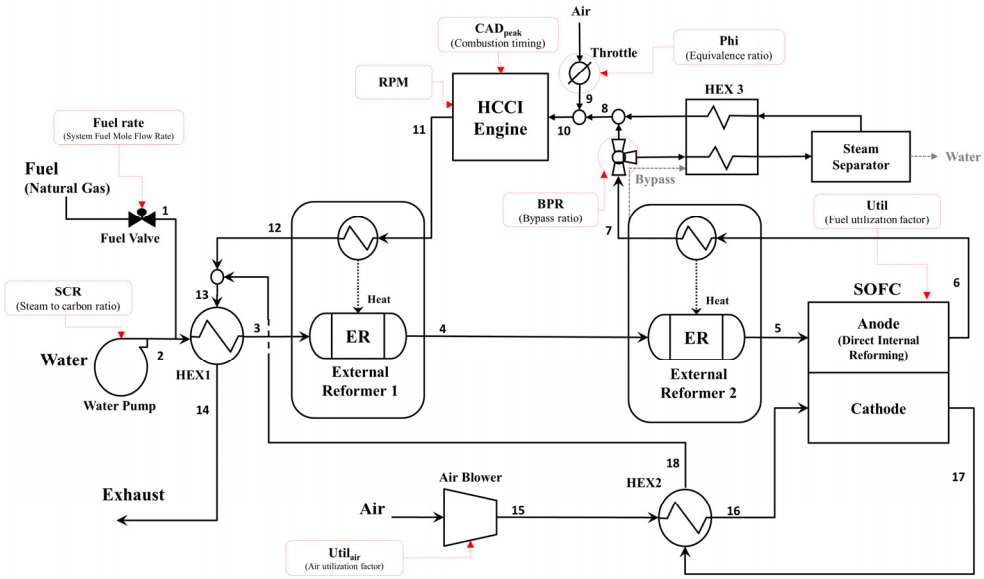

Figure 2.2. Control parameters of the SOFC–HCCI engine hybrid system

Figure 2.2 shows the eight control parameters, with dashed lines, that affect the system operation: the system fuel flow rate (hereinafter referred to as the Fuel rate), steam-to-carbon ratio (hereinafter referred to as SCR), fuel utilization factor of the SOFC (hereinafter referred to as Util), air utilization factor of the SOFC (hereinafter referred to as $Util_{air}$), bypass ratio to the steam separator (hereinafter referred to as BPR), the amount of air entrained into the HCCI engine (hereinafter referred to as Phi), combustion timing of the HCCI engine (hereinafter referred to as CAD_{peak}), and engine rpm (hereinafter referred to as RPM). The effect of each control parameter is described in the following.

Three control parameters (Fuel rate, SCR, and $Util_{air}$) affect the system operation by determining the flow rate of the input substances (natural gas, water, and air). The Fuel rate refers to the flow rate of the fuel into the system. This parameter is expressed in kW (for reference, a lower heating value is used for the calculation). SCR refers to the ratio of the molar flow rate of steam to carbon. SCR determines the flow rate of water,

which is input into the system for steam–methane reforming, when the flow rate of natural gas is pre-determined by the value of the Fuel rate. $Util_{air}$ refers to the ratio of the amount of air to be used in the SOFC to the amount of air supplied to the SOFC. $Util_{air}$ determines the flow rate of air supplied to the SOFC cathode when the amount of fuel reacting in the SOFC is pre-determined by the values of the Fuel rate and Util.

Util refers to the ratio of the amount of fuel to be used in the SOFC to the amount of fuel supplied to the SOFC. Therefore, Util is one of the control parameters that determine the system's performance. Util affects the operation of not only the SOFC but also the HCCI engine by influencing the flow rate and composition of the SOFC anode off-gas. Therefore, Util affects the SOFC and HCCI engine simultaneously and acts as a parameter that determines the load distribution of both generators.

Four parameters (BPR, Phi, CAD_{peak}, and RPM) directly affect the HCCI engine operation; however, since the HCCI engine is closely interconnected with the SOFC and external reformer, the HCCI engine operation influences the operation of the system. As a result, these four parameters also affect the operation of the system, including the SOFC. BPR represents the amount of gas bypassed to the steam separator to control the amount of H_2O in the engine intake gas. Therefore, because the value of BPR affects the composition, flow rate and temperature of the HCCI engine intake and exhaust gas, the external reforming rate and system operation result are also affected. In this dissertation, the value of BPR is considered to be varied freely by changing the design specifications of the bypass flow path.

Phi is a parameter that represents the equivalence ratio of the HCCI engine intake gas. Phi is calculated based on the amount of air and fuel components (H_2 and CO) entrained in the HCCI engine; thus, the value of Phi determines the amount of air entrained in the HCCI engine together with the SOFC anode off-gas. Similar to BPR,

Phi affects not only the HCCI engine operation but also the external reforming rate and system operation results by influencing the thermodynamic states of the HCCI engine intake and exhaust gas. Phi can be controlled by changing the angle of the throttle.

CAD_{peak} represents the timing of combustion in the HCCI engine. Changes in combustion timing affect the HCCI engine operation and, accordingly, affect the overall system operation. The thermodynamic state of the engine intake gas determines the combustion phase of the HCCI engine since HCCI combustion is achieved by the auto-ignition caused by compression. Therefore, CAD_{peak} can be controlled by changing the thermodynamic state of the intake gas. Finally, RPM refers to the engine rpm, which determines the volume flow rate of the engine intake gas. RPM affects not only the combustion phase of the HCCI engine but also the temperature and pressure of the engine intake gas, thereby affecting the overall system operation.

Chapter 3
Experimental Study of HCCI engine fuelled by SOFC anode off-gas

3.1. Introduction

To experimentally investigate the hybrid system, since the SOFC and HCCI engines continuously provide feedback to each other in the hybrid system, a complete understanding of the operation of the HCCI engine fuelled by SOFC anode off-gas is essential for analysing the overall system operation. Therefore, the analysis of the HCCI engine should precede the other analysis. However, thus far, such analysis has not been performed. Although the studies on the operation of HCCI engine fuelled by syngas have been conducted, the composition of syngas in previous literatures are different from that of SOFC anode off-gas.[24, 25, 31, 32] The amount of diluent in SOFC anode off-gas is much larger than that of syngas in the literatures; especially, the steam dilution in SOFC anode off-gas is much larger. More importantly, it is essential to analyse how the HCCI engine will operate under various system operating conditions, but such studies have not been conducted.

This chapter aims at analysing HCCI engine operation in SOFC–HCCI engine hybrid system by conducting an experimental study of HCCI engine operation fuelled by SOFC anode off-gas. Specifically, there are three objectives for this experimental study, which can be summarized as follows. The first objective is to verify the feasibility of HCCI engine operation fuelled by SOFC anode off-gas to demonstrate the feasibility of the SOFC–HCCI engine hybrid system. The second objective is to confirm experimentally how the HCCI engine operation changes when various control parameters of the system change and to analyse the causes of these experimental results.

The third objective is to identify the ranges of system control parameters for successful HCCI engine operation from these experimental results.

For these purposes, the main body of this chapter consists of three parts: experiment, results, and discussion. In the experiment section, the experimental equipment is described. The experimental methods and the experimental conditions are also explained in this section. Additionally, the control parameters of the HCCI engine, which determine the experimental condition, and their effects on engine operation are examined. In the results section, the experimental results of the HCCI engine operation for various control parameter values are introduced. From the experimental results, the feasibility and performance of the HCCI engine operation are verified. In the discussion section, various experimental results are summarized, and the general principles of HCCI engine operation are determined. Finally, possible problems facing HCCI engine operation fuelled by SOFC anode off-gas are discussed.

Although this chapter focuses on analysing only HCCI engine operation in the SOFC–HCCI engine hybrid system, it is also very important to understand how HCCI engine operation affects the system and the SOFC and, conversely, how the system affects the HCCI engine. Therefore, chapter 4 in this dissertation focus on this effect. Moreover, in chapter 5, the design-point of HCCI engine operation is determined from an entire-system point of view.

3.2. Experiment

3.2.1. Experimental setup

3.2.1.1. Outline of experimental setup

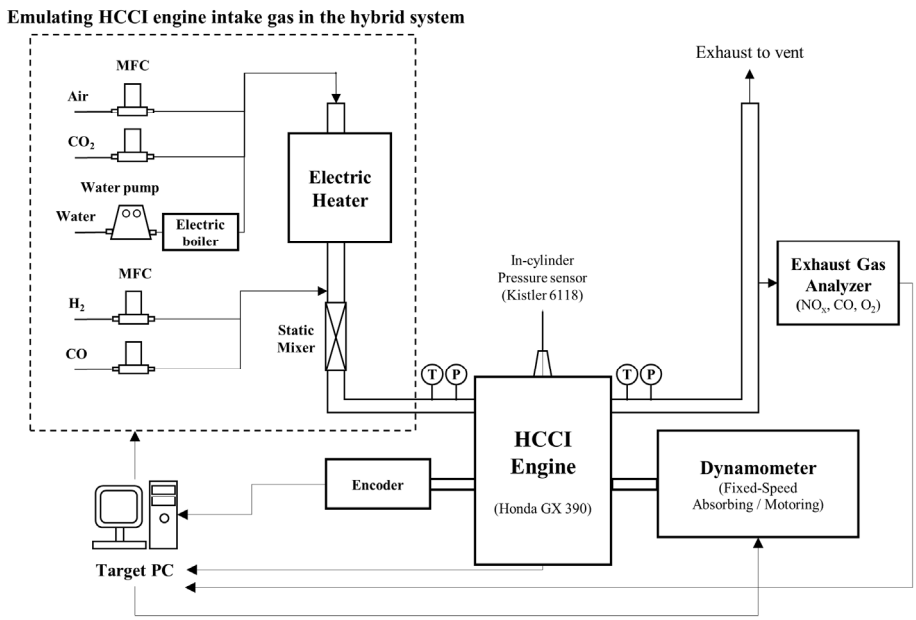

Figure 3.1. Experimental apparatus

Figure 3.1 is a schematic view showing the experimental setup. Based on functionality, it can be divided into two parts. The first part includes the experimental equipment that emulates the HCCI engine intake gas of the SOFC–HCCI engine hybrid system. The second part includes the HCCI engine and its peripherals.

All experimental equipment is controlled by a host computer and a target computer. The host computer operates using Mathworks MATLAB Simulink/Real-Time Workshop, and the target computer operates using the Mathworks xPC operating system. To enable real-time signal sensing and actuating via computers, the target computer is equipped with an NI DAQ 6259 board capable of digital-to-analogue and analogue-to-digital data conversion and an MCC PCI QUAD 04 encoder board dedicated to the encoder signal of the engine.

For reference, the experimental set up are explained with pictures in appendix A. Therefore, it is recommended to refer the appendix A for the detailed description of experimental set up.

3.2.1.2. Emulator of HCCI engine intake gas in the SOFC–HCCI engine hybrid system

The HCCI engine intake gas in the hybrid system is hot gas consisting of H_2, CO, H_2O, CO_2, and air (O_2 and N_2). To accurately emulate the thermodynamic state of the HCCI engine intake gas, mass flow controllers (MFCs), a water pump, an electric boiler, and an electric heater are used. To prevent an uncontrolled ignition in the intake system, the fuel components (H_2 and CO) are not put into the electric heater with O_2. Instead, the gases, except for H_2 and CO, are put into an electric heater, and H_2 and CO are mixed later using a static mixer.

3.2.1.3. HCCI engine and peripherals

In this chapter, the HCCI engine, the size of which is matched to that of the 5 kW-class SOFC–HCCI engine hybrid system, is experimented on. More specifically, the HCCI engine used in the experiment was made by modifying Honda's GX390 model. First, the throttle and the fuel carburettor were removed, and a proper intake manifold, which can input the HCCI engine intake gas, emulated by the equipment described in section 3.2.1.2., into the HCCI engine, was fabricated. The spark plug was replaced with a Kistler pressure transducer (Kistler 6118) to measure the in-cylinder pressure. The piston and engine head, which have one intake valve and one exhaust valve, were not modified. Therefore, the engine valve timing, compression ratio, and displacement volume were maintained at their original values. The detailed specifications of the HCCI engine are shown in table 3.1.

Table 3.1. HCCI engine specifications

Number of cylinders	1
Bore	88 mm
Stroke	64 mm
Displacement	389 cc
Compression ratio	8.2
Engine Speed	1800 rpm
Oil Temperature	110±5 °C

A dynamometer consisting of a motor and an inverter was connected to the crankshaft of the engine so that it could rotate the engine crankshaft at a fixed speed regardless of the engine's combustion conditions. As mentioned before, RPM was maintained at 1800 rpm in all experiments. The crankshaft of the engine was also connected to the encoder so that the crank angle degree of the current engine could be measured.

The intake gas temperature was measured using a thermocouple installed approximately 5 cm upstream of the intake valve in the intake manifold. The exhaust gas temperature was measured using a thermocouple installed approximately 10 cm downstream of the exhaust valve in the exhaust manifold. In addition, a pressure transducer was installed in each manifold to measure the static pressures of the intake gas and exhaust gas. The pollutant emissions in the engine exhaust gas were measured using an exhaust gas analyser set (Eurotron GreenLine MK2). CO and NO_x emissions, which are major pollutants of the engine, were measured using this analyser set.

There was no separate cooling water for the engine, as the engine was an air- and oil-cooled engine. However, to enable similar engine cooling conditions in all experiments, the oil temperature in the engine was monitored and maintained near 110 °C using an external oil conditioner.

3.2.2. Description of control parameters

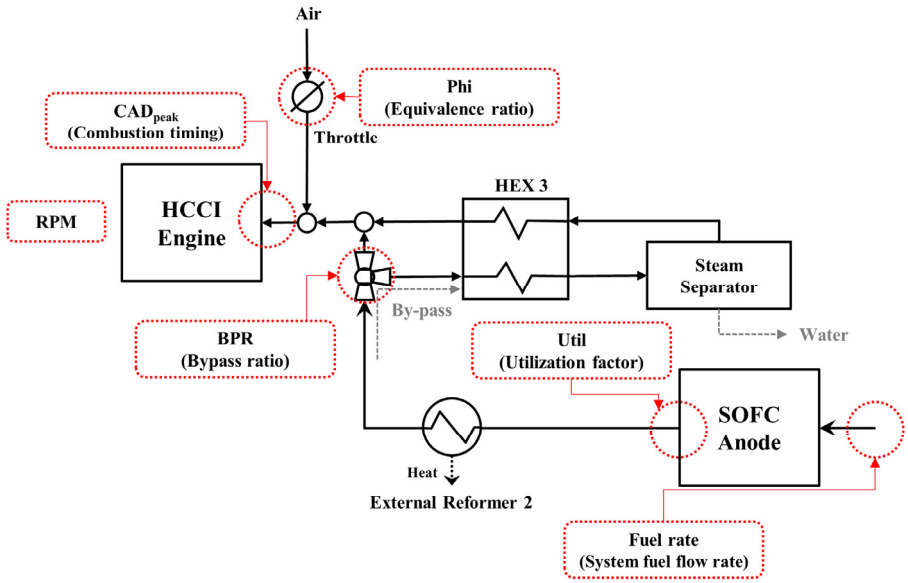

Figure 3.2. Control parameters of HCCI engine operation

Figure 3.2 shows the HCCI engine part of the hybrid system with the HCCI engine control parameters emphasized. In this system, there are six control parameters affecting the HCCI engine operation: system fuel flow rate (Fuel rate), fuel utilization factor of the SOFC (Util), bypass ratio with regard to the steam separator (BPR), amount of air entrained in the HCCI engine (Phi), combustion timing of the HCCI engine (CAD_{peak}), and engine rpm (RPM). The effect of each control parameter is explained in the following.

First, the Fuel rate refers to the amount of fuel, i.e., natural gas, that enters the hybrid system. The Fuel rate affects the power generation load of the entire system. Util refers to the proportion of the fuel used in the SOFC. Therefore, Util determines the load distribution between the SOFC and HCCI engine in the system. At a given Fuel rate, a larger Util results in a higher load on the SOFC and a lower load on the HCCI engine. From the HCCI engine point of view, Util determines the amount of diluent (H_2O and CO_2) relative to the amount of fuel (H_2 and CO) in the gas delivered to the HCCI engine.

In other words, when Util increases, the HCCI engine intake gas has a high dilution level and a low fuel level. BPR adjusts the amount of gas bypassed to the steam separator and ultimately controls the amount of H_2O in the engine intake gas. If BPR is high, which means that a large amount of gas is bypassed to the steam separator for water to be condensed out, then the amount of H_2O in the engine intake gas will decrease accordingly. Phi implies the amount of air entrained through the throttle and fed into the HCCI engine. Specifically, the amount of O_2 and N_2 in the engine intake gas is controlled according to the desired value of Phi. Taken together, the four above-mentioned parameters determine the composition and flow rate of the engine intake gas.

The timing of HCCI combustion is another control parameter of the HCCI engine. Because the HCCI engine achieves combustion only via the compression of a premixed charge inside the cylinder, the combustion timing is determined by the thermodynamic state of the engine intake gas. Specifically, the composition, pressure, and temperature of the engine intake gas determine the combustion timing, in a given geometric profile of the engine hardware. Therefore, the combustion timing can be changed if the engine intake gas temperature is varied even though the flow rate and composition of the engine intake gas are fixed via the determination of the above four parameters. In this chapter, CAD_{peak} is used to indicate the combustion timing. CAD_{peak} denotes the crank angle degree (CAD) of the engine at which the peak pressure occurs. In this chapter, if the peak pressure occurs at the same CAD, it is considered to be the same combustion timing. Finally, the engine rpm (RPM) determines the volume flow rate of the engine intake gas. RPM also determines the physical duration of an engine cycle, which affects the combustion and heat transfer characteristics of the HCCI engine. In this chapter, however, RPM is fixed at 1800 rpm (60 Hz), which is equal to the frequency of the Korean AC power, for efficient power generation.

Therefore, in this chapter, various experiments are performed to determine how the HCCI engine operation is changed when the above five control parameters (Fuel rate, Util, BPR, Phi, and CAD_{peak}) are varied. Additionally, by analysing these results, we can confirm the ranges of the optimal control parameters for proper HCCI engine operation.

3.2.3. Experimental approach

The main goals of the experiment are to verify the feasibility of HCCI engine operation fuelled by SOFC anode off-gas, to see how the experimental results of HCCI engine operation are changed when various control parameters are varied and to determine the ranges of control parameters that enable proper HCCI engine operation. For this purpose, the experiment was performed while varying the values of five control parameters (Fuel rate, Util, BPR, Phi, and CAD_{peak}).

The experiment was performed in the following manner. First, the experimental conditions, that is, the values of each control parameter, were determined. Then, the composition and flow rate of the engine intake gas corresponding to these control parameters were calculated. The method of this calculation is described in detail in appendix B. Next, the engine intake gas, with the calculated composition and flow rate, was created using the experimental equipment described in section 3.2.1.3; then, this gas was input into the HCCI engine, and combustion was achieved within the HCCI engine. At this time, the combustion timing of the HCCI engine was measured in real time, and the intake gas temperature was controlled by the electric heater to match the desired combustion timing.

Table 3.2. Effects of control parameters

Control parameter	Effect of parameter variation
Fuel rate	Fuel flow rate of engine intake gas
Util	Fuel flow rate and dilution
BPR	H_2O dilution level of engine intake
Phi	Air dilution level of engine intake gas
CAD_{peak}	Combustion phase

Table 3.2 summarizes the effect of each control parameter of the HCCI engine. The experimental results for different values of these parameters are introduced in the following order. First, in section 3.3.1, the flow rate of the fuel components (H_2 and CO) in the HCCI engine intake gas is fixed by determining the Fuel rate and Util, while the H_2O and air diluent flow rate of the intake gas are changed by varying BPR and Phi. The aim of this section is to understand the effects of the dilution level of the intake gas on HCCI engine operation. In section 3.3.2, the values of other parameters are fixed, but the value of Util is changed. According to changes in Util, the flow rate characterizing the fuel components and the dilution level of the engine intake gas change simultaneously. Therefore, the aim of this section is to understand the effect of these simultaneous changes, or Util, on HCCI engine operation. The range of Util in which the HCCI engine can operate properly is also confirmed in this section. In section 3.3.3, other parameters are fixed, but the Fuel rate is varied. This helps us confirm how the HCCI engine operation changes when the overall flow rate of the engine intake gas changes and thereby the engine load changes while the fuel and dilution level of the intake gas remain fixed. In sections 3.3.1 to 3.3.3, the experiments are performed with fixed combustion timing and a CAD_{peak} value of 372 CAD. On the other hand, in section

3.3.4, the experiments are performed with the values of the other parameters being fixed, except the combustion timing. This procedure helps us to identify the effect of the combustion timing on HCCI engine operation.

The experimental conditions of each section are summarized in table 3.3. In each section, the fixed value is determined as a value that is suitable for efficient and stable system operation or a value that can well represent the change in HCCI engine operation caused by varying the values of the other control parameters. Specifically, in sections 3.3.1, 3.3.3, and 3.3.4, different values of Util are selected to well represent the changes in engine operation caused by changing the control parameters in each section.

Table 3.3. Experimental conditions of each section

Control parameter	**3.3.1**	**3.3.2**	**3.3.3**	**3.3.4**
Fuel rate	10.0 kW	10.0 kW	**Variation**	10.0 kW
Util	0.65	**Variation**	0.7	0.75
BPR	**Variation**	0	0	0
Phi	**Variation**	**Variation**	0.9	0.9
CAD_{peak}	372 CAD	372 CAD	372 CAD	**Variation**

3.3. Results

It should be noted that all the experimental results shown in this section are the result of averaging the experimental results from 15-second engine operating durations (approximately 220 engine cycles at 1800 rpm). In particular, the in-cylinder pressure and CAD were measured at a speed of approximately 1 sample / 0.15 ms, and these data were averaged at the same position in the engine cycle. The pollutant emissions were measured under dry conditions and corrected to a 15% O_2 level so that they could be objectively compared to various experimental results. In addition, although it is possible to overcharge the engine over 1 atm by supplying intake gas using the MFCs, only the experimental results for which the intake manifold pressure is less than 1 atm are introduced. This is because the engine intake pressure cannot exceed 1 atm, as air is supplied through the throttle in an actual SOFC–HCCI engine hybrid system.

3.3.1. BPR/Phi variations

Table 3.4. Molar flow rates and lower heating value (LHV) of HCCI engine intake gas in section 3.3.1

	Molar flow rate (mol/s)
H_2	0.0147
CO	0.0027
H_2O	0.0137~0.0417
CO_2	0.01
Air (O_2 & N_2) [1]	0.0413~0.0826
LHV	39.0 kJ/mol
Supplied energy [2]	4.3 kW

[1] O_2: N_2 = 0.21: 0.79 [2] Supplied energy = LHV × Molar flow

In this section, the results of an experiment with a fixed Fuel rate of 10.0 kW, Util of 0.65, CAD_{peak} of 372 CAD, and variable BPR and Phi, are introduced. BPR is varied from 0 to 0.8, and Phi is varied from 0.5 to 1. With these control parameter ranges, the composition of the HCCI engine intake gas is changed, as shown in table 3.4. Through these experiments, the manner in which HCCI engine operation is affected when varying the diluent (air and H_2O) flow rate under a fixed fuel (H_2 and CO) flow rate is investigated. Particularly, the goal is to investigate whether proper HCCI combustion is achieved even under a high dilution level of the engine intake gas and to determine the types of problems that exist in the case of a high dilution level.

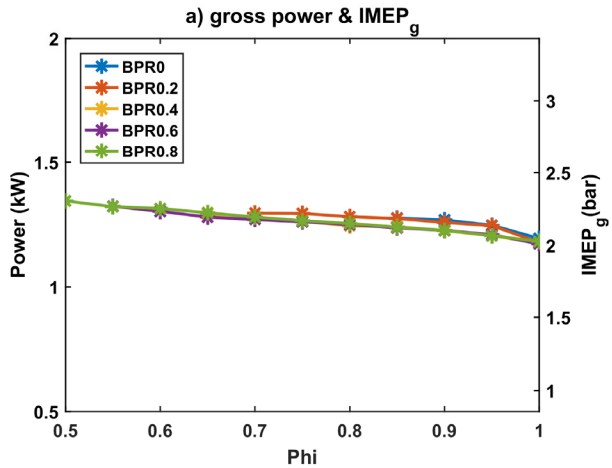

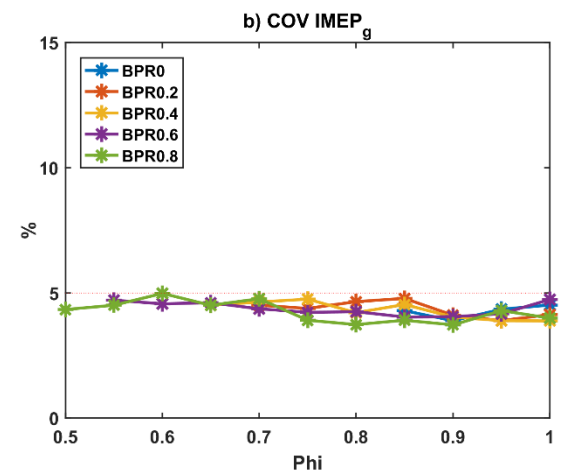

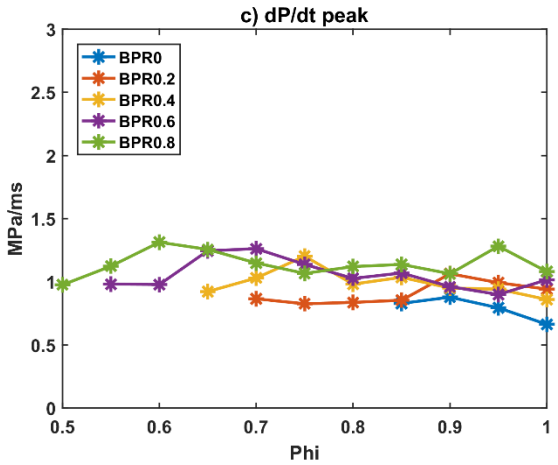

Figure 3.3. Stability of HCCI engine operation with BPR/Phi variations: a) gross power and $IMEP_g$; b) COV $IMEP_g$; c) dP/dt peak

To verify whether the HCCI engine fuelled by SOFC anode off-gas operates well, three parameters are checked in figure 3.3. First, figure 3.3 a) shows the gross indicated power produced by the engine as a function of BPR and Phi. The graph shows that under all tested conditions, approximately 1.3 kW of gross indicated power (or $IMEP_g$, i.e., gross indicated mean effective pressure ~ 2.2 bar) and approximately 30% efficiency (~1.3 kW of power out of 4.3 kW of fuel input) are achieved. Considering that the engine used in the experiment is a small single-cylinder engine, it can be considered that the power is produced with promising efficiency. Figure 3.3 b) shows the COV $IMEP_g$, i.e., the coefficient of variance of the gross indicated mean effective pressure, which indicates the cycle-to-cycle variation of the HCCI engine and is used to determine if the HCCI combustion is stable. It can be seen that the COV $IMEP_g$ is maintained at 5% or less. The upper limit of the COV IMEP for stable combustion varies from 5% to 10% depending on the references.[23, 33-35] In this dissertation, a COV $IMEP_g$ of less than 5% is set as the stable combustion range. Therefore, it can be considered that the combustion is stable under every experimental condition of this

section. Finally, the peak dP/dt of the HCCI engine is shown in figure 3.3 c); it is used to determine if the pressure rise occurs too quickly, thereby degrading engine durability. As shown in figure 3.3 c), when BPR decreases, that is, when the amount of H_2O diluent in the engine intake gas increases, the value of the peak dP/dt tends to decrease, but the difference in value is not large. The values of the peak dP/dt are near 1 MPa/ms for all cases. In general, HCCI combustion is considered to be safe for typical engine harware when the value of the peak dP/dt is under 5 MPa/ms.[36] Therefore, the values of the peak dP/dt are in the stable range for all cases. Thus, from the values of these three parameters, it can be confirmed that proper HCCI engine operation is achieved even with low BPR and Phi, that is, a large amount of diluent in the engine intake gas, under the conditions considered in this section, i.e., a Fuel rate of 10.0 kW, Util of 0.65, and CAD_{peak} of 372 CAD.

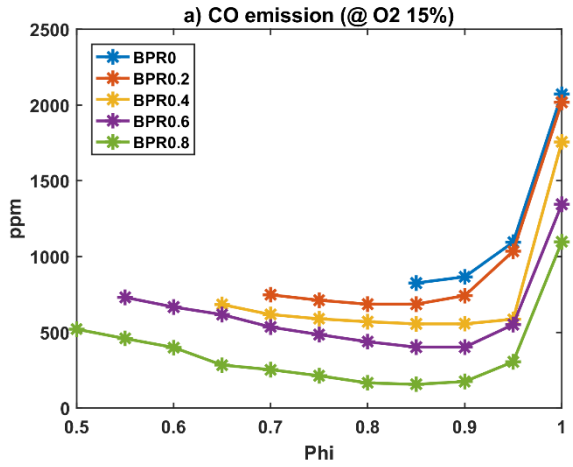
a) CO emission (@ O2 15%)
BPR0
BPR0.2
BPR0.4
BPR0.6
BPR0.8
ppm
Phi
2500
2000
1500
1000
500
0
0.5
0.6
0.7
0.8
0.9
1

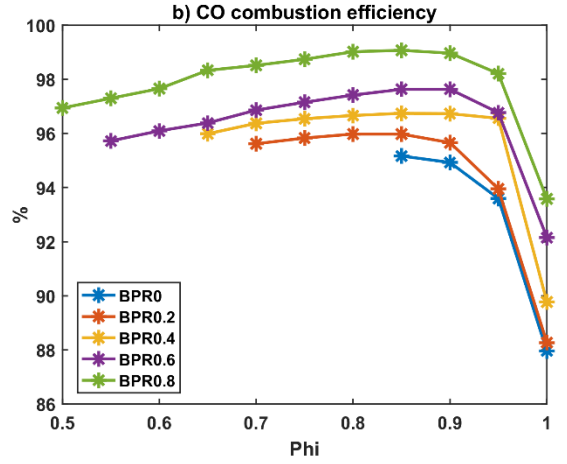
b) CO combustion efficiency
BPR0
BPR0.2
BPR0.4
BPR0.6
BPR0.8
%
Phi
100
98
96
94
92
90
88
86
0.5
0.6
0.7
0.8
0.9
1

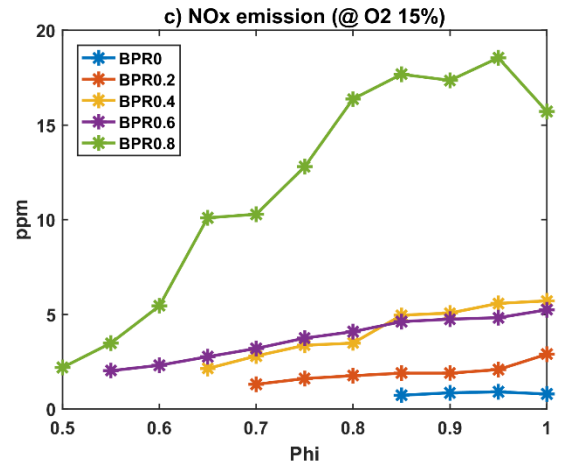
c) NOx emission (@ O2 15%)
BPR0
BPR0.2
BPR0.4
BPR0.6
BPR0.8
ppm
Phi
20
15
10
5
0
0.5
0.6
0.7
0.8
0.9
1

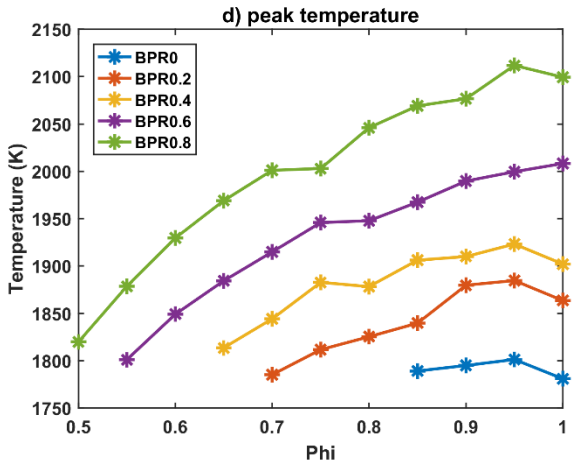

Figure 3.4. Pollutant emission characteristics of HCCI engine with BPR/Phi variations: a) CO emissions; b) CO combustion efficiency; c) NO_x emission; d) peak temperature

Figure 3.4 shows the pollutant emissions of the HCCI engine. Because the fuel of the HCCI engine in the hybrid system is composed only of H_2 and CO, which are originally included in the SOFC anode off-gas, unburned hydrocarbon and soot emissions are barely produced, unlike what occurs in the general internal combustion engine operation. Therefore, the major pollutant emissions of the HCCI engine fuelled by SOFC anode off-gas can be regarded as CO and NO_x. In addition, the CO emissions are caused by the unburned CO rather than incomplete combustion of the hydrocarbons, which is the major cause for general internal combustion engines. For reference, in this dissertation, H_2 is assumed to have combusted completely. To simplify the experiments, the H_2 emissions in the exhaust gas were not measured via gas chromatography under all the experimental conditions but rather were only measured for some selected operating points. At the selected operating points, the amount of H_2 emissions was measured via gas chromatography and found to be overall below the measurement error. The detailed measuremental results of H_2 emission is described in section 5.3.4. In

addition, the fact that the ignition temperature of H_2 is approximately 1100 K, which is much lower than the ignition temperature of CO, and the fact that the oxidation reaction rate of H_2 is very fast, support this assumption.[32]

Since the HCCI engine generally has a relatively low temperature after combustion, it produces lower NO_x emissions and higher CO emissions than the spark ignition engine.[37] Figure 3.4 a) shows the CO emissions. The graph shows that the CO emissions are less than approximately 1000 ppm (@ O_2 15%), except when Phi is equal to 1. Since ppm is a relative unit, the combustion efficiency of CO is shown in figure 3.4 b) for an absolute comparison. In this dissertation, the combustion efficiency of CO is calculated using the following equation. In this equation, $\dot{m_{CO,in}}$ can be calculated from the values of the control parameters, and $\dot{m_{CO,out}}$ is calculated inversely from the measured CO fraction (ppm) in the exhaust gas. The calculated CO combustion efficiency is greater than 95%, except when Phi is equal to 1.

$$\text{CO combustion efficiceny} = 1 - {\dot{m_{CO,out}}}\Big/{\dot{m_{CO,in}}} \quad (3.1)$$

The trend of the CO emissions can be explained based on the following three aspects. The first trend characterizing the CO emissions is that as Phi approaches 1, regardless of BPR, the CO emissions increase rapidly, and the combustion efficiency of the CO drastically decreases. There are two reasons for this. The first reason is that when the value of Phi is close to 1, a locally rich region (Phi >1) can be formed inside the cylinder due to inevitable inhomogeneity. The second reason is that when Phi is close to 1, there is no extra oxygen for the oxidation reaction; thus, the O_2 concentration is remarkably low, and the CO oxidation reaction does not occur properly at the end of the CO oxidation reaction process. The second trend characterizing the CO emissions is that when Phi is less than 0.9, the combustion efficiency decreases as Phi decreases. The third trend is that as BPR increases, the combustion efficiency of CO increases. These

second and third trends show that as the diluent flow rate increases, the combustion efficiency of CO decreases. The cause of these trends is that when the diluent flow rate of the engine intake gas is increased and the fuel flow rate remains constant, the in-cylinder temperature during combustion decreases, which reduces the CO combustion efficiency. Figure 3.4 d) shows the calculated peak temperature inside the cylinder for one averaged engine cycle. The graph shows that the trends of the CO combustion efficiency and the peak temperature are very similar, except for cases where Phi is close to 1 (Phi 0.95 ~ 1). The correlation between the CO combustion efficiency and peak temperature is discussed further in the discussion section.

Figure 3.4 c) shows the NO_x emissions. The NO_x emissions decrease as BPR and Phi decrease. This implies that the NO_x emissions decrease as the dilution level of the engine intake gas increases, that is, the peak temperature decreases. These experimental results are in good agreement with theory, as it is well known that NO_x formation is sensitive to the combustion temperature.[38] More specifically, the experimental results show that when BPR is 0.6 or less, the NO_x emissions generated are less than approximately 5 ppm, and when BPR is 0, the measured NO_x emissions are lower than the measurement limit of the analyser. In addition, it is confirmed that the HCCI engine generates NO_x emissions at approximately 20 ppm even for the case of a BPR value of 0.8. Therefore, it can be concluded that an HCCI engine fuelled by SOFC anode off-gas generally produces minimal NO_x emissions.

In summary, both the CO emissions and NO_x emissions of the HCCI engine fuelled by SOFC anode off-gas are greatly influenced by the dilution level of the engine intake gas and the subsequent combustion temperature. However, if the dilution level increases and the peak temperature decreases, the NO_x emissions decrease and the CO emissions increase, indicating that the two major pollutant emissions of an HCCI engine fuelled

by SOFC anode off-gas are characterized by a trade-off relationship with the dilution level.

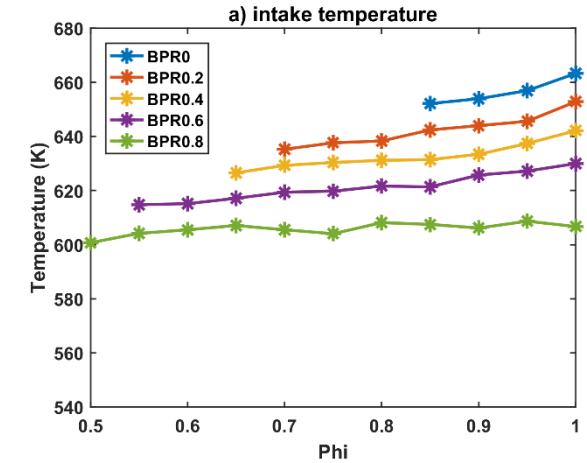

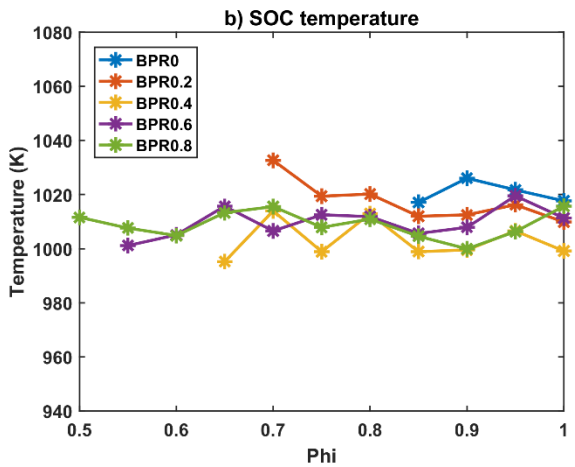

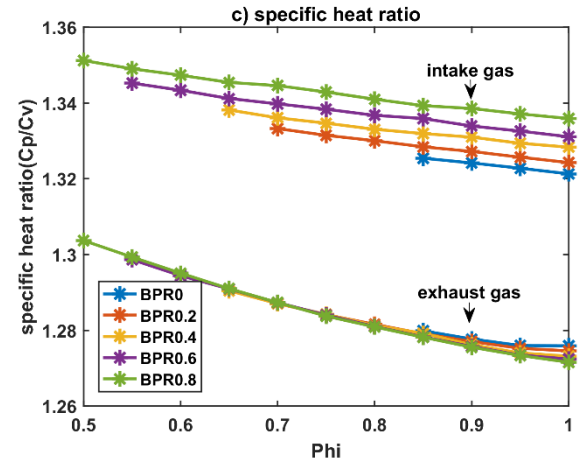

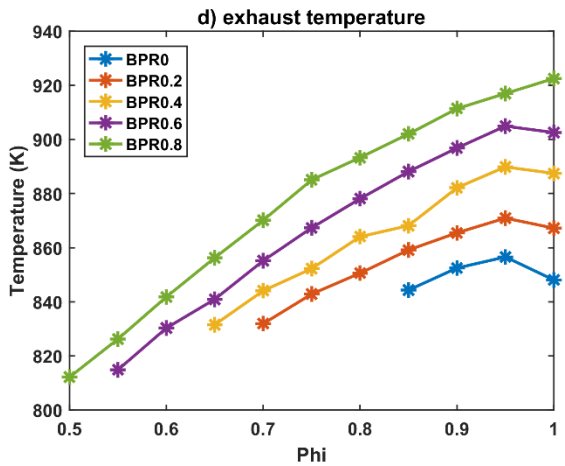

Figure 3.5. Intake and exhaust gas temperature characteristics of HCCI engine with BPR/Phi variations: a) intake gas temperature; b) SOC temperature; c) specific heat ratio; d) exhaust gas temperature

As shown in figure 3.3, HCCI combustion occurred properly for all operating points. To achieve this HCCI combustion, a relatively high intake gas temperature was required. Figure 3.5 shows the temperatures of the intake gas and exhaust gas. As shown in figure 3.5 a), an engine intake gas temperature of over 600 K is required to achieve HCCI combustion at the given combustion timing (CAD_{peak} of 372 CAD) with a given engine compression ratio of 8.2, which is relatively small for typical HCCI engine operation.

Meanwhile, in the SOFC–HCCI engine hybrid system, the intake and exhaust gas temperatures of the HCCI engine are important properties that determine the feedback of the HCCI engine to and from the system. Since the HCCI engine uses SOFC anode off-gas as the fuel, the operational results of the SOFC and the consequent thermodynamic state of the SOFC anode off-gas directly affect the engine intake gas temperature. Additionally, since the HCCI engine exhaust gas is used as the heat source for the external reformer, the engine exhaust gas temperature affects the external reforming rate, which affects the operation of the SOFC. Therefore, understanding the trends of the intake and exhaust gas temperatures is essential for predicting the operation of the SOFC–HCCI engine hybrid system.

Figure 3.5 a) shows two trends of the intake gas temperature. First, when BPR decreases, that is, the amount of H_2O diluent in the engine intake gas increases, the required intake temperature increases. Second, a higher intake temperature is required as Phi approaches the stoichiometric condition, i.e., Phi equal to 1. Since the combustion of the HCCI engine results from the autoignition of the intake gas due to compression, there are two main factors that determine the required intake gas temperature for a given combustion timing. The first factor is the start of the combustion temperature (hereafter called the SOC temperature). If the SOC temperature is affected significantly by BPR and Phi, the required intake temperature will also be affected by BPR and Phi. The second factor is the specific heat ratio of the engine intake gas. The value of the specific heat ratio affects the required intake gas temperature because the increment of temperature caused by compression is influenced by the value of the specific heat ratio. Figure 3.5 b) shows the SOC temperature. The graph shows that the values of the SOC temperature for various BPR and Phi values remained almost constant without any significant changes (for reference, the method for determining the SOC timing is

described in detail in appendix B). On the other hand, figure 3.5 c) shows how the specific heat ratio of the engine intake gas varies for different BPR and Phi values (for reference, the specific heat ratio was calculated using the Cantera thermodynamic tool box[39]). The trend of the specific heat ratio of the engine intake gas in figure 3.5 c) is exactly the opposite of the trend of the intake gas temperature in figure 3.5 a). Therefore, it can be said that an intake gas with a low specific heat ratio requires a high intake temperature to reach the SOC temperature after compression, or vice versa. Therefore, it can be concluded that the most dominant factor that determines the intake temperature of an HCCI engine fuelled by SOFC anode off-gas is the value of the specific heat ratio of the engine intake gas.

Figure 3.5 d) shows the engine exhaust gas temperature. The graph shows that the exhaust gas temperature decreases as BPR and Phi decrease. Specifically, the higher the dilution level, the lower the exhaust gas temperature. There are two main parameters that determine the exhaust gas temperature. The first factor is the peak temperature shown in figure 3.4 d). The peak temperature can be regarded as the starting point for determining the exhaust gas temperature because the exhaust gas temperature is obtained from the peak temperature via the expansion and exhaust process. Therefore, as shown in figure 3.4 d) and figure 3.5 d), a lower peak temperature results in a lower exhaust gas temperature. The second factor is the specific heat ratio of the engine exhaust gas. The specific heat ratio of the engine exhaust gas determines the decrement in temperature during the expansion process. As shown in figure 3.5 c), the specific heat ratio of the engine exhaust gas does not change significantly with BPR but rather increases as Phi decreases. Therefore, a lower value of Phi results in a greater decrease in temperature during the expansion process. Thus, this point contributes to the exhaust gas temperature decreasing when Phi decreases.

An additional interesting note regarding the tendency of the intake and exhaust gas temperatures is that the slope of the intake gas temperature with increasing Phi decreases as BPR increases. Particularly, when BPR is 0.8, it can be said that the intake gas temperature hardly increases as Phi increases. This tendency occurs because the sensible energy of the residual gas (or internal exhaust gas recirculation) remaining in the engine cylinder from the previous engine cycle affects the required intake gas temperature of the next engine cycle. In general, the in-cylinder gas of an engine cycle consists of the fresh intake gas of this engine cycle and the residual gas remaining in the clearance volume of the engine from the previous engine cycle. Therefore, a larger sensible energy of the residual gas may result in a lower intake temperature required to induce HCCI combustion. Because of this, as Phi increases, the exhaust gas temperature increases, and the sensible energy of the residual gas also increases. This relationship affects the required intake gas temperature, causing it to decrease as Phi increases. On the other hand, as mentioned above, the decrease in the specific heat ratio of the engine intake gas as Phi increases causes the required intake gas temperature to be increased. Therefore, when Phi increases, the two effects on the required intake gas temperature present a trade-off relationship. Meanwhile, when BPR increases, the amount of H_2O in the engine intake gas is reduced, which decreases the flow rate of the engine intake gas. As a result, when BPR increases, the ratio of the residual gas to the total in-cylinder gas increases, as the flow rate of the intake gas is decreased but the amount of residual gas is fixed at the level of the engine clearance volume. Therefore, if the influence of the sensible energy of the residual gas becomes sufficiently dominant as BPR increases, the required intake gas temperature hardly increases even though Phi increases.

For reference, in this chapter, it is assumed that the required engine intake gas temperature is always achievable from the system operation. Whether the required

engine intake gas is achievable for each BPR and Phi and how the engine exhaust gas temperature affects the external reforming rate are discussed in chapter 5.

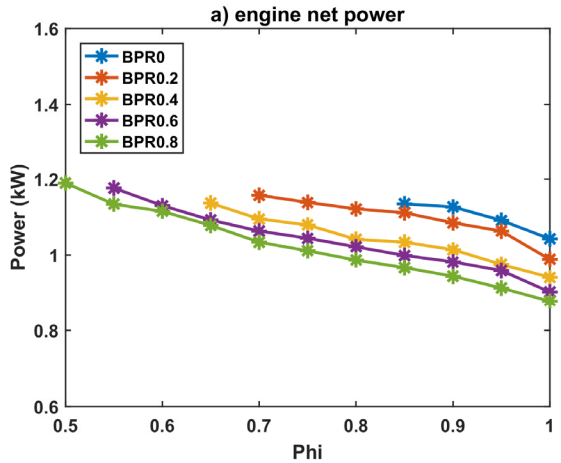

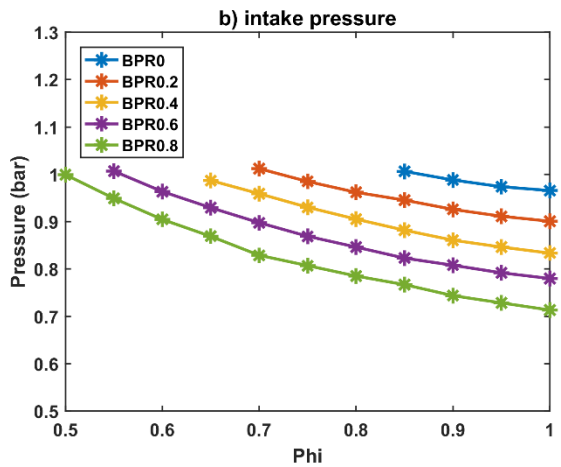

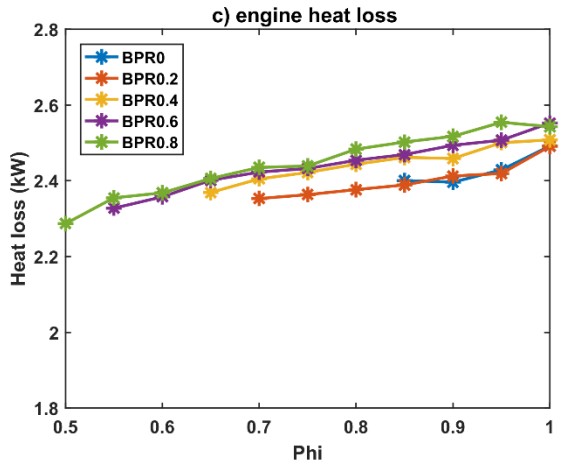

Figure 3.6. Energy transfer characteristics of HCCI engine with BPR/Phi variations: a) engine net power; b) intake pressure; c) engine heat loss

Figure 3.6 shows the energy transfer characteristics of the HCCI engine. Figure 3.6 a) shows the engine net indicated power. The net indicated power of the engine is calculated by subtracting the pumping loss, which is the amount of energy required to pump in-cylinder gas from the intake pressure to the exhaust pressure, from the gross indicated power. As shown in the graph, lower BPR and Phi, i.e., higher diluent flow rates, result in greater engine net indicated power. In figure 3.3 a), the gross indicated power is hardly affected by BPR and Phi; thus, this trend characterizing net power is mainly attributed to the change in pumping loss. As the flow rate of the diluent increases, i.e., BPR and Phi decrease, the intake gas flow rate increases, which causes the engine intake pressure to be increased, as shown in figure 3.6 b). Therefore, the pumping loss is decreased, and the engine net power is increased as BPR and Phi decrease. It is noted that the engine exhaust pressure is almost the same as the atmospheric pressure regardless of the values of the control parameters. For this reason, the trends characterizing the engine net power and engine intake pressure are quite similar.

Figure 3.6 c) shows the total heat loss of the HCCI engine. The engine heat loss is

calculated using the first law of thermodynamics based on the temperatures, flow rates, and compositions of the intake and exhaust gases and the engine net indicated power. Therefore, the engine heat loss here also includes the heat transfer in both the intake and exhaust manifolds of the engine. In contrast to the engine net power, the heat loss decreases as the diluent flow rate increases, that is, BPR and Phi decrease. This result is attributed to the fact that as the flow rate of the diluent increases, a drop in the in-cylinder temperature after combustion is observed, which reduces the overall engine heat loss. Meanwhile, it can be said that the value of heat loss is approximately twice the value of the engine net power. This result is due to three reasons. First, unlike normal engine operating conditions, this engine has a very high intake gas temperature, resulting in relatively large heat loss throughout the engine cycle. Second, the engine used in the experiments is a small single-cylinder engine, which also results in increased heat loss because of the high surface-to-volume ratio. Third, the engine load is maintained at low values ($IMEP_g \sim 2$ bar), which results in relatively large heat transfer amount as compared to that of power.[23, 40]

Therefore, the results of this section can be summarized as follows. First, the feasibility of an HCCI engine fuelled by SOFC anode off-gas was verified, as it was confirmed that stable HCCI engine operation is achieved under a Fuel rate of 10.0 kW, Util of 0.65, and CAD_{peak} of 372 CAD, even if the dilution level of the intake gas is very high. In addition, an increase in the dilution level, i.e., a decrease in BPR and Phi, increases the intake pressure and net power and decreases the peak temperature, heat loss, and NOx emissions. Therefore, it can be concluded that, in contrast to concerns that a high dilution level may disturb engine operation, choosing the lowest BPR and Phi under the conditions considered in this section helps to improve most of the HCCI engine performance aspects, although there is a problem regarding the increase in CO

emissions. Moreover, changes in BPR and Phi affect the intake and exhaust gas temperatures of the HCCI engine. The most important factor for determining the intake temperature is the specific heat ratio of the intake gas and that the most important factor for determining the exhaust temperature is the peak temperature.

3.3.2. Fuel utilization factor of SOFC variations

Table 3.5. Molar flow rates and lower heating value (LHV) of SOFC anode off-gas in section 3.3.2

Molar flow rate (mol/s)	Util 0.55	Util 0.6	Util 0.65	Util 0.7	Util 0.75	Util 0.8
H_2	0.0188	0.0167	0.0147	0.0126	0.0105	0.0084
CO	0.0035	0.0031	0.0027	0.0023	0.0019	0.0015
Fuel total	0.0223 (32%)	0.0198 (29%)	0.0174 (25%)	0.0149 (22%)	0.0124 (18%)	0.0099 (14%)
H_2O	0.0375	0.0396	0.0417	0.0437	0.0458	0.0479
CO_2	0.0092	0.0096	0.0100	0.0104	0.0108	0.0112
Diluent total	0.0467 (68%)	0.0492 (71%)	0.0517 (75%)	0.0541 (78%)	0.566 (82%)	0.0591 (86%)
LHV	45.4 kJ/mol	42.4 kJ/mol	39.0 kJ/mol	35.4 kJ/mol	31.2 kJ/mol	26.6 kJ/mol
Supplied energy[1]	5.54 kW	4.92 kW	4.31 kW	3.69 kW	3.08 kW	2.46 kW

[1] Supplied energy = LHV × Molar flow rate

In section 3.3.1, the flow rate of the fuel components (H_2 and CO) entering the HCCI engine was fixed by setting the Fuel rate and Util constant, and the flow rate of the diluent (H_2O, CO_2, and Air) was varied by varying BPR and Phi. In this section, engine experiments with varying Util values are performed to observe how the engine operation results change when the flow rate of the fuel as well as the diluent entering the HCCI engine change simultaneously. As mentioned earlier, Util determines the load distribution of the SOFC and HCCI engine. Because of this, understanding how the

HCCI engine operation changes when Util changes is very important. In this section, the experiments are performed while varying Util from 0.55 to 0.8 with a fixed Fuel rate of 10.0 kW, BPR of 0, and CAD_{peak} of 372 CAD. The compositions and flow rates of the SOFC anode off-gas under these conditions are shown in table 3.5. The table shows that as Util increases, the fuel flow rate of the SOFC anode off-gas decreases and the diluent flow rate increases, which may result in the engine load decreasing. Meanwhile, from the system efficiency point of view, it may be advantageous to operate under the condition of a high Util, which means that more system fuel is used in the SOFC, which generally has a higher efficiency than that of an engine. Therefore, in this section, the goal is to determine the upper range of Util within which the HCCI engine can operate.

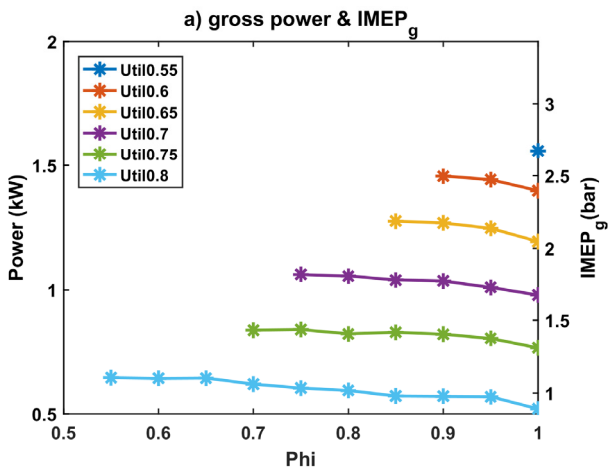

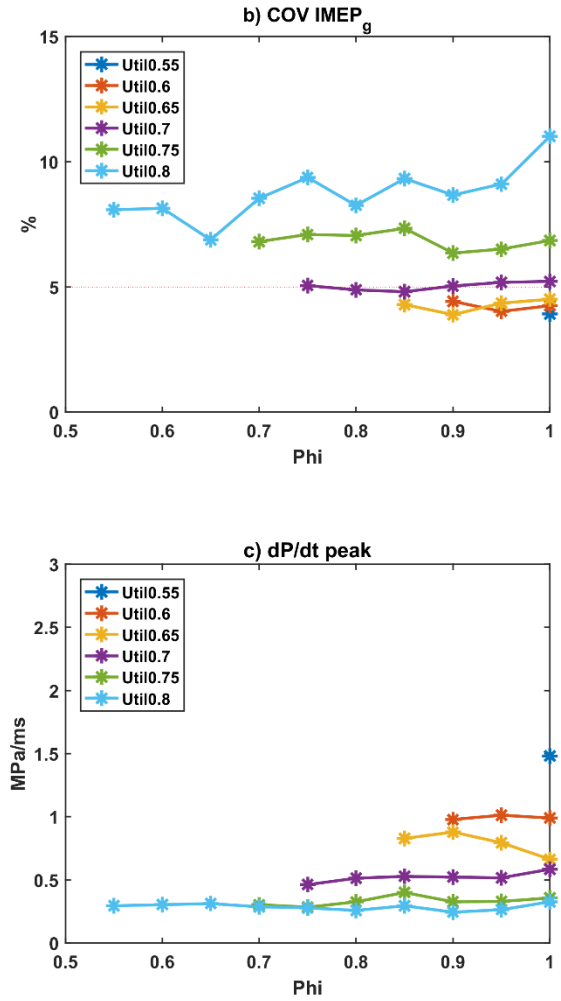

Figure 3.7. Stability of HCCI engine operation with Util/Phi variations: a) gross power and IMEP$_g$; b) COV IMEP$_g$; c) dP/dt peak

To verify that HCCI engine operation has occurred properly for each Util value, three parameters are analysed in figure 3.7. As shown in figure 3.7 a), the load of the engine decreases continuously as Util increases. Particularly, when Util is 0.8, IMEP$_g$, which indicates the engine load, is approximately 1 bar, which is very low. To determine whether the HCCI combustion is stable for each case, the values of the COV IMEP$_g$ are also calculated. As shown in figure 3.7 b), COV IMEP$_g$ increases remarkably with increasing Util. In particular, when Util is 0.75 ~ 0.8, COV IMEP$_g$ exceeds 5%, and

HCCI engine operation becomes unstable. Therefore, it can be seen that as Util increases, which causes the engine load to decrease and the dilution level to increase, the stability of the combustion degrades. However, it is unclear whether the cause of the combustion instability is the decreased engine load or the excessive dilution level. This will be discussed in greater detail in section 3.3.3 and in the discussion section. Meanwhile, as shown in figure 3.7 c), the value of the peak dP/dt increases as Util decreases because the engine load increases and because the dilution level of the intake gas decreases. However, even under the condition of Util equal to 0.55, the value of the peak dP/dt is still much less than 5 MPa/ms, which is the upper limit at which engine durability problems may occur. Therefore, in summary, as Util increases, the engine load decreases and the combustion stability is degraded, but the peak dP/dt decreases. Overall, stable HCCI combustion occurs at Util range of 0.55 ~ 0.7 under the conditions considered in this section, i.e., a Fuel rate of 10.0 kW, BPR of 0, and CAD_{peak} of 372 CAD.

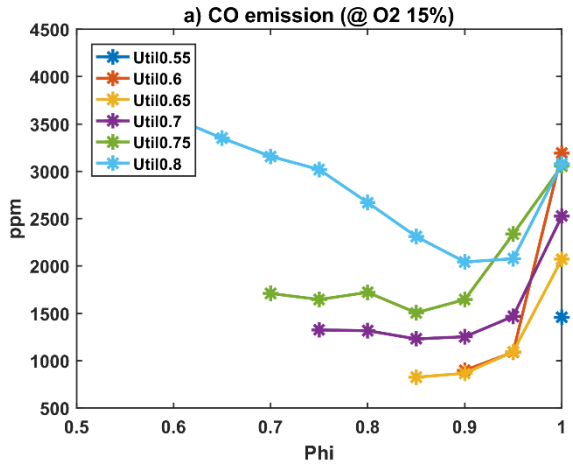
a) CO emission (@ O2 15%)
Util0.55
Util0.6
Util0.65
Util0.7
Util0.75
Util0.8
ppm
Phi
4500
4000
3500
3000
2500
2000
1500
1000
500
0.5
0.6
0.7
0.8
0.9
1

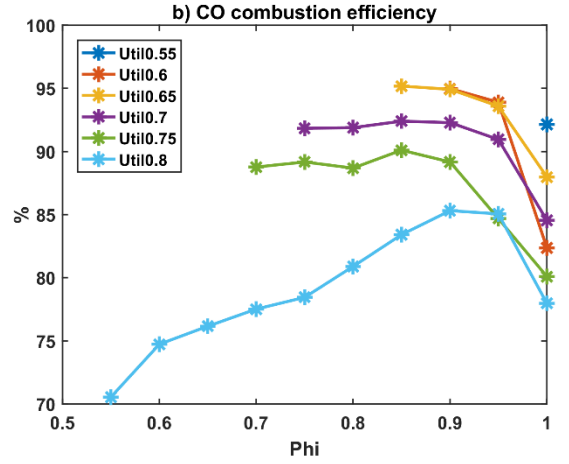
b) CO combustion efficiency
Util0.55
Util0.6
Util0.65
Util0.7
Util0.75
Util0.8
%
Phi
100
95
90
85
80
75
70
0.5
0.6
0.7
0.8
0.9
1

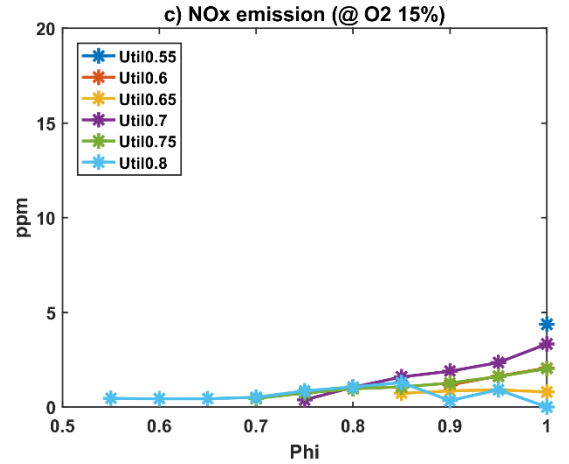
c) NOx emission (@ O2 15%)
Util0.55
Util0.6
Util0.65
Util0.7
Util0.75
Util0.8
ppm
Phi
20
15
10
5
0
0.5
0.6
0.7
0.8
0.9
1

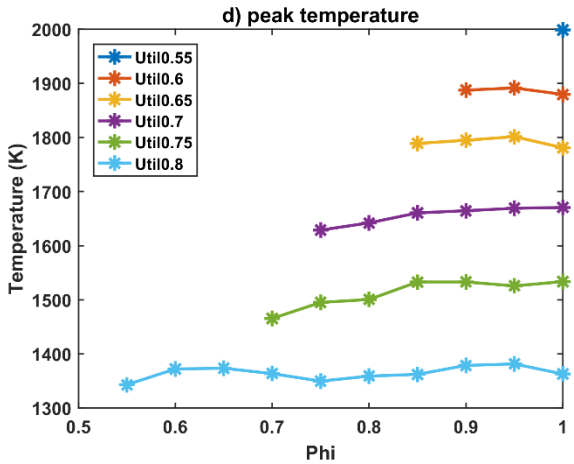

Figure 3.8. Pollutant emission characteristics of HCCI engine with Util/Phi variations: a) CO emissions; b) CO combustion efficiency; c) NOx emissions; d) peak temperature

Figure 3.8 shows the emission characteristics when varying Util. Figures 3.8 a) and b) show that as Util increases, CO emissions generally increase and the CO combustion efficiency decreases. It is experimentally confirmed that the CO combustion efficiency falls below 90% when Util is 0.75 or higher. Moreover, when Util is 0.8, the CO combustion efficiency is very bad, being as high as 70 to 80%. The cause of this phenomenon can be found by considering the trend characterizing the peak temperature. As shown in figure 3.8 d), when Util increases, the peak temperature decreases because the ratio of the fuel decreases and the ratio of the diluent increases. Particularly, when Util is 0.8, the peak temperature is lowered to approximately 1300 ~ 1400 K, which is an insufficient temperature for CO oxidation to occur.

Figure 3.8 c) shows the NO_x emissions. When Util decreases, the NOx emissions show a tendency to increase but not to greater than 5 ppm even for the condition wherein Util equals 0.55. This occurs because even if Util decreases, the dilution level still remains high because BPR is fixed at 0 in these experiments. Because of the large

amount of H_2O dilution caused by a BPR of 0, the peak temperature is not high, and the amount of NO_x emissions for HCCI engine operation fuelled by SOFC anode off-gas is negligible for most Util values.

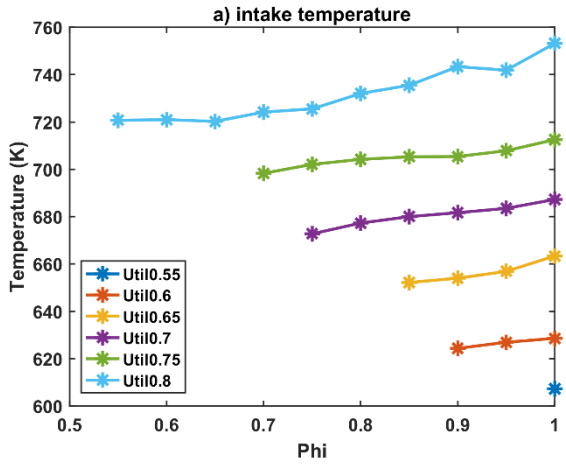

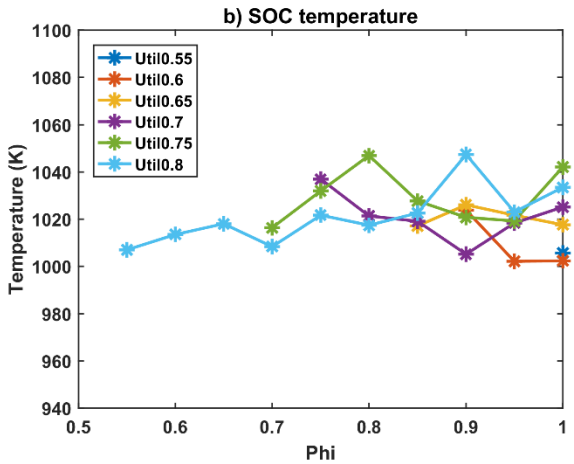

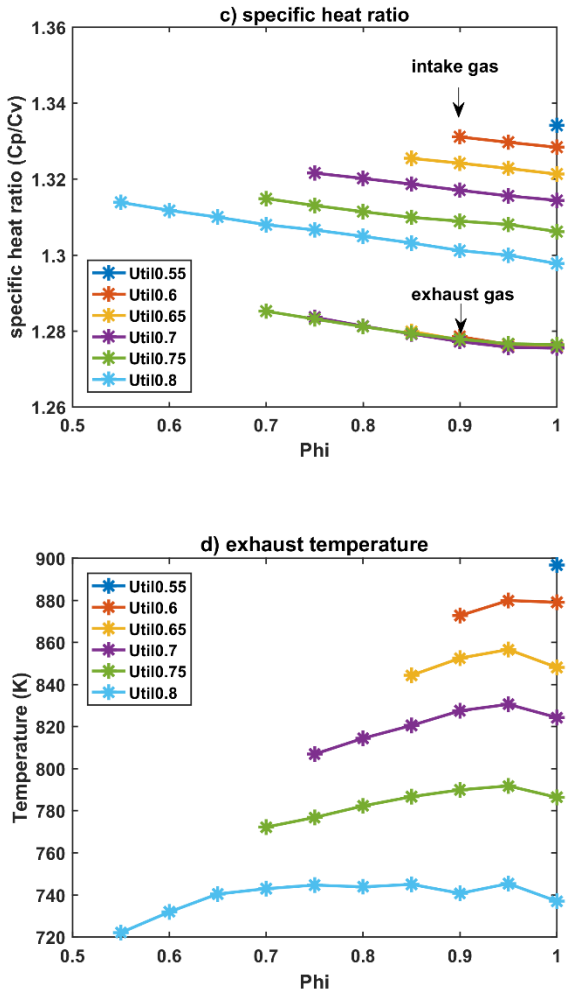

Figure 3.9. Intake and exhaust gas temperature characteristics of HCCI engine with Util/Phi variations: a) intake gas temperature; b) SOC temperature; c) specific heat ratio; d) exhaust temperature

Figure 3.9 shows how the intake and exhaust gas temperature of the HCCI engine change as Util changes. First, figure 3.9 a) shows the required intake gas temperature for HCCI combustion under each Util and Phi condition. It can be seen that as Util increases and Phi increases, the required intake gas temperature also increases. As mentioned in section 4.1, there are two possible parameters that affect the value of the required intake gas temperature: the SOC temperature and the specific heat ratio of the

engine intake gas. Figure 3.9 b) shows the SOC temperature for each condition. From the graph, it can be confirmed that changes in Util and Phi do not affect the SOC temperature significantly. On the other hand, as shown in figure 3.9 c), the trend characterizing the specific heat ratio of the engine intake gas is opposite to the trend characterizing the engine intake gas temperature. Therefore, again, it can be concluded that the specific heat ratio is an important parameter in the determination of the intake gas temperature.

Meanwhile, figure 3.9 d) shows the exhaust gas temperature. As shown in the graph, as Util increases, the exhaust gas temperature decreases. The trend of the exhaust gas temperature is very similar to that of the peak temperature shown in figure 3.8 d). Therefore, it can be confirmed again that the peak temperature is an important factor for determining the exhaust temperature.

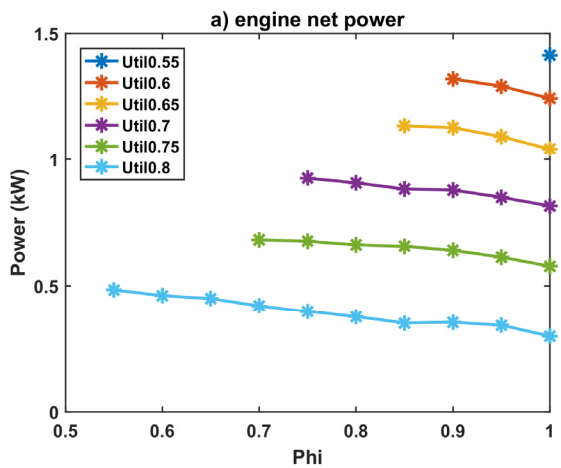

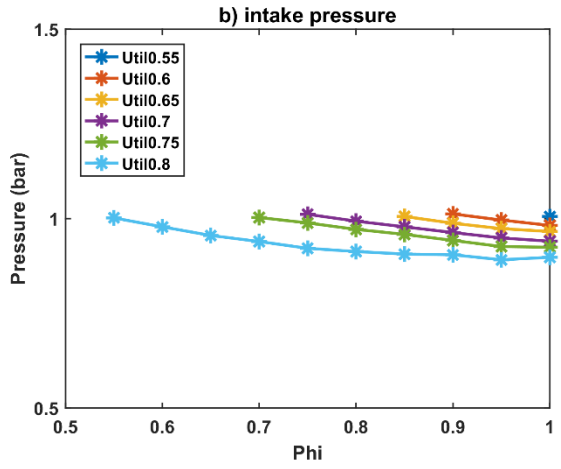

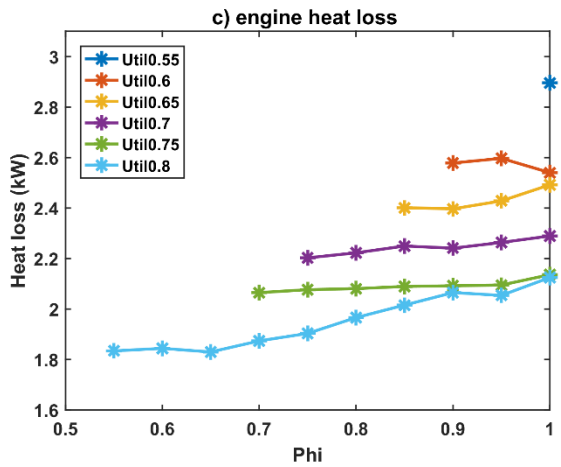

Figure 3.10. Energy transfer characteristics of HCCI engine with Util/Phi variations: a) engine net power; b) intake pressure; c) engine heat loss

Figure 3.10 shows the energy transfer characteristics of the HCCI engine. As shown in figures 3.10 a) and c), as Util increases, the engine net power decreases due to the decrease in fuel flow rate of the engine intake gas, and accordingly, the engine heat loss also decreases. However, the decrease in heat loss is smaller than the decrease in engine net power. Therefore, as Util increases, the ratio of heat loss to net power increases. Meanwhile, the decrease in net power with increasing Phi is not much different from the decrease in gross power. This is because the engine intake pressure does not

decrease as much as Phi increases, as shown in figure 3.10 b).

The results of this section can be summarized as follows. First, when the value of Util increases, engine load decreases and the stability of HCCI engine operation decreases. More specifically, when Util equal to 0.75 or more, it is confirmed that the HCCI combustion becomes unstable under the given conditions of this section. In addition, when Util increases, the CO emission is increased, which causes the CO combustion efficiency to worsen, and the efficiency of the engine is decreased. It is also confirmed that when Util is changed within a given range, only a negligible amount of NO_x of less than ~ 5 ppm is emitted. Overall, increasing Util yields poor HCCI engine performance regarding most aspects. Therefore, operating an HCCI engine with a high Util value is not appropriate from the HCCI engine operation point of view. However, as mentioned earlier, increasing Util may be advantageous from the system efficiency point of view, as an SOFC is generally more efficient than an HCCI engine. Therefore, there is a trade-off relationship, and it is necessary to identify the optimal operating point from not only the HCCI engine operation but also the overall system aspect. This optimal value of Util, from the overall system operation point of view, is analysed in chapter 5.

3.3.3. Fuelling rate variations

In this section, experimental results obtained for fixed Util, BPR, Phi and CAD_{peak} values and different Fuel rate are presented. These experiments were performed with two purposes. First, we investigate the independent effect of engine load on HCCI engine operation, while keeping the fuel and dilution level of the engine intake gas at fixed values, unlike the cases in sections 4.1 and 4.2. Second, these conditions of the experiments can actually be observed when the hybrid system changes the power

generating load from the design point to partial load or overload. Therefore, we attempt to determine how the HCCI engine operates under this type of load variation. Specifically, the experimental condition of this section is as follows. Util is fixed at 0.7, BPR is fixed at 0, Phi is fixed at 0.9, and CAD_{peak} is fixed at 372 CAD, and the Fuel rate is varied from 60% to 120% of 10.0 kW.

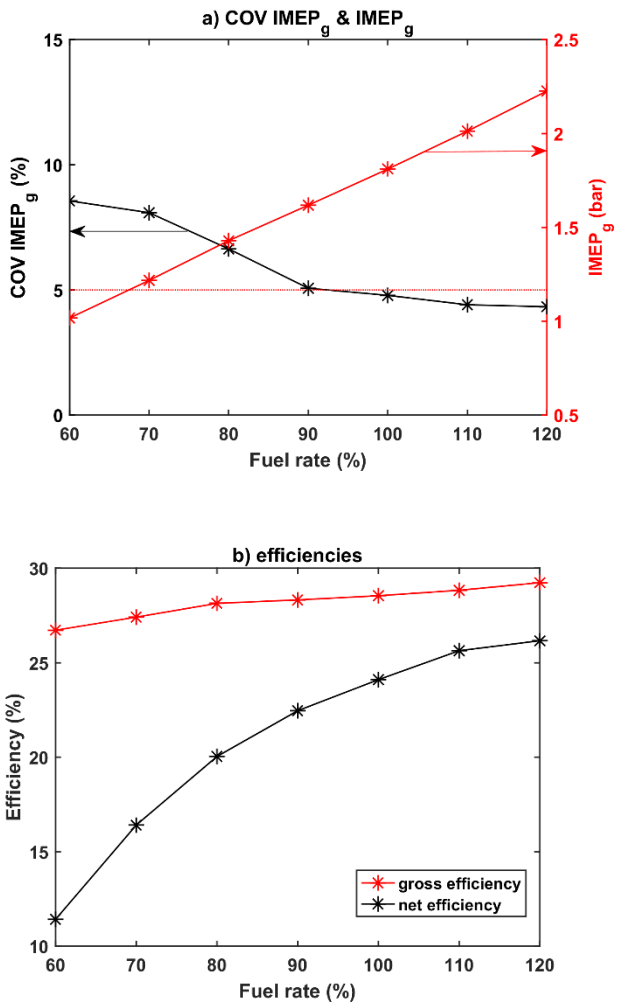

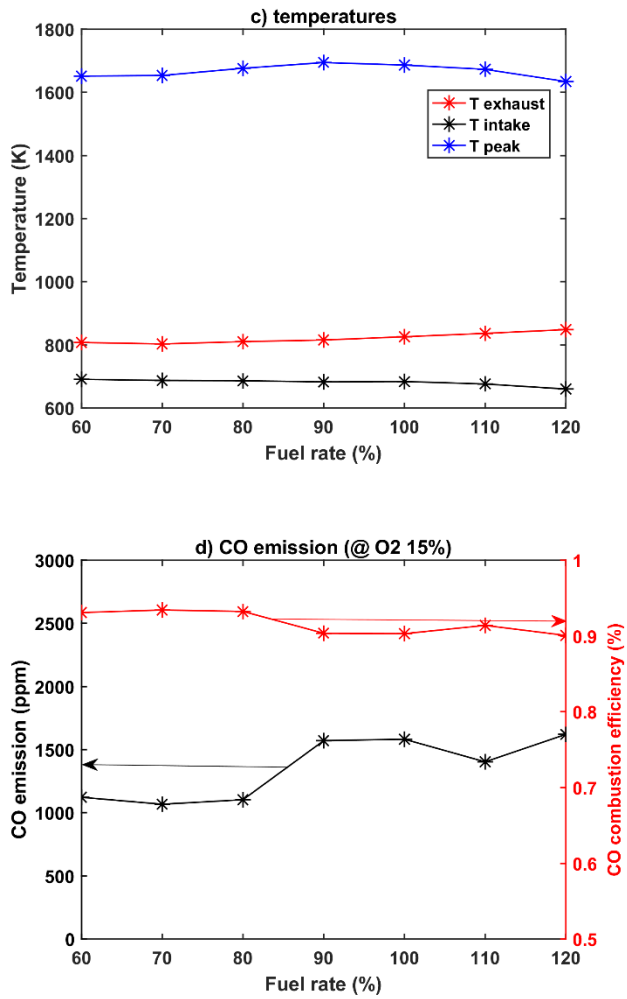

Figure 3.11. HCCI engine operation results with Fuel rate variations: a) COV IMEP$_g$ and IMEP$_g$; b) efficiencies; c) temperatures; d) CO emission (@ O_2 15%)

Figure 3.11 a) shows that the HCCI engine operation becomes markedly unstable when the Fuel rate and the consequent engine load are reduced. In figure 3.7 b) of section 3.3.2, it was seen that the COV IMEP$_g$ value increases as Util increases, but it was difficult to identify whether the exact cause of the increase in COV IMEP$_g$ was the increase in dilution level or the decrease in engine load. However, the results in figure 3.11 a) clearly show that combustion stability has a significant relationship with engine

load. Apart from this, it is also necessary to check whether the dilution level affects the combustion stability or not, which will be presented in the discussion section.

Figure 3.11 b) shows that the gross and net efficiencies decrease as the Fuel rate decreases. The reason for the decrease in gross efficiency is the increase in the amount of heat loss per unit amount of the in-cylinder gas. According to Woschni's correlation, the total amount of heat transferred to the engine wall is proportional to the (in-cylinder pressure)$^{0.8}$.[23, 41] On the other hand, the total flow rate of the engine intake gas is proportional to the in-cylinder pressure in the case of fixed engine rpm. Therefore, the amount of heat transfer per unit amount of in-cylinder gas is proportional to (in-cylinder pressure)$^{-0.2}$. Because of this, for the experimental conditions of this section, as the Fuel rate decreases, the flow rate of the engine intake gas decreases, that is, the in-cylinder pressure decreases; thus, the amount of heat transfer per unit amount of in-cylinder gas increases. For reference, the in-cylinder temperature, which also influences on the amount of heat transfer, changes insignificantly when the Fuel rate changes.

In addition, the rate of decrease of the net efficiency due to the decrease in the Fuel rate is larger than the rate of decrease of the gross efficiency. This occurs mainly because when the flow rate is decreased at a given engine rpm, the intake pressure is decreased, and the pumping loss is increased. Additionally, figure 3.11 c) shows that as the Fuel rate decreases, the intake temperature increases, and the exhaust temperature decreases. As mentioned above, because more heat is lost during the engine operation as the Fuel rate decreases, the intake temperature required to achieve HCCI combustion increases, while the exhaust temperature decreases. It can also be seen in figure 3.11 c) that the peak temperature does not change significantly even if the Fuel rate is changed. Therefore, the CO emissions and the CO combustion efficiency also do not change significantly, as shown in figure 3.11 d).

To summarize the results of this section, if the Fuel rate decreases while the other parameters remain constant, the engine load decreases and COV $IMEP_g$ increases, resulting in unstable HCCI combustion. Therefore, the engine load was recognized as one of the major factors that would affect COV $IMEP_g$ of such an HCCI engine in the hybrid system. Additionally, because the amount of heat loss per unit flow rate of the in-cylinder gas increases as the Fuel rate decreases, the efficiency also decreases. Overall, a reduction in the Fuel rate while maintaining other control parameters as constant is not good for engine performance. Therefore, this type of problem should be considered, especially when the system switches to partial load operation.

3.3.4. Combustion timing variations

In sections 3.3.1 ~ 3.3.3, the experiment was performed with a fixed combustion timing. In this section, the experimental results for various combustion timings and fixed values of the other control parameters are presented. It was noted from the experimental results in sections 3.3.1 ~ 3.3.3, that although HCCI engine operation fuelled by SOFC anode off-gas was found to be feasible, there could be three major issues that might arise: COV $IMEP_g$, CO emissions, and heat transfer. In this section, the experiments are performed under certain conditions (a Fuel rate of 10.0 kW, Util of 0.75, BPR of 0, and Phi of 0.9), which can reveal these issues, to investigate whether changing the combustion timing can solve some of these problems.

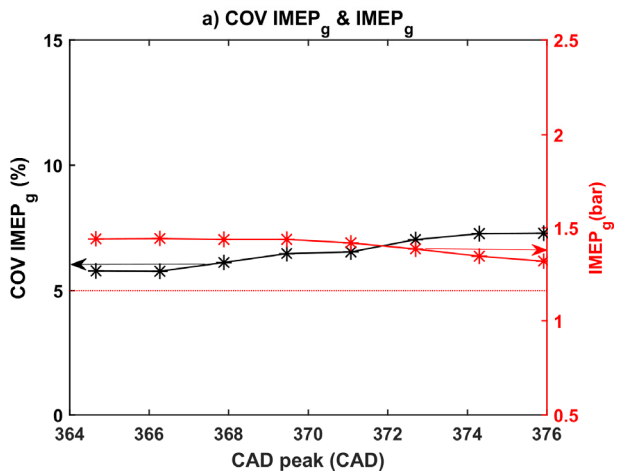

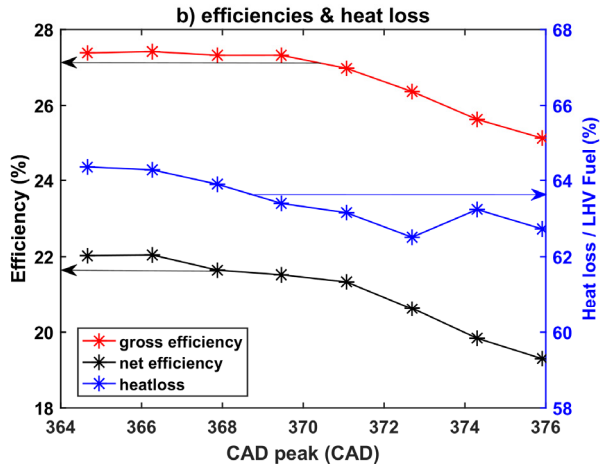
b) efficiencies & heat loss
Efficiency (%)
Heat loss / LHV Fuel (%)
CAD peak (CAD)
gross efficiency
net efficiency
heatloss

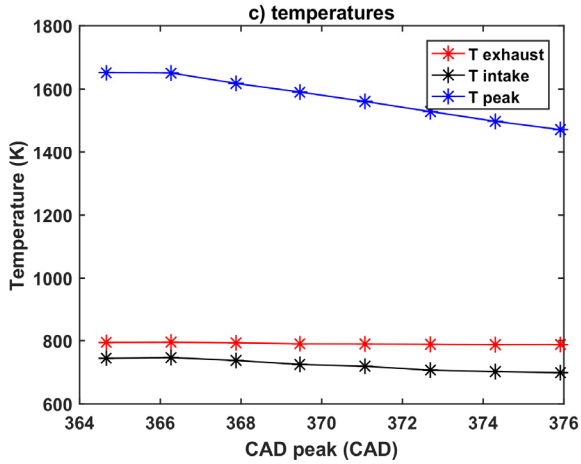
c) temperatures
Temperature (K)
CAD peak (CAD)
T exhaust
T intake
T peak

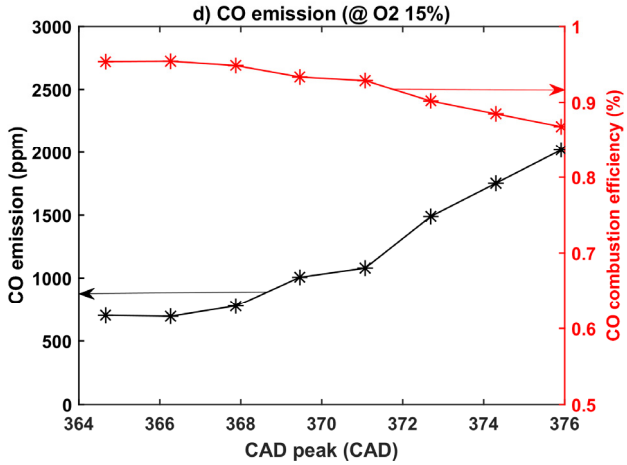
d) CO emission (@ O2 15%)
CO emission (ppm)
CO combustion efficiency (%)
CAD peak (CAD)

Figure 3.12. HCCI engine operation results with combustion timing variations: a) COV $IMEP_g$ and $IMEP_g$; b) efficiencies and heat loss; c) temperatures; d) CO emission (@ O_2 15%)

The experiment was performed while advancing the combustion timing from a CAD_{peak} of 376 CAD to 364 CAD. In a given operating condition, when the combustion timing was retarded to values later than a CAD_{peak} of 376 CAD by lowering the engine intake temperature, misfire was observed.

Figure 3.12 a) first shows the load and stability of the engine operation. The graph shows that as the combustion timing advances, the engine load, i.e., $IMEP_g$, increases slightly, and the stability of engine operation, i.e., COV $IMEP_g$, improves accordingly. Despite the flow rate and composition of the engine intake gas not changing at all, the engine load was increased due to increased efficiency. Figure 3.12 b) shows that the gross efficiency increases as the combusting timing advances. This result is mainly attributed to two reasons. First, as the combustion timing advances, the timing of ignition advances, and the peak pressure and temperature also increase. Increased peak pressure is helpful for generating more power. Second, the increased peak temperature facilitates the oxidization of more CO and increases the CO combustion efficiency, as shown in figure 3.12 d). For these two reasons, as the combustion timing advances, $IMEP_g$ increases and, accordingly, COV $IMEP_g$ decreases. In particular, it was possible to reduce COV $IMEP_g$ to ~ 5% from ~ 7% and increase the CO combustion efficiency to ~ 95% from ~ 85% under the given condition of this section by advancing the combustion timing. Therefore, advancing the combustion timing can be considered as the method for operating an HCCI engine more stably when otherwise unstable, e.g., at such a high Util of 0.75 in the present experiment. However, advancing the combustion timing beyond CAD_{peak} equal to 364 CAD is not expected to improve the engine

performances significantly because the amount of heat loss also increases as the combustion timing advances. As the combustion timing advances the peak temperature increases, and accordingly, the amount of heat loss also increases. Because of this, the improvement in engine performances is barely improved for CAD_{peak} values of 364 ~ 368 CAD, as shown in figures 3.12 b) and d).

Meanwhile, figure 3.12 c) shows that when the combustion timing is advanced from CAD_{peak} 376 CAD to 364 CAD, the engine intake gas temperature is increased by approximately 50 to 60 K, but the engine exhaust gas temperature is almost unchanged. This is mainly because the amount of energy transfer, i.e., not only the engine power but also the engine heat loss, from the engine to its surroundings is increased. As the combustion timing advances, the amount of power produced by the HCCI engine increases, and simultaneously, the heat loss to the engine wall is partially increased due to the increase in peak temperature. Therefore, even though increasing the engine intake temperature, i.e., advancing the combustion timing, improves the engine performances to certain extent, more heat energy from the hybrid system is required, as well as heat loss of the engine is increased. Therefore, it is necessary to consider from the system point of view whether advancing the combustion timing is more advantageous for the whole system.

3.4. Discussion

In this chapter, the experimental results for an HCCI engine fuelled by SOFC anode off-gas with varying control parameter values were analysed. Overall, it was confirmed that HCCI combustion can occur even with a very high dilution level and very low fuel flow rate, covering a large portion of the possible anode off-gas of SOFC in the hybrid system.

However, a relatively high engine intake gas temperature was required to achieve such HCCI combustion. In the results section, it was mentioned that the most important factor determining the required intake gas temperature is the specific heat ratio of the intake gas. To confirm this more clearly, all the experimental results presented in the results section are shown in figure 3.13 a). Although not introduced in the results section, the experimental results obtained by performing the same experiment as in section 3.3.1 for Util equal to 0.7 instead of Util equal to 0.65 are also shown in this graph. Therefore, each point in this graph represents one of 113 experimental conditions. The graph clearly shows that the required intake gas temperature and the specific heat ratio of the engine intake gas are inversely proportional. Therefore, it can be concluded that the specific heat ratio is the most important factor determining the required intake gas temperature. Meanwhile, it was mentioned in the results section that the exhaust gas temperature is most strongly influenced by the peak temperature. Similar to the intake gas temperature, the exhaust gas temperatures under all experimental conditions are shown in figure 3.13 b) together with the peak temperatures. As shown in the graph, the exhaust gas temperature is significantly influenced by the peak temperature. Meanwhile, the peak temperature is strongly influenced by the mole fraction of the fuel components (H_2 and CO) of the engine intake gas, as shown in figure 3.13 c). Therefore, it can also be concluded that the exhaust gas temperature is most strongly influenced by the mole fraction of the fuel components or the dilution level of the engine intake gas.

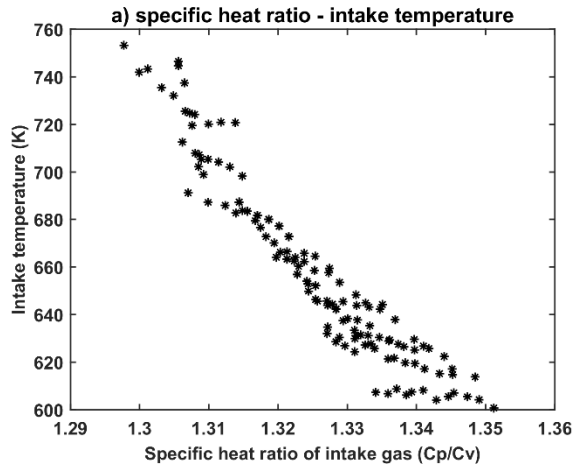
a) specific heat ratio - intake temperature
Intake temperature (K)
760
740
720
700
680
660
640
620
600
1.29
1.3
1.31
1.32
1.33
1.34
1.35
1.36
Specific heat ratio of intake gas (Cp/Cv)

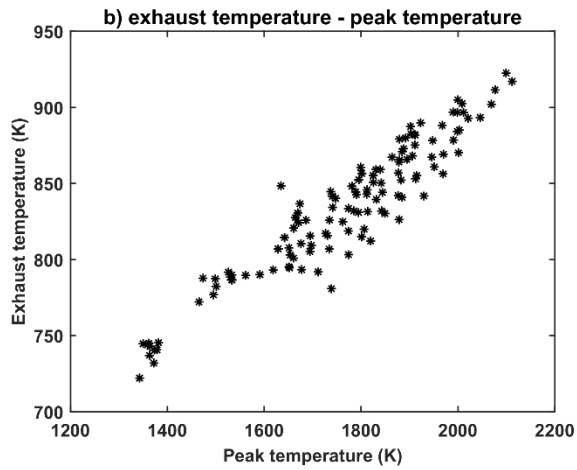
b) exhaust temperature - peak temperature
Exhaust temperature (K)
950
900
850
800
750
700
1200
1400
1600
1800
2000
2200
Peak temperature (K)

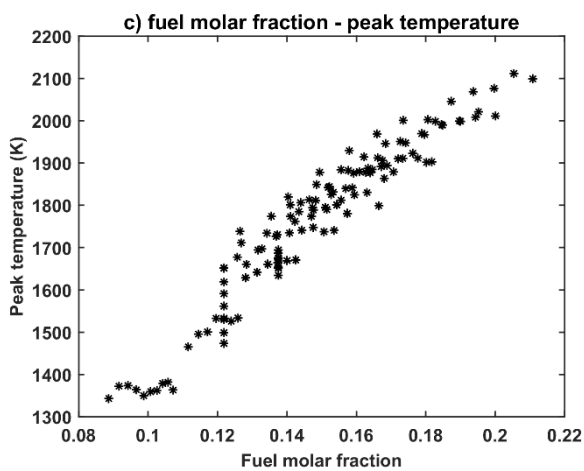
c) fuel molar fraction - peak temperature
Peak temperature (K)
2200
2100
2000
1900
1800
1700
1600
1500
1400
1300
0.08
0.1
0.12
0.14
0.16
0.18
0.2
0.22
Fuel molar fraction

Figure 3. 13. Major factors determining the intake, exhaust and peak temperatures: a) specific heat ratio – intake temperature; b) exhaust temperature – peak temperature; c) fuel molar fraction – peak temperature

If a sufficient intake gas temperature was supplied, HCCI combustion occurred and the HCCI engine both produced a stable and meaningful power and emitted almost negligible NO_x under almost all conditions. However, it was also found that HCCI engine operation fuelled by SOFC anode off-gas suffered from the following two problems depending on the values of the control parameters.

The first problem is a large amount of CO emissions. The HCCI engine generally presents high CO emissions due to the low combustion temperature; this characteristic can also be seen when SOFC anode off-gas is used as the fuel of the HCCI engine. More specifically, it was shown in the results section that when the control parameter is varied, CO is emitted at rates ranging from 500 ppm to 3500 ppm at a 15% O_2 level. Considering that the CO emission is generally very small during SOFC operation, this result can be considered as a problem facing the SOFC–HCCI engine hybrid system.[42] In addition, since the CO emissions are unburned CO instead of CO emissions due to the incomplete combustion of the hydrocarbons, the combustion efficiency becomes worse when the CO emissions are large. Therefore, it is essential to analyse the CO emissions and improve the emission characteristics so that the SOFC–HCCI engine hybrid system can be regarded as an environmentally friendly power generation device.

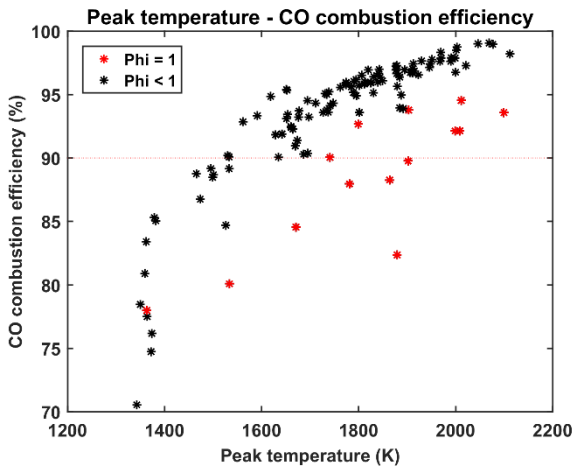

Figure 3. 14. Peak temperature – CO combustion efficiency

In the results section (section 3.3), it was estimated that there is a significant correlation between the CO emission and peak temperature results. Figure 3.14 shows a plot of peak temperature versus CO combustion efficiency for all 113 operating points. The graph shows a significant inverse trend between peak temperature and CO combustion efficiency. Particularly, except for the operating points at which Phi is equal to 1, which are marked in red, the CO combustion efficiency clearly drops with a certain trend when the peak temperature decreases. There are two reasons for this result. First, the rate constant of the CO oxidation reaction is proportional to the exponential of the temperature.[43] Therefore, it can be considered that the CO combustion efficiency is very sensitive to changes in temperature. Second, a lower peak temperature results in a greater quenching effect of the engine cylinder wall. In the paper of Aceves, it was found that when HCCI combustion occurs, the temperature inside the cylinder is decreased in the boundary layer near the wall due to the quenching effect of the wall, and the main unburned fuel emissions occur in the zone where the temperature of the zone is insufficient.[44] Likewise, if the peak temperature is lowered, the size of the zone with an insufficient temperature to cause CO emission in the boundary layer increases, which

may lead to an increase in unburned CO emissions.

Therefore, to reduce the CO emission and increase the combustion efficiency, it is necessary to control the dilution level by choosing proper values of the control parameters so that the peak temperature, as a representative indicator, is not too low. Additionally, at Phi equal to 1, the emission of CO becomes very high; thus, Phi would better be adjusted to operate at a value of less than 1, to prevent significant CO emission. In addition, for CO emissions, which are generated even after this adjustment, an oxidation catalyst that cleans up the CO can be added downstream of the engine. If the engine is operated when Phi is less than 1, sufficient amount of oxygen to react with unburned CO will remain in the exhaust gas. Therefore, it can be relatively easy to clean up all the pollutant emissions of the HCCI engine by adding a simple oxidation catalyst, as there is almost no NOx emission. In addition, the oxidation of this additional CO also has the advantage of increasing the temperature of the exhaust gas than otherwise, which in turn can increase the thermal energy that can be delivered to the system.

The second problem is the stability of combustion, which is indicated by COV $IMEP_g$. In the results section, it was found that COV $IMEP_g$ increases when the dilution level of the engine intake gas increases or the engine load decreases. However, the parameter that most strongly affects the stability of combustion was not identified clearly. For this, all the results of the 113 operating points are shown in Figure 3.15.

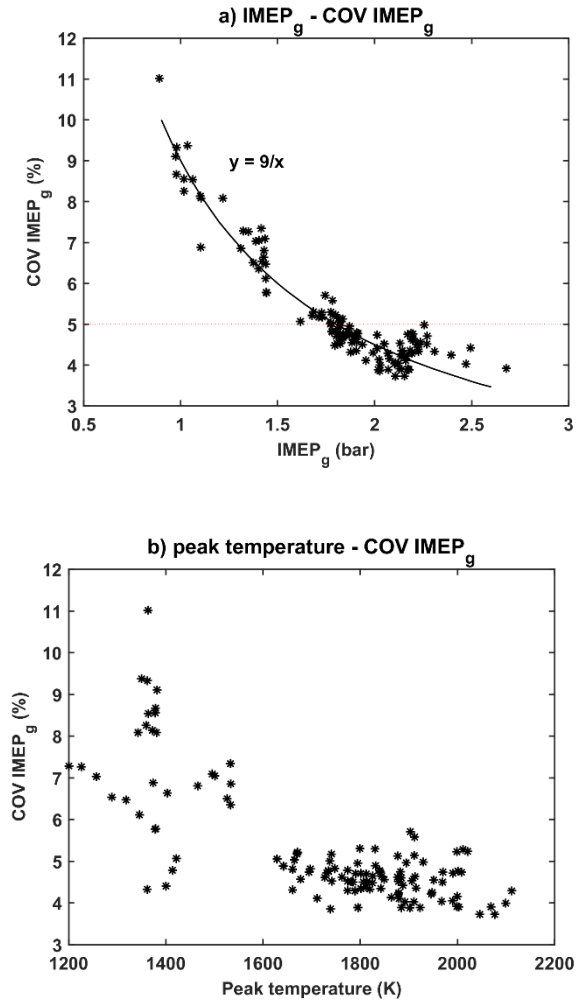

Figure 3.15. a) IMEP$_g$ – COV IMEP$_g$; b) peak temperature – COV IMEP$_g$

Figure 3.15 a) shows the significant inverse relationship between IMEP$_g$ (which indicates the engine load) and COV IMEP$_g$. It is not clear whether the engine combustion stability has a strong relationship with the peak temperature, as shown in figure 3.15 b). Therefore, it can be said that the decrease in engine load, rather than the decrease in peak temperature or the increase in the dilution level, has more influence on the decrease of combustion stability. In addition, all the experimental results shown in Figure 3.15 a) agree very well with the following trend equation.

$$\text{COV IMEP}_g\ (\%) = \frac{9}{\text{IMEP}_g\ (\text{bar})} \quad (3.2)$$

Considering that COV $IMEP_g$ is, by definition, "variance / $IMEP_g$", this result shows that the variance is almost constant even if $IMEP_g$ changes. Specifically, even if various engine control parameters change, there exists a certain variance for $IMEP_g$.

In summary, this analysis shows that for stable operation, an engine should not be operated at especially low loads. Particularly, if a COV $IMEP_g$ of less than 5% is set as the upper limit of stable operation, an approximate $IMEP_g$ value of roughly 1.8 bar becomes the low load limit of HCCI engine operation fuelled by SOFC anode off-gas at the given engine specifications.

3.5. Conclusions

In this chapter, HCCI engine operation fuelled by SOFC anode off-gas was experimentally investigated. The experimental results showed that, in general, HCCI engine operation can yield significant power production (w/ 25-30% gross indicated efficiency) while producing significantly fewer NOx emissions (<5 ppm @ O_2 15%) via a stable HCCI combustion (<5% COV $IMEP_g$). Considering that the experiment was performed using a small single-cylinder engine, these experimental results show that the HCCI engine has the potential to be used as the bottoming cycle of the SOFC in an SOFC hybrid system.

HCCI engine experiments were performed for different control parameter values. HCCI combustion occurred under all 113 experimental conditions. Even for some cases in which the dilution level of the engine intake gas was very high or the fuel flow rate of the engine intake gas was very low, it was confirmed that HCCI combustion occurred. However, a sufficient engine intake gas temperature was required to cause such combustion, and it was found that approximately 600 ~ 750 K was required for the engine (with a compression ratio of 8.2) used in the experiments. The most important factor determining the required intake temperature for combustion was found to be the specific heat ratio of the engine intake gas. Moreover, the most dominant factor in determining the engine exhaust gas temperature, which was an important factor affecting the external reforming rate in the hybrid system, was the peak temperature of the in-cylinder gas in an engine cycle. In addition, it was found that the major factor determining the peak temperature was the ratio of diluent in the engine intake gas.

The ranges of control parameters for proper HCCI engine operation were also analysed. Experiments in which the Fuel rate was 10.0 kW, Util was 0.65 and CAD_{peak} was 372 CAD showed that HCCI engine operation was performed successfully even

when BPR was 0, i.e., when no steam was removed from the SOFC anode off-gas. However, when Phi was close to 1, the CO emissions suddenly increased, causing a problem. On the other hand, it was confirmed that HCCI engine operation was generally successful when Phi was less than 1. In addition, if Util was increased to 0.75 or more under the given conditions (Fuel rate: 10.0 kW, BPR: 0, and CAD_{peak}: 372 CAD), the COV $IMEP_g$ exceeded 5%, which means that the combustion became unstable, and the CO emission efficiency became less than 90%.

Some experimental conditions cause high CO emissions and high COV $IMEP_g$. These two problems can be regarded as major problems facing HCCI engine operation fuelled by SOFC anode off-gas. Based on the experimental results, it was found that the most dominant effect on the CO emission was the peak temperature of the engine in-cylinder gas. Therefore, to reduce CO emissions, it is necessary to control the peak temperature by controlling the amount of diluent in the engine intake gas. Moreover, the experimental results corresponding to COV $IMEP_g$ fit very well with the trend line expressed as $\mathrm{COV\ IMEP_g(\%)} = \frac{9}{\mathrm{IMEP_g(bar)}}$, that is, COV $IMEP_g$ was found to be mainly determined by the engine load. Therefore, to improve the stability of the HCCI engine operation, the engine load should be maintained to some extent. More specifically, it was found that $IMEP_g$, which indicates the engine load, should be kept above 1.8 bar to keep the values of COV $IMEP_g$ below 5%.

Chapter 4
Operation characteristics of the SOFC under the hybrid system and design point performance of the hybrid system

4.1. Introduction

In chapter 3, the first experimental study of an HCCI engine fuelled by SOFC anode off-gas was conducted. The significance of chapter 3 can be summarized as follows. First, chapter 3 proved the feasibility of HCCI engine operation fuelled by SOFC anode off-gas through an experimental demonstration. Second, chapter 3 showed experimentally how the HCCI engine operation changes when various system control parameters change and analysed the causes of those results. Third, based on those experimental results, the proper ranges of control parameter values for successful HCCI engine operation were determined.

However, in chapter 3, the HCCI engine was analysed independently from the hybrid system; thus, there was a limitation in assessing the operation of the entire system. Therefore, in the next step of the system demonstration, it is necessary to investigate the influence of the HCCI engine operation on a system including the SOFC and to assess the operation results of the entire system.

Therefore, this chapter attempts to analyse the operation of the entire SOFC–HCCI engine hybrid system. The objectives of this chapter can be summarized into three goals. The first objective is to analyse how the combined operation with the HCCI engine affects the SOFC, external reformer, and other system components in the hybrid system. Specifically, whether the SOFC can be operated successfully in the hybrid system with the HCCI engine is determined. The second objective is to analyse how the SOFC–

HCCI engine hybrid system operation changes when various control parameter values change and to determine the causes of the system operation results. The third objective is to investigate the ranges of the control parameters that enable successful operation of the SOFC–HCCI engine hybrid system and to determine the design point of operation based on the analysis.

In this chapter, to accomplish these goals, the HCCI engine of the hybrid system is analysed through experiments, the other components are analysed through simulations, and the overall system operation is assessed by combining the results of the experiments and simulations. There is no well-known simulation model for an HCCI engine operated with SOFC anode off-gas, which is a new part of the SOFC system. Therefore, the analysis of the HCCI engine is performed experimentally to improve the accuracy of the analysis. It is noted that the experimental results described in chapter 3 are used for the experimental analysis of the HCCI engine in this chapter. On the other hand, simulation models are used for the other components, including the SOFC. For this purpose, the SOFC simulation model is constructed based on a well-known simulation model for direct internal reforming SOFC. This analysis method is effective for understanding the operation of a system before performing an experimental study on the entire system and in determining the control direction of each control parameter for successful system operation.

The main body of this chapter is organized as follows. In section 4.2 (Methodology), the simulation modelling methods for the system components, including the SOFC, and the experimental methods of the HCCI engine are described. In addition, a method for analysing the entire SOFC–HCCI engine hybrid system by combining the simulation and experimental results is described. In section 4.3 (Results), the operating characteristics of the SOFC under the SOFC–HCCI engine hybrid system are

determined. In addition, the operation of the SOFC–HCCI engine hybrid system when various control parameters are varied is analysed, and the design point of the system operation is determined based on these results. In section 4.4 (Discussion), based on the results of this chapter, a comprehensive evaluation of the HCCI engine as the bottoming cycle of the SOFC is presented.

4.2. Methodology

4.2.1. Outline of the methodology

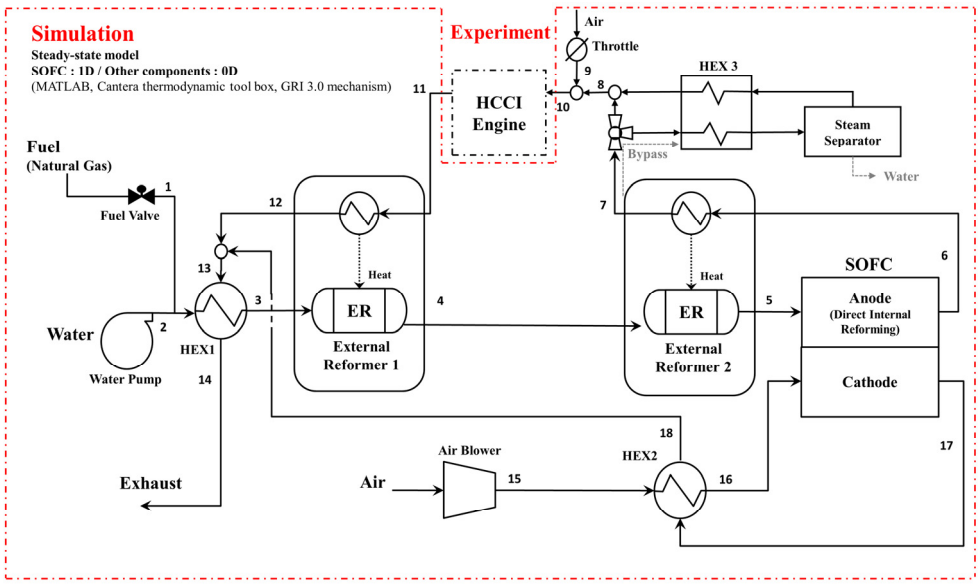

Figure 4.1. Methodology for system analysis

In this chapter, as shown in figure 4.1, the results of the system operation are derived by combining the experimental results of the HCCI engine and the simulation models of the remaining system components. The methods for deriving the system operation results are described in the following sections. In section 4.2.2, the simulation models of various system components, including the SOFC, are described. First, the modelling methodology of the SOFC is described, and the results of the validation with the SOFC experimental data are explained. Additionally, the method used to model external reformers, heat exchangers, a steam separator and a blower is explained. Section 4.2.3 explains how the simulation model and experimental results of the HCCI engine are combined and analysed to obtain the overall system operation results.

4.2.2. Simulation models

Steady-state simulation models were constructed for all system components, except for the HCCI engine. Specifically, a one-dimensional model was constructed for the SOFC to simulate the internal phenomenon in which the electrochemical reaction and the internal reforming reaction simultaneously affect each other. For the other system components, a zero-dimensional model was constructed to reduce the computational complexity. MATLAB, developed by Mathworks, was used to construct all simulation models. Additionally, the Cantera thermodynamic toolbox and the GRI 3.0 mechanism were used with MATLAB.[39, 45] By utilizing this software, the thermodynamic state and thermal conductivity of each stream in the system, as well as the thermodynamic equilibria and chemical reactions, are calculated.

4.2.2.1. Solid oxide fuel cell (SOFC)

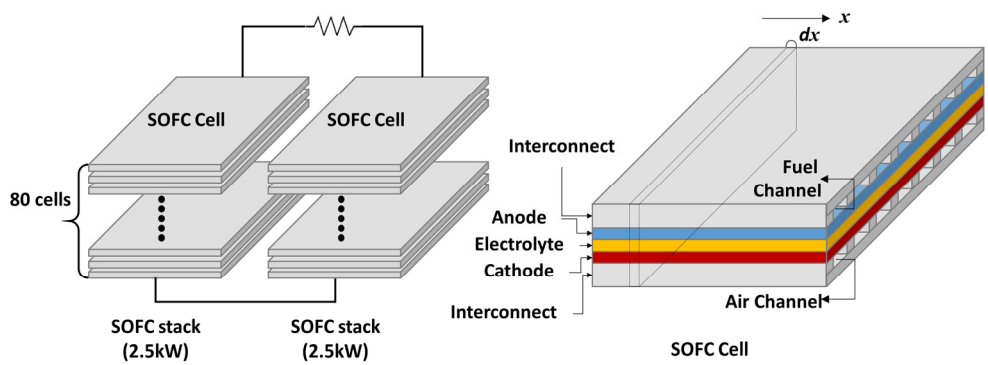

Figure 4.2. SOFC model description

Figure 4.2 shows how the SOFC is modelled. The SOFC model is written in a form that simulates the 5 kW SOFC of the MiCo corporation. First, the SOFC is composed of two 2.5 kW-class SOFC stacks that are connected in parallel; thus, the SOFC has a total nominal power of 5 kW. The SOFC stack consists of 80 cells that are connected in series. Each cell of the SOFC is modelled as an anode-supported planar type and

consists of anode, electrolyte, cathode, and interconnect. Additionally, the fuel channel is considered to be formed by the junction of the anode and the interconnect, and the air channel is formed by the junction of the cathode and the interconnect. It is assumed that the SOFC model is operated in co-flow, for which the directions of the fuel gas and air are the same. The flow direction is set as along the *x* direction.

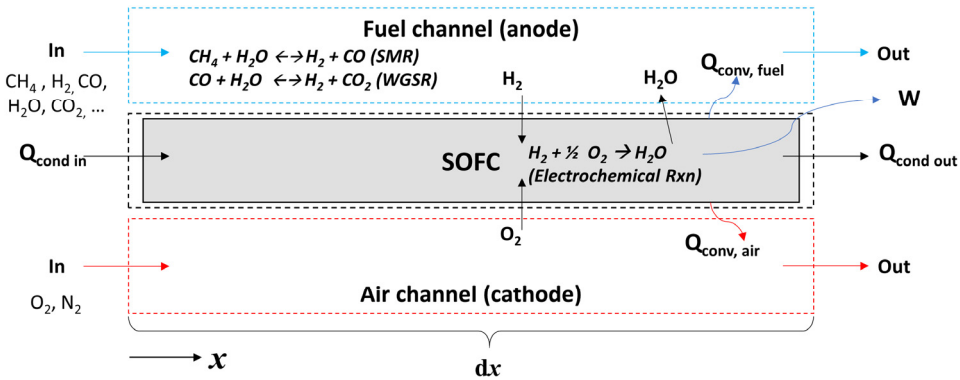

Figure 4.3. Control volumes of infinitesimal SOFC cells

To model each SOFC cell, the cell is divided along the *x* direction into infinitesimal SOFC cells. Each infinitesimal SOFC cell consists of three control volumes, as shown in figure 4.3. Each control volume is set as follows. First, the SOFC body part, consisting of the anode, cathode, and interconnects, is set as one control volume called the 'SOFC control volume', as shown in figure 4.3. Therefore, in this chapter, it is assumed that there is no temperature difference between the subcomponents, e.g., the anode and cathode, in the infinitesimal SOFC cell to simplify the calculation. Second, the control volume for the gas in the fuel channel is set as one control volume and called the 'fuel channel control volume'. Third, the control volume for the gas in the air channel is set as one control volume and called 'air channel control volume'.

A mass and energy conservation model is adopted for each control volume, and an electrochemical reaction model, an internal reforming reaction model, and a water-gas shift reaction model are considered together. For heat transfer, the conduction ($Q_{cond\ in}$

and $Q_{cond\ out}$) between the infinitesimal cell's SOFC body part and the convection ($Q_{conv,fuel}$ and $Q_{conv,air}$) between the SOFC body and the gases passing through the air and fuel channel are considered. It is assumed that there is no heat loss from the SOFC to the surroundings. The internal reforming reaction and the water-gas shift reaction are considered to occur in the fuel channel, and the electrochemical reaction is considered to occur in the SOFC control volume. The parameters used in the SOFC model and the key equations are summarized in tables 4.1 and 4.2. It is noted that the parameters related to the SOFC geometry are determined by referring to the data from MiCo and various publications on anode-supported intermediate-temperature SOFCs.[46-48] Additional details on the equations and parameters used in the SOFC model can be found in appendix C. Appendix C provides a detailed description of the SOFC model.

Table 4.1. Parameters of the SOFC model

Parameters of the SOFC geometry		
	Number of stacks	2 ea
	Number of cells (per stack)	80 ea
	Active cell area	110.25 cm^2
L	Side length of a cell	10.5 cm
d_{an}	Anode thickness	500 ㎛
d_{ca}	Cathode thickness	50 ㎛
d_{el}	Electrolyte thickness	20 ㎛
d_{int}	Interconnect thickness	500 ㎛
$d_{h,channel}$	Fuel and air channel height	1.5 mm
Parameters of the heat transfer characteristics		
	Thermal conductivity of SOFC cell	10 W/(m K)
	Nusselt number of fuel and air channel	3.09
Parameters of the activation loss		
γ_{an}	Pre-exponential coefficient for anode	1.5×10^{11} A/m^2
γ_{ca}	Pre-exponential coefficient for cathode	5×10^{9} A/m^2
$E_{act,an}$	Activation energy for anode	120 kJ/mol
$E_{act,ca}$	Activation energy for cathode	120 kJ/mol
Parameters of the concentration loss		
r	Pore diameter for anode and cathode	0.5 ㎛
ε_{an}	Porosity of anode	0.5
ε_{ca}	Porosity of cathode	0.3
τ	Tortuosity for anode and cathode	6

Table 4.2. Equations of the SOFC electrochemical model

Nernst equation

$$V_{nernst} = E_0 + \frac{RT}{n_e F} ln\left(\frac{(p_{an,H2}/p_{atm})(p_{ca,O2}/p_{atm})^{0.5}}{p_{an,H2O}/p_{atm}}\right)$$

Ohmic loss

$$V_{ohm} = R_{ohm} \times j$$

$$R_{ohm} = \sum \rho_{components} \times d_{components}$$

$$\rho_{components} = \rho_0 \times exp\left(-\frac{\Delta G_{act}}{RT}\right)$$

Activation loss

$$V_{act} = \frac{2RT}{n_e F} \sinh^{-1}\left(\frac{j}{2j_0}\right)$$

$$j_{0,an} = \gamma_{an} \times \left(\frac{p_{H_2}}{p_{atm}}\right) \times \left(\frac{p_{H_2O}}{p_{atm}}\right) \times exp\left(-\frac{E_{act,an}}{RT}\right)$$

$$j_{0,ca} = \gamma_{ca} \times \left(\frac{p_{O_2}}{p_{atm}}\right)^{0.25} \times exp\left(-\frac{E_{act,ca}}{RT}\right)$$

Concentration loss

$$V_{conc,an} = \frac{RT}{2F} ln\left[\frac{1 + \left(\frac{RT}{2F}\right)\left(\frac{d_{an}}{D_{an}^{eff} p_{an,H_2O}}\right)j}{1 - \left(\frac{RT}{2F}\right)\left(\frac{d_{an}}{D_{an}^{eff} p_{an,H_2}}\right)j}\right]$$

$$V_{conc,ca} = -\frac{RT}{4F} ln\left[\frac{\frac{p_{ca}}{\alpha_{O_2}} - \left(\frac{p_{ca}}{\alpha_{O_2}} - p_{ca,O_2}\right) exp\left(\left(\frac{RT}{4F}\right)\left(\frac{\alpha_{O_2} d_{ca}}{p_{ca} D_{ca}^{eff}}\right)j\right)}{p_{ca,O_2}}\right]$$

The model is validated with experimental results from MiCo's 5 kW SOFC. Validation is performed for three cases. In case 1, gas consisting of 50% H_2 and 50% N_2 is input into the anode of the SOFC. Case 1 attempts to determine whether the operation of the SOFC in the situation whereby direct internal reforming is not required is well validated. In cases 2 and 3, a partially reformed gas is input into the anode of the SOFC. In these two cases, direct internal reforming occurs inside the SOFC, and the goal is to determine whether the model accurately simulates the experimental results even in the presence of direct internal reforming. Two cases are validated to assess whether the model simulates the experimental results well even when the external reforming rate is different. The experimental conditions for the three cases are shown in table 4.3. For reference, the external reforming rate is defined as follows.

$$External\ reforming\ rate = \frac{(LHV\ of\ partially\ reformed\ gas - LHV\ of\ non-reformed\ gas)}{(LHV\ of\ fully\ reformed\ gas - LHV\ of\ non-reformed\ gas)} \quad (4.1)$$

Figure 4.4 compares the simulation results of the model with the experimental results for the three cases. Figure 4.4 shows that the simulation results and the experimental results are similar in all three cases. Therefore, through this validation, we confirm that the SOFC 1D model can reliably predict the operation of an SOFC in the range of the general operation conditions to be tested below.

Note that as this model doesn't reflect the heat transfer to the outside, the amount of heat loss caused by SOFC operation cannot be predicted. Constructing more accurate simulation model that reflect the heat loss remains as the future work of this dissertation.

Table 4.3. Validation conditions of the SOFC model

			Case 1	Case 2	Case 3
Pressure (bar)	Anode		1.05	1.02	1.03
	Cathode		1.04	1.06	1.04
Temperature (K)	Anode		730	712	715
	Cathode		739	731	725
Molar flow rate (mol/s)	Anode	H_2	0.0387	0.0268	0.0188
		CO	-	0.0024	0.0008
		H_2O	-	0.0183	0.0216
		CO_2	-	0.0049	0.0041
		CH_4	-	0.0028	0.0051
		N_2	0.0387	-	-
	Cathode	O_2	0.0450	0.0540	0.0450
		N_2	0.1692	0.2033	0.1692
External reforming rate			-	66.6	45.9

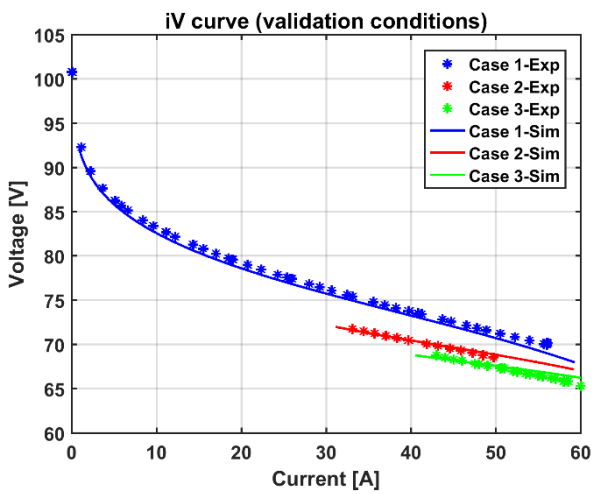

Figure 4.4. iV curve of the validation conditions

4.2.2.2. External reformers

There are two external reformers in the SOFC–HCCI engine hybrid system proposed in this dissertation. Both external reformers are heat exchanger types that receive heat from the gas entering the hot side of the external reformer and cause a reforming reaction on the cold side. The external reformers are modelled based on a simple counter-flow heat exchanger model that uses the heat exchange effectiveness to calculate the amount of heat transmitted to the cold side from the hot side. It is also assumed that the gas hourly space velocities of the external reformers are sufficiently small and that the reformers are filled with a sufficient amount of catalyst so that the reforming reaction can always be in equilibrium when heat exchange occurs. The specific formulas used in the model are as follows.

$$Q_{max,h} = H_{h,i} - H_{h,o@T_{c,i}}\ ,\ Q_{max,c} = H_{c,o@T_{h,i}} - H_{c,i}\ ,\ Q_{max} = min\left(Q_{max,h}, Q_{max,c}\right) \quad (4.2)$$

$$Q = Q_{max} \times \eta_{effectiveness} \quad (4.3)$$

First, the maximum amount of heat that can be transferred from the hot side to the cold side in the external reformers is calculated. In equation (4.2), $H_{h,i}$ denotes the inlet enthalpy of the hot-side gas, and $H_{h,o@T_{c,i}}$ denotes the enthalpy of the hot-side gas when the temperature of the hot-side gas becomes the inlet temperature of the cold-side gas. Because there is no reaction on the hot side of the external reformers, $H_{h,i} - H_{h,o@T_{c,i}}$ denotes the enthalpy change caused by only the temperature reduction. In contrast to the hot side of the external reformer, on the cold side, the reforming reaction occurs in addition to the temperature increase. Therefore, $H_{c,o@T_{h,i}}$ denotes the enthalpy of the cold-side gas when the temperature of the cold-side gas becomes the inlet temperature of the hot-side gas, and the reforming reaction of the cold-side gas reaches equilibrium. Finally, Q_{max}, the maximum amount of heat that can be

transferred to the cold side from the hot side, is set as the smaller of $Q_{max,h}$ and $Q_{max,c}$. As shown in equation (4.3), Q, the actual amount of heat transferred, is calculated from Q_{max} and the heat exchanger effectiveness ($\eta_{effectiveness}$).

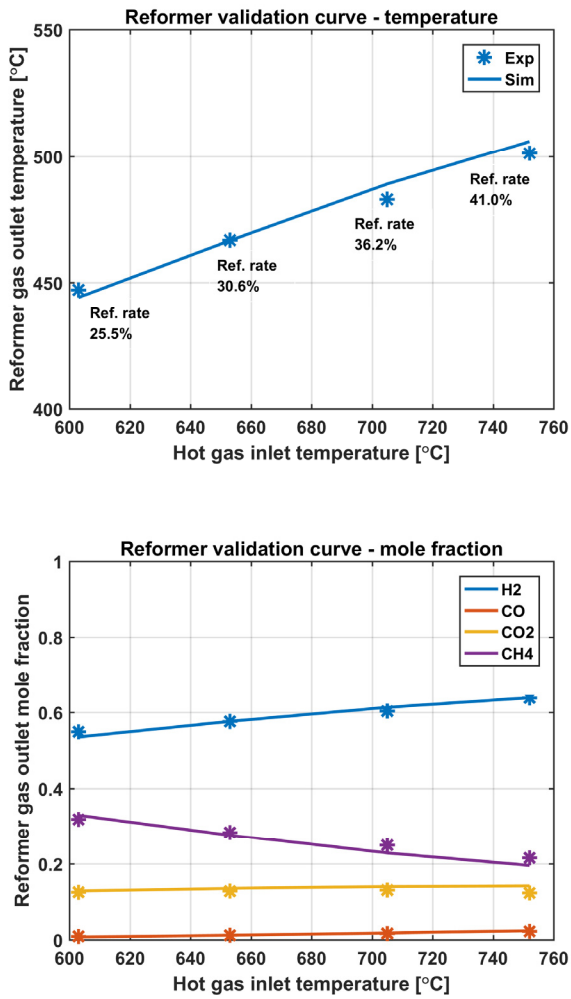

Figure 4. 5. Validation curve of the external reformer simulation model

Figure 4.5 shows the validation results of the external reformer simulation model. The experimented reformer was developed by Chungnam National University and it was experimented at Korea Institute of Machinery and Materials (KIMM).[49, 50] The temperatures of gases were measured by thermocouples located inside the reformer and the mole fractions were measured by a gas chromatography. Validation is performed

for four cases by varying the hot gas inlet temperature. As shown in the figure, although the simulation model of external reformer is relatively simple, the results of simulation are adequately validated with the experimental results for all cases. One of the major assumptions in the simulation model is that the reformer is large enough and is filled with enough amount of catalyst to make the equilibrium of reformer outlet gas. From the validation, it is confirmed that this assumption is pertinent. Note that as the simulation model doesn't reflect the heat loss to the outside, the model has limitation to calculate heat loss. For constructing more accurate simulation model, the heat loss model should be considered.

4.2.2.3. Other components

There are three heat exchangers (HEX1, HEX2, and HEX3) in the SOFC–HCCI engine hybrid system proposed in this dissertation. Each heat exchanger is considered to be a counter-flow heat exchanger. The heat exchanger model is constructed with a relatively simple model using the heat exchanger effectiveness. Equations (4.2) and (4.3) are also used to model heat exchangers, such as external reformers; however, the calculation of the equilibrium state is not necessary in the case of heat exchangers since no reactions occur in the heat exchangers.

For the steam separator, it is assumed that the steam is separated at 60 ℃; consequently, the steam in the inlet gas of the steam separator is liquefied, except for the amount corresponding to 0.1964 bar, which is the saturation pressure of steam at 60 ℃. In addition, it is assumed that the work of blowing the coolant (e.g., cooling water) in the steam separator is small and negligible.

A blower is used in the system to input air into the cathode side of the SOFC. The work used by the blower is calculated using equations (4.4) and (4.5). It is assumed that

the differential pressure on the cathode side is 3 kPa based on the SOFC experimental results.[51] The differential pressure is assumed to constant even if various control parameters are changed.

$$h_i - h_o = q - w = -w \quad (4.4)$$

$$w = \frac{h_{o,s} - h_i}{\eta_{blower}} \quad (4.5)$$

In addition to the above-mentioned system components, the system includes a water pump, a fuel valve and a throttle. For the water pump, it is assumed that the energy consumed is negligible because the working fluid (water) is a liquid; thus, not a large amount of energy is consumed in pumping. In addition, the SOFC–HCCI engine hybrid system in this dissertation operates at near atmospheric pressure; however, because the natural gas is usually supplied at several bars above atmospheric pressure, the amount of fuel supplied is controlled by the fuel valve. It is also assumed that the amount of energy used in controlling the fuel valve is negligible. Finally, the energy used to control the throttle for controlling the amount of air entrained in the HCCI engine is also assumed to be negligible.

4.2.3. System operation

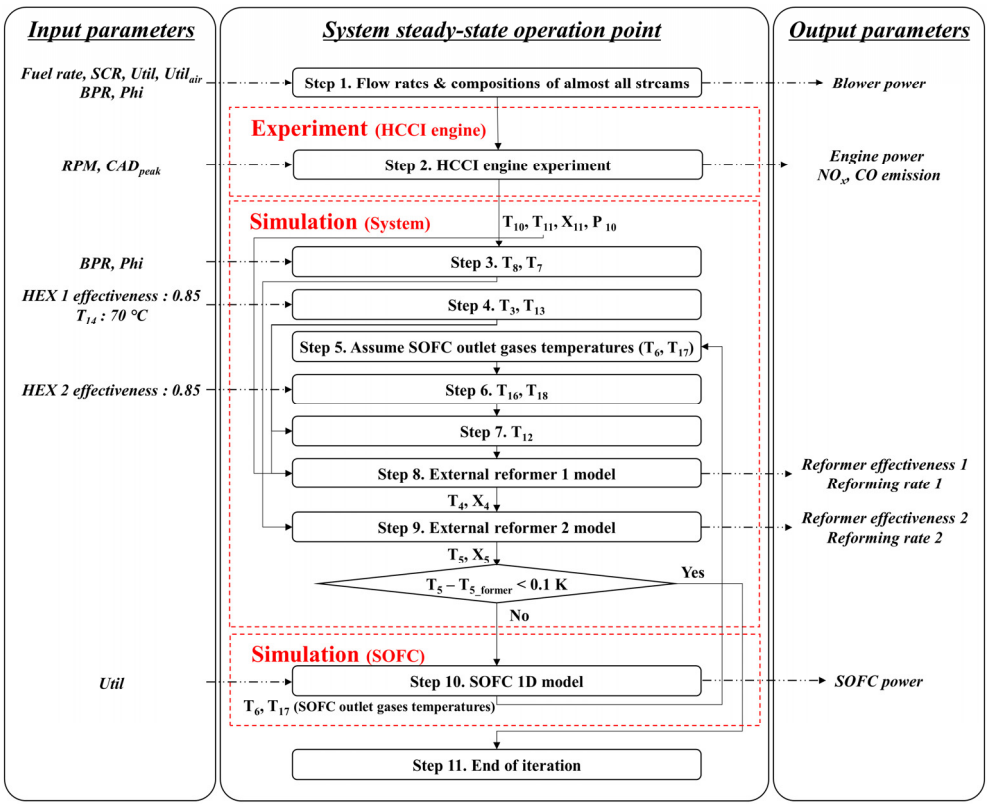

Figure 4.6. Algorithm for determining the steady-state operation point of the SOFC–HCCI engine hybrid system

Figure 4.5 shows the algorithm for deriving the system operation results when combining the experimental HCCI engine results and the system simulation model. The detailed processes of the algorithm are explained as follows. In the first step, the system operating conditions to be analysed are selected by determining the control parameters (Fuel rate, SCR, $Util_{air}$, Util, BPR, and Phi). Then, with two following assumptions, the mass flow rates of all the streams are determined. The compositions of almost all streams, except streams 4 through 5 and 11 through 14 (in figure 4.1), which require information about the external reforming rates and the unburned CO emissions of the engine exhaust gas, are determined. The first assumption is that the input gas is fully

reformed inside the SOFC; therefore, there is no CH_4 in the SOFC anode off-gas. According to the experiment results of the MiCo SOFC at the system operating range considered in this chapter, CH_4 is discharged to the downstream of the SOFC at approximately 0.00001 or less based on mole fraction. Therefore, it is confirmed that this is an appropriate assumption. The second assumption is that the composition of the anode off-gas is set to the equilibrium composition of the water-gas shift reaction at 750 ℃. In the system operating range used in this chapter, the temperature of the SOFC anode off-gas is approximately 700 ~ 900 ℃, and the equilibrium composition of the anode off-gas varies by approximately 0.02% or less within this temperature range. These changes do not have a significant effect on the HCCI engine operation; therefore, the system operation results do not vary greatly with this change. This assumption is included to prevent an increased number of iterations for a negligible improvement in accuracy.

After step 1, the information about the HCCI engine intake gas is transferred to the HCCI engine experiment part, i.e., step 2. In step 2, the gas with the determined flow rate and composition is emulated by the experimental equipment, and the HCCI engine is experimented upon with the emulated gas. RPM and CAD_{peak} are also determined for the engine experiment. As the results of the experiment, the engine performance (in terms of produced power and NO_x and CO emissions) is confirmed. Additionally, the engine intake and exhaust gas temperature, exhaust gas composition, and intake gas pressure, which are parameters used in the system simulation, are measured and transmitted to the system simulation model. For reference, it is possible to overcharge the engine over 1 atm in the HCCI engine experiment since the engine intake gas is supplied by the MFCs and water pump. However, during actual operation of the SOFC–HCCI engine hybrid system, engine operation is only possible at an intake pressure of

less than 1 atm because the air of the engine intake gas is entrained through the throttle. Therefore, only conditions with an intake pressure of less than 1 atm are analysed.

In the system simulation model, the temperatures of the stream before mixing with the air entrained through the throttle (stream 8) and the stream before bypassing to the steam separator (stream 7) are derived from the engine intake gas temperature, which is obtained from the engine experiment, and the flow rates of the entrained air and bypassed SOFC anode off-gas, which are calculated from BPR and Phi. It is assumed that the temperature of the air entering through the throttle is ambient temperature (25 °C). The temperature of stream 14, which is the exhaust gas of the system, is assumed to be 70 °C. The effectiveness of the heat exchangers (HEX 1, 2, and 3) is assumed to be 0.85. The thermodynamic states of streams 3 and 13 are calculated based on the effectiveness under the assumption that water and natural gas are also input into the system at ambient temperature (25°C). Then, we assume the temperatures of streams 6 and 17, which are SOFC outlet gases, as the initial value, e.g., 750 °C, and determine the temperatures of streams 16 and 18 using the effectiveness of HEX 2. Then, from the information of streams 13 and 18, the temperature of stream 12 is determined. The assumed values of the parameters are summarized in table 4.4.

Table 4.4. Assumed system parameters

Temperatures (°C)	
Ambient temperature (T_1, T_2, T_9, T_{15})	25
System exhaust temperature (T_{14})	70
Steam condensation temperature	60
System component design parameters	
HEX 1, 2, 3 effectiveness	0.85
Blower isentropic efficiency	0.88

Because the thermodynamic states of streams 11, 12 and 3 are determined from the above-mentioned calculations, the amount of heat to be exchanged between the cold side and the hot side in external reformer 1 can be calculated. Therefore, from equations (4.2) and (4.3), the effectiveness of external reformer 1 in delivering this amount of heat can also be calculated. Whenever the system operation condition is varied, the effectiveness of external reformers is inversely calculated in this way. This method cannot be regarded as the proper method for analysing the effects of the system control parameters on the system operation after the specifications of the external reformers are determined. However, one of the purposes of this chapter is to identify the most successful operating point of the system; therefore, it is assumed that for all the system operating conditions, the external reformers can be designed to transfer the most appropriate amount of heat. Therefore, based on these analyses, how the effectiveness of each external reformer should be designed for optimal operation is analysed. However, the effectiveness of the external reformers is limited to being no greater than 0.85, which is close to the maximum value of the heat exchanger effectiveness used in engineering practice.

Meanwhile, the thermodynamic state of stream 4 is calculated based on the amount

of heat exchanged in external reformer 1. External reforming rate 1 is calculated using equation (4.1) based on the thermodynamic state of stream 4. Similarly, from the information about the thermodynamic states of steams 4, 6 and 7, the amount of heat to be transferred and the effectiveness of external reformer 2 are calculated. Then, the thermodynamic state of stream 5 and the external reforming rate 2 are calculated. The total external reforming rate denotes the sum of external reforming rate 1 and external reforming rate 2. Finally, the calculated thermodynamic states of the SOFC inlet gas conditions (steams 5 and 16) are transferred to the SOFC simulation model.

The SOFC simulation model calculates how the SOFC will operate under conditions whereby the information of the SOFC inlet gases are given from the system simulation model and the amount of current to be drawn is determined from the value of Util. Specifically, the cell voltage of the SOFC, the temperature and the current density distribution of the cell, and the produced power are calculated in the SOFC simulation model. The temperatures of the SOFC outlet gases can be obtained as the results of the SOFC simulation, and this temperature information is used to repeat the iteration at step 5 (in figure 4.5). This iteration stops when the temperature difference of stream 5 during the previous and current iteration cycles is less than 0.1 K.

4.2.4. Ranges of control parameters

In this chapter, of the eight parameters, the values of five parameters (Fuel rate, SCR, $Util_{air}$, CAD_{peak}, and RPM) are fixed to typical values. First, the Fuel rate is fixed at 10.0 kW, which is considered to be appropriate for a 5 kW-class system. SCR is fixed at 2.5, which is typically the minimum value to prevent carbon coking in the reformer. $Util_{air}$ is fixed at 0.3 to prevent overcooling and undercooling of the SOFC. CAD_{peak}, i.e., the combustion timing of the HCCI engine, is fixed at 372 CAD. According to various

experimental results for HCCI engines, stable and efficient operation is achieved at this combustion timing. Finally, RPM is fixed at 1800 rpm (60 Hz), corresponding to the frequency of Korean AC power, for efficient power generation. Therefore, in this chapter, changes in system operation with changes in three control parameters (Util, BPR, Phi) are analysed.

4.3. Results

The central goals of the system analysis were to investigate how combined operation with the HCCI engine affects the overall system operation, including the SOFC, and to determine the necessary controls that enable successful system operation. For these purposes, the system analysis was performed in the following order. First, in section 4.3.1, SOFC operation under the SOFC–HCCI engine hybrid system is analysed under one representative system operating condition. Based on the results of the analysis, in this section, the typical characteristics of SOFC operation under the hybrid system are described in detail, and the feasibility of SOFC operation is ascertained.

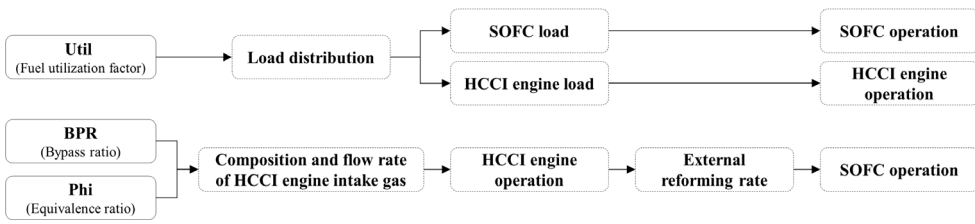

Figure 4.7. Effects of each control parameter on the SOFC and HCCI engine operation

In section 4.3.2, the changes in the system operation as the three control parameters (Util, BPR, and Phi) are varied were analysed to determine the effects of each control parameter on the system operation.

As mentioned in chapter 2 and section 4.2.4, these three control parameters are important control parameter because they significantly affect not only HCCI engine operation but also SOFC operation. Figure 4.6 re-summarizes the outline of how each control parameter influences SOFC operation as well as HCCI engine operation. In sections 4.3.2.1 and 4.3.2.2, the effects of each control parameter on the system operations are analysed quantitatively. In section 4.3.2.1, the system analysis is performed with varying BPR and Phi while the other parameters are fixed. In section

4.3.2.2, the other control parameters are fixed, and the system analysis is performed while varying Util. In section 4.3.2.3, the design point of system operation, that is, the values of BPR, Phi and Util that produce the optimal system operation, was determined based on the results of sections 4.3.2.1 and 4.3.2.2. In addition, the system operation results at the design point are introduced in detail.

The system analysis conditions of each section are summarized in table 4.5. In each section, the fixed values are determined as the values that are appropriate for stable and efficient system operation or the values that clearly represent the change in system operation caused by varying the other control parameters. It is noted that the operating conditions of sections 4.3.2.1 and 4.3.2.2 are the same as the operating conditions of sections 3.3.1 and 3.3.2 of chapter 3, respectively. Therefore, for additional details about HCCI engine operation under these conditions, the reader is referred to chapter 3.

Table 4.5. System analysis conditions of each result section

Control parameters	**4.1.**	**4.2.1.**	**4.2.2.**
Util (Fuel utilization factor of SOFC)	0.65	0.65	**Variation**
BPR (Bypass ratio)	0	**Variation**	0
Phi (Equivalence ratio of HCCI engine)	0.85	**Variation**	**Variation**
Fuel rate (System fuel flow rate)	10.0 kW		
SCR (Steam to carbon ratio)	2.5		
$Util_{air}$ (Air utilization factor of SOFC)	0.3		
CAD_{peak} (Combustion timing of HCCI engine)	372 CAD		
RPM (HCCI engine rpm)	1800 rpm		

4.3.1. SOFC operation in the SOFC–HCCI engine hybrid system

In this section, the characteristics of SOFC operation under the SOFC–HCCI engine hybrid system are analysed. The most important characteristic of SOFC operation under the SOFC–HCCI engine hybrid system is that the SOFC should be operated with the SOFC anode inlet gas, which has relatively low temperature and low reforming rate. In the SOFC stand-alone system, the SOFC anode off-gas is usually combusted in the catalytic combustor to produce heat for external reforming. However, the hybrid system produces additional power from the sensible and chemical energy of the SOFC anode off-gas; therefore, the amount of heat for external reforming is reduced in the hybrid system. As a result, the external reforming rate is lowered, and the temperature of the anode inlet gas is decreased. Therefore, the main objective of this section is to introduce the SOFC operation results under these operating conditions.

To achieve this objective, one representative system operating condition (Util of 0.65, BPR of 0, and Phi of 0.85) is selected for obtaining the SOFC operation results under the hybrid system. Although the results of SOFC operation will change if the values of the system control parameters vary from the selected values, the main characteristics of SOFC operation will not change significantly. At the given operating point, the SOFC inlet gas's properties obtained from the system analysis are presented as follows. The temperature of the anode inlet gas is approximately 783 K, and the external reforming rate is approximately 36.8%. The temperature of the cathode inlet gas is approximately 954 K, and the pressures of the anode and cathode are maintained as atmospheric pressure.

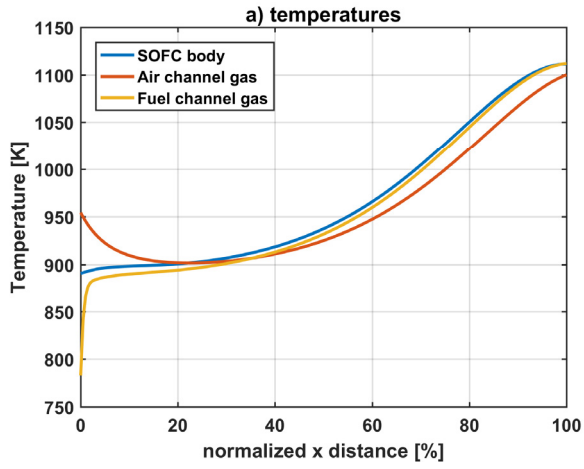
a) temperatures
SOFC body
Air channel gas
Fuel channel gas
Temperature [K]
normalized x distance [%]

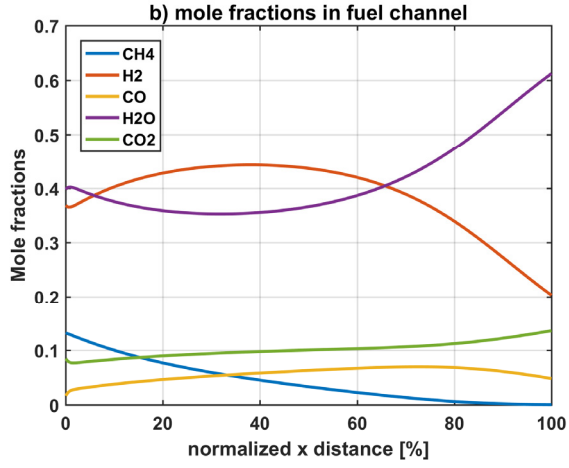
b) mole fractions in fuel channel
CH4
H2
CO
H2O
CO2
Mole fractions
normalized x distance [%]

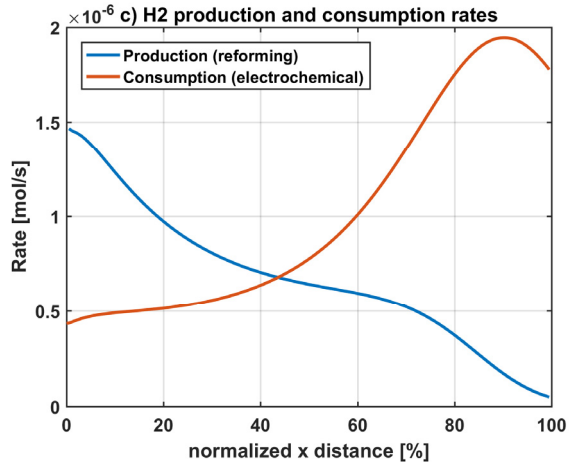
×10-6 c) H2 production and consumption rates
Production (reforming)
Consumption (electrochemical)
Rate [mol/s]
normalized x distance [%]

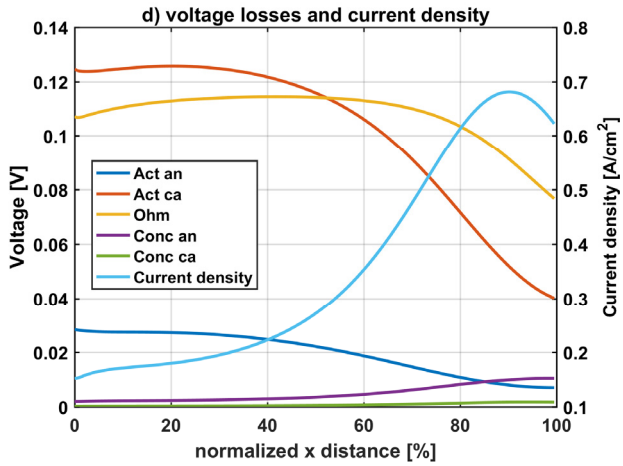

Figure 4.8. Typical SOFC performance of the hybrid system with an HCCI engine: a) temperatures; b) mole fractions in fuel channel; c) H_2 production and consumption rates; d) voltage losses and current density

Figure 4.7 shows the SOFC operation results under the given system operating conditions. Figure 4.7 a) shows the temperature distributions of the SOFC body, fuel channel gas and air channel gas in the *x* direction. As shown in the graph, the temperature of the fuel channel inlet gas (~783 K) is approximately 170 K lower than the temperature of the air channel inlet gas (~954 K). In steady-state operation, the temperature of the SOFC body starts at approximately 891 K, which is between the two inlet gas temperatures. Therefore, the SOFC body receives heat from the air channel gas and transfers heat to the fuel channel gas. As *x* increases, the temperature of the air channel gas gradually drops, whereas the temperature of the fuel channel gas rapidly increases. The rate of increase of the fuel channel gas temperature is very large because the mass flow rate of the fuel channel gas is approximately 1/10 of that of the air channel gas.

This rapid temperature rise results in a fast internal reforming reaction. Figure 4.7 b) shows that the mole fraction of H_2 in the fuel channel increases until normalized *x* equals

to ~ 40% because the rate of H_2 production caused by reforming reactions is higher than the rate of H_2 consumption caused by electrochemical reactions in the entrance of the SOFC. The comparison of the H_2 production rate with the H_2 consumption rate in figure 4.7 c) shows that the profiles of the two rates cross when normalized x is approximately 40%. This crossing is attributed to the fact that as the reforming reaction occurs, the partial pressure of H_2 increases and the partial pressure of CH_4 decreases, and these changes in partial pressure accelerated the electrochemical reaction and decelerated the reforming reaction.

Whereas reforming is an endothermic reaction, the electrochemical reaction is exothermic; therefore, the temperature of the SOFC body does not increase significantly at the entrance of the SOFC. However, the temperature increases greatly from the point where the electrochemical reaction becomes more dominant than the reforming reaction. This increased temperature leads to an additional increase in current density while improving the performance of the SOFC. An increase in current density means an increase in the rate of electrochemical reactions because the electrons are produced from the electrochemical reactions. Therefore, it can be concluded that there is a continuous positive feedback between temperature and current density: an increase in the electrochemical reaction rate increases the temperature which improves the SOFC performances, and thus, the current density, i.e., electrochemical reaction rate, increases further. This positive feedback continues until normalized x is approximately 90%. When normalized x increases beyond 90%, the current density, now decreases because the H_2 partial pressure decreases too much due to the electrochemical reactions in the previous part (normalized $x < 90\%$).

These temperature and current density profiles also affect the voltage losses, which are shown in figure 4.7 d). The voltage losses show that the ohmic and activation losses,

which are the dominant losses, follow similar trends. These voltage losses tend to increase slightly when x increases and decrease after a certain point. These trends are caused by the simultaneously increasing temperature and current density. Because ohmic and activation losses tend to increase as the current density increases and decrease as the temperature increases, there is a trade-off when the temperature and current density increase simultaneously. Meanwhile, the concentration losses increase at the back end, where the current density is large. This result is attributed to the increase in current density, the decrease in H_2 partial pressure, and the increase in H_2O partial pressure as x increases. Combining these voltage losses, the cell voltages at all x should be the same. Therefore, the Nernst potential (open-circuit voltage) increases slightly as x increases and decreases when approaching the exit. In the entrance part of the SOFC, as x increases, the partial pressure of H_2 increases and the partial pressure of H_2O decreases; therefore, the Nernst potential increases. However, when x exceeds a certain point, the increase in temperature, the decrease in H_2 partial pressure and the increase in H_2O partial pressure cause the Nernst potential to decrease.

The results of section 4.3.1 are summarized as follows. The greatest feature of SOFC operation in the SOFC–HCCI engine hybrid system is that the anode inlet gas has a low external reforming rate (~ 36.8% under the conditions considered in this section) and low temperature (~ 783 K). These characteristics of the anode inlet gas reduce the temperature of the SOFC, resulting in the requirement that the SOFC should be able to operate at approximately 900 K, which is in intermediate temperature range for SOFC operation.[52] Therefore, the SOFC, which can operate well at intermediate temperature, should be chosen for the SOFC–HCCI engine hybrid system. Additionally, the use of the anode-supported SOFC in this system was adequate with respect to the fact that the ohmic loss in the electrolyte, which can be increased significantly at

intermediate temperature, could be reduced since the thickness of the electrolyte is small in an anode-supported-type SOFC.[53] Meanwhile, although the temperature difference between the anode inlet gas and the cathode inlet gas is large, the temperature of the fuel gas approaches that of the SOFC body quickly since the flow rate of the fuel gas is small. Therefore, the low temperature of the anode inlet gas does not induce a significant additional temperature gradient in the height direction between the anode and the cathode.

Additionally, comparison of the results in section 4.3.1 with well-known 1D simulation results for anode-supported intermediate-temperature direct internal reforming SOFC shows that the trends of the mole fractions, voltage losses, and current density are similar.[46] This comparison confirms the reliability of the simulation model in this dissertation.

4.3.2. Parametric study to determine the design point of system operation

In this section, the changes in the operation results of the entire SOFC–HCCI engine hybrid system, including the SOFC and HCCI engine, when three control parameters (Util, BPR, and Phi) change are analysed. Based on this analysis, the values of control parameters able to achieve not only high performance but also stable system operation are investigated, and the design point of the system is determined. Section 4.3.2.1 is aimed at analysing how the system operation changes as the values of BPR and Phi change and understanding the effects of two control parameters on system operation. In particular, the values of BPR and Phi that can be used to improve the external reforming rate, which is usually low in the hybrid system, and accordingly SOFC operation are analysed in this section. Section 4.3.2.2 is aimed at analysing how the system operation varies when the value of Util changes and investigating the effect of Util on system operation. Specifically, the value of Util that can best distribute the power generation load to two devices for achieving high performance as well as stable system operation is investigated in this section. In section 4.3.2.3, the design point of system operation is determined, and the system operation results at the design point are described in detail.

4.3.2.1. BPR/ Phi variations

As mentioned above, BPR controls the amount of steam, and Phi regulates the amount of air in the HCCI engine intake gas. Therefore, they affect the composition and flow rate of the HCCI engine intake gas and accordingly directly influence the HCCI engine operation.

BPR and Phi also indirectly affect system operation, including the SOFC. When BPR and Phi change, the temperature and flow rate of the engine exhaust gas change;

therefore, the amount of heat that can be transferred in external reformer 1 (in figure 4.1) varies. Similarly, when BPR and Phi change, the temperature and flow rate of the engine intake gas also change, and the amount of heat that can be transferred in external reformer 2 (in figure 4.1) is also varied. Therefore, BPR and Phi affect the amount of heat used in the external reformers and therefore affect the total external reforming rate. As a result, BPR and Phi also affect SOFC operation.

This section attempts to investigate quantitatively how changes in BPR and Phi directly and indirectly affect HCCI engine operation, SOFC operation, and finally the entire system operation. To this end, system analysis is performed while BPR and Phi are changed from 0 to 0.8 and from 0.5 to 1, respectively, whereas Util is fixed as 0.65.

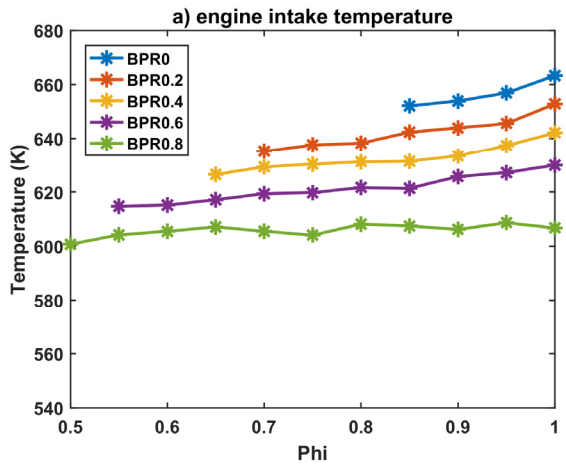

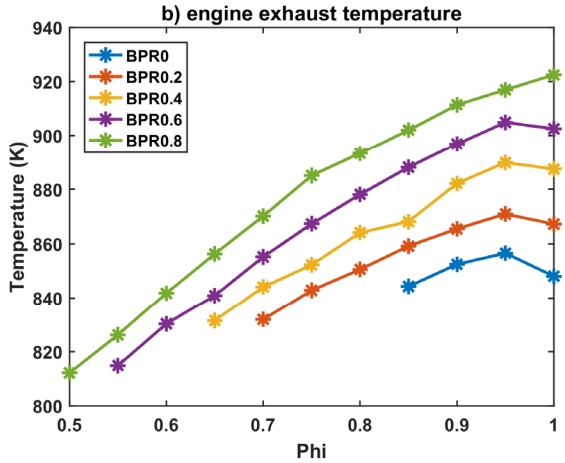
b) engine exhaust temperature
BPR0
BPR0.2
BPR0.4
BPR0.6
BPR0.8
Temperature (K)
Phi

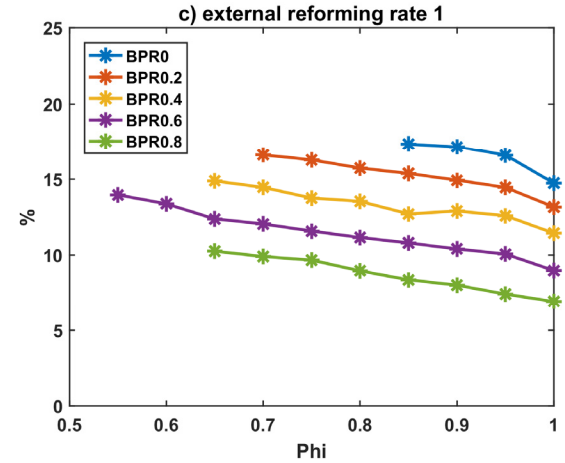
c) external reforming rate 1
BPR0
BPR0.2
BPR0.4
BPR0.6
BPR0.8
%
Phi

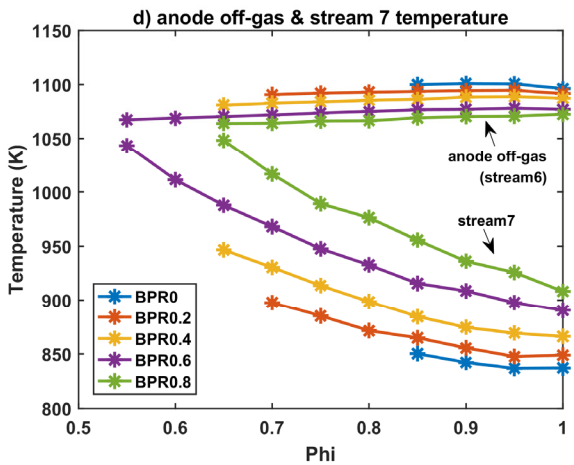
d) anode off-gas & stream 7 temperature
anode off-gas
(stream6)
stream7
BPR0
BPR0.2
BPR0.4
BPR0.6
BPR0.8
Temperature (K)
Phi

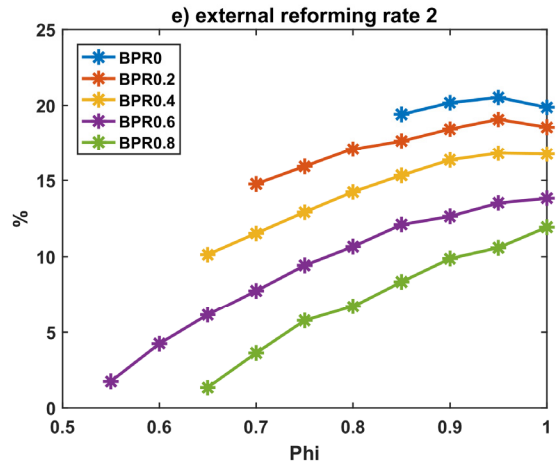

Figure 4.9. Temperatures and external reforming rates:

a) engine intake gas temperature; b) engine exhaust gas temperature;

c) external reforming rate 1; d) anode off-gas and stream 7 temperature;

e) external reforming rate 2; f) total external reforming rate

Figures 4.8 a) and b) show the temperatures of the engine intake and exhaust gas as a function of BPR and Phi. The intake gas temperature in the graph denotes the required gas temperature to cause HCCI combustion, which means the autoignition of the intake gas achieved only by the compression of the engine intake gas. The exhaust gas temperature is the temperature of the gas emitted from the engine when such

combustion occurs. Chapter 3 showed that even if the amounts of air and steam in the engine intake gas change due to variations in BPR and Phi, the ignition temperature does not vary greatly. It was concluded that the specific heat ratio of the engine intake gas is the predominant factor determining the required intake gas temperature. Therefore, as BPR decreases and Phi increases, the amount of steam increases and the amount of air decreases; therefore, the specific heat ratio of the engine intake gas decreases, resulting in an increase in the required intake gas temperature. Chapter 3 also showed that larger amounts of diluent in the engine intake gas resulted in lower combustion and exhaust temperatures. Therefore, as BPR and Phi decrease, the exhaust gas temperature decreases.

As mentioned above, changes in BPR and Phi influence the external reforming rate. In external reformer 1, the engine exhaust gas supplies the heat required for reforming; therefore, the flow rate and the temperature of the exhaust gas determine external reforming rate 1. It is interesting to note that as BPR and Phi decrease, the flow rate of the engine exhaust gas increases, but the exhaust gas temperature decreases. Therefore, the increased flow rate and decreased temperature exhibit a trade-off effect with respect to the external reforming rate. Figure 4.8 c) shows the calculated value of external reforming rate 1 considering these two effects. As shown in the graph, the effect of an increase in flow rate is greater than the effect of a decrease in temperature, and eventually, as the amount of diluent increases, external reforming rate 1 also increases. Therefore, external reforming rate 1 increases as BPR decreases, which means less steam separation, and as Phi decreases, a larger amount of air is entrained in the engine.

In external reformer 2, the SOFC anode off-gas supplies the heat for reforming. Because the flow rate of the SOFC anode off-gas does not change even when BPR and Phi are varied, the temperature of the SOFC anode off-gas is important for determining

external reforming rate 2. Additionally, the temperature of the SOFC anode off-gas should not be lowered beyond the temperature required to supply the required engine intake gas temperature to prevent misfiring in the HCCI engine. Figure 4.8 d) shows the temperature of stream 7 (in figure 4.1) necessary to achieve the required engine intake temperature in figure 4.8 a). It is interesting to note that although the required intake gas temperature increases as BPR decreases and Phi increases, the required temperature of stream 7 shows the opposite tendency. This is because even if the required engine intake gas temperature is high, it is easier to reach this temperature with less steam separation, which induces heat losses from stream 7, and with a lower amount of ambient air entrained in the engine, which causes the temperature of the stream to decrease since the ambient air is colder than the stream. For these reasons, as BPR decreases and Phi increases, the temperature difference between the SOFC anode off-gas (stream 6) and stream 7 increases, resulting in an increase in the amount of heat that can be transferred in external reformer 2. On the other hand, when BPR is 0.6 or more, there are some points where the temperature of stream 6 is lower than the required temperature of stream 7. In this case, required engine intake temperature for occurring the HCCI combustion cannot be achieved and the HCCI engine cannot produce power. Therefore, the graphs related with system operation in this section does not include these cases. As explained in section 4.2.3, it is assumed that the design and effectiveness of the external reformers can be changed under each set of operating conditions to deliver the exact amount of heat based on the difference between the temperature of the SOFC anode off-gas and the required temperature of stream 7. Therefore, external reformer 2 delivers exactly this amount of heat, and external reforming rate 2 increases as BPR decreases and Phi increases.

External reforming rates 1 and 2 are added to obtain the total external reforming rate,

as shown in figure 4.8 f). As shown in the graph, a lower BPR results in a higher total external reforming rate because a lower BPR results in higher external reforming rates 1 and 2. Meanwhile, the total external reforming rate is maximized when Phi is 0.9 because as Phi decreases, external reforming rate 1 increases, but external reforming rate 2 decreases. Ultimately, the total external reforming rate affects the operating temperature and performance of the SOFC.

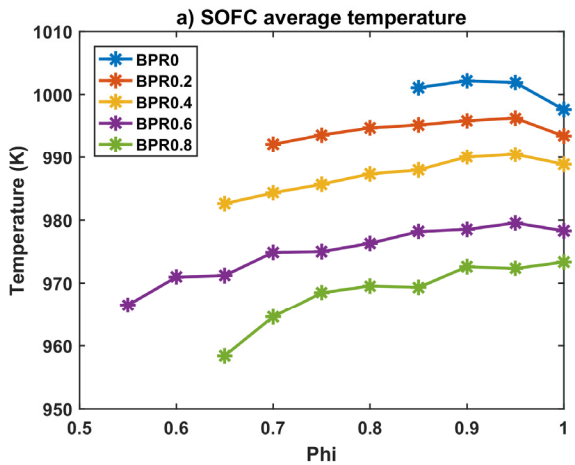

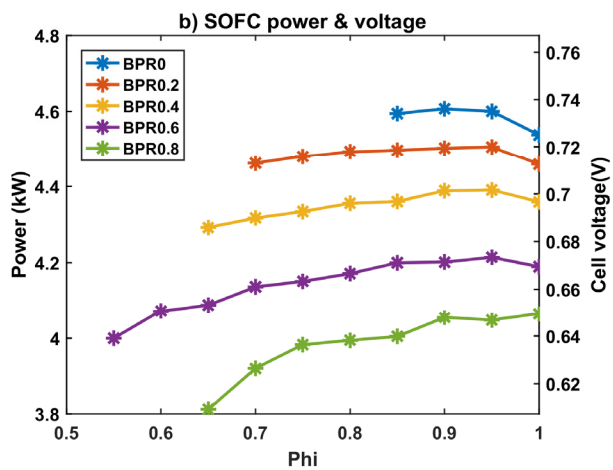

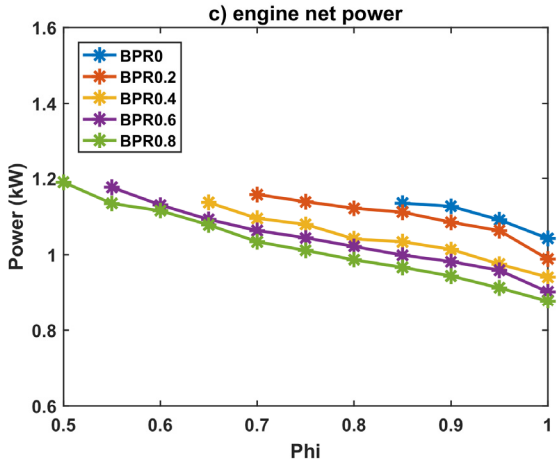
c) engine net power
BPR0
BPR0.2
BPR0.4
BPR0.6
BPR0.8
Power (kW)
Phi
1.6
1.4
1.2
1
0.8
0.6
0.5
0.6
0.7
0.8
0.9
1

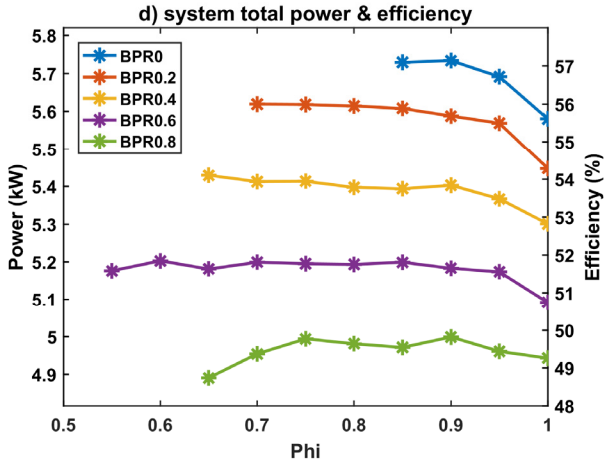
d) system total power & efficiency
BPR0
BPR0.2
BPR0.4
BPR0.6
BPR0.8
Power (kW)
Efficiency (%)
Phi
5.8
5.7
5.6
5.5
5.4
5.3
5.2
5.1
5
4.9
57
56
55
54
53
52
51
50
49
48
0.5
0.6
0.7
0.8
0.9
1

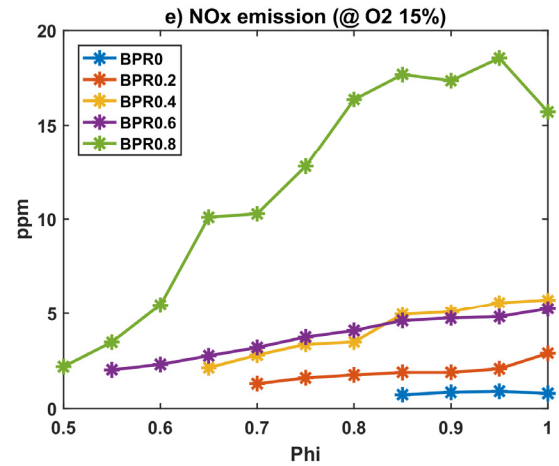
e) NOx emission (@ O2 15%)
BPR0
BPR0.2
BPR0.4
BPR0.6
BPR0.8
ppm
Phi
20
15
10
5
0
0.5
0.6
0.7
0.8
0.9
1

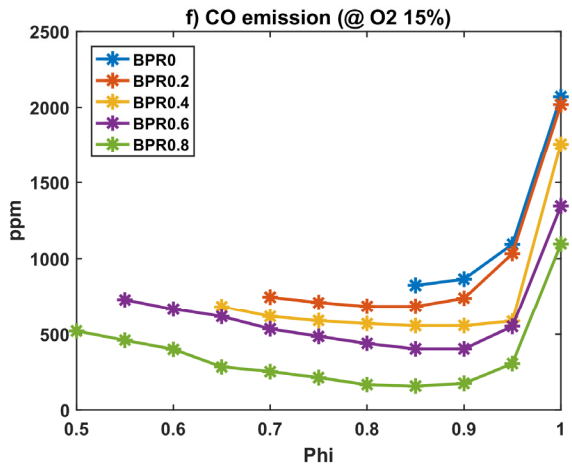

Figure 4.10. System performance: a) SOFC average temperature; b) SOFC power and cell voltage; c) engine net power; d) system total power and efficiency; e) NO_x emission (@ O_2 15%); f) CO emission (@ O_2 15%)

Figure 4.9 a) shows the average temperature of the SOFC body. The trend of the graph is similar to the trend of the total external reforming rate, as shown in figure 4.8 f), because when the total external reforming rate increases, the amount of reforming that should be performed in the SOFC decreases. Accordingly, the overall SOFC temperature can be increased. The temperature of the SOFC also directly affects the performance of the SOFC. Figures 4.9 a) and b) show similar trends: as the temperature of the SOFC increases, the voltage losses decrease and thus the voltage of the SOFC cell increases, which increases the amount of power produced in the SOFC.

Meanwhile, figure 4.9 c) shows the net indicated power of the HCCI engine, which was confirmed from the engine experiment. According to chapter 3, lower values of BPR and Phi result in higher amounts of diluent and greater engine intake pressures at fixed rpm. Hence, the pumping loss decreases, and the net indicated power increases. The total system power, which is the sum of the SOFC power and the HCCI engine net

power, is calculated and shown in figure 4.9 d). As BPR decreases, the system power increases since both the SOFC power and the HCCI engine power increase. Additionally, when Phi is less than 0.9, the total system power does not vary greatly because the engine power increases as Phi decreases, whereas the SOFC power decreases when Phi is less than 0.9. Therefore, under the operating conditions considered in this section, the system efficiency is maximized when BPR is 0 and Phi is 0.9 or lower.

Figures 4.9 e) and f) show the emission characteristics of the system. The graphs show the NO_x and CO emissions measured at the exhaust manifold of the HCCI engine. Since SOFC is known to emit almost no pollutants, these results can be regarded as the emissions of the entire hybrid system.[54] In chapter 3, it was shown that as the amount of diluent increases, NO_x emissions decrease and CO emissions increase since the combustion temperature decreases. Additionally, it was confirmed in chapter 3 that when Phi is 0.9 or more, a locally rich region can be generated within the engine cylinder, and the CO emissions rapidly increase. Confirming the emission characteristics under the conditions of a BPR of 0 and Phi of 0.9, which result in good system efficiency, less than 1 ppm NO_x is generated and approximately 800 ppm CO is emitted based on an O_2 level of 15%.

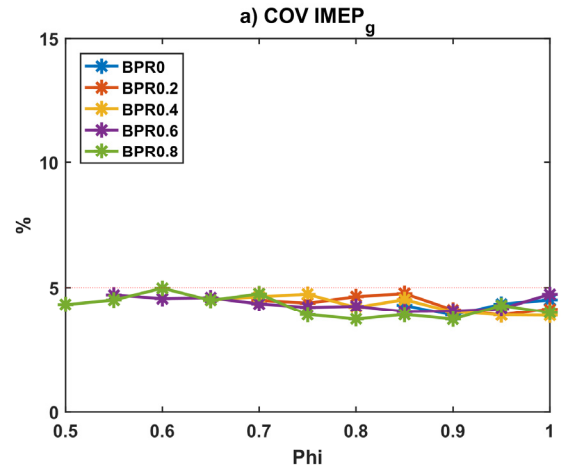
a) COV IMEP g
15
10
5
0
%
0.5
0.6
0.7
0.8
0.9
1
Phi
BPR0
BPR0.2
BPR0.4
BPR0.6
BPR0.8

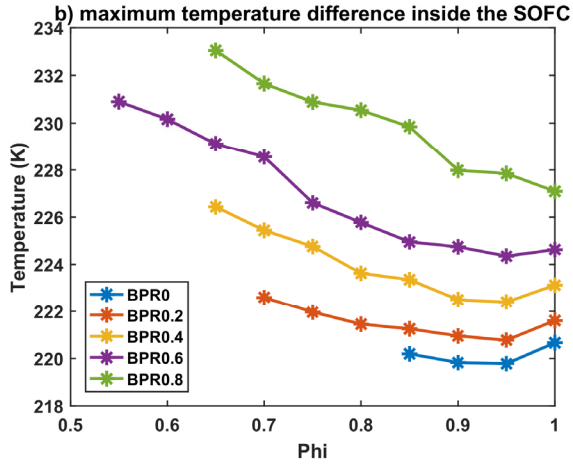
b) maximum temperature difference inside the SOFC
234
232
230
228
226
224
222
220
218
Temperature (K)
0.5
0.6
0.7
0.8
0.9
1
Phi
BPR0
BPR0.2
BPR0.4
BPR0.6
BPR0.8

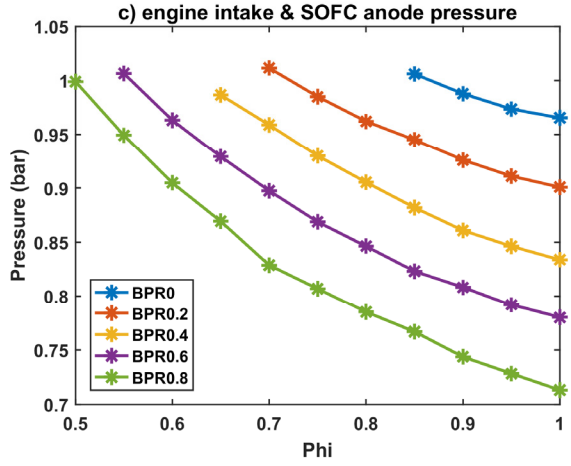
c) engine intake & SOFC anode pressure
1.05
1
0.95
0.9
0.85
0.8
0.75
0.7
Pressure (bar)
0.5
0.6
0.7
0.8
0.9
1
Phi
BPR0
BPR0.2
BPR0.4
BPR0.6
BPR0.8

Figure 4.11. Constraints on system operation:
a) COV $IMEP_g$; b) maximum temperature difference inside the SOFC; c) engine intake and SOFC anode pressure

However, system operation can be unstable even if the system achieves great performances. Figure 4.10 shows the three factors that can affect the stability of system operation. The first factor is the stability of HCCI engine operation. Figure 4.10 a) shows the values of COV $IMEP_g$ (the coefficient of variance of the gross indicated mean effective pressure), which is a parameter that represents the cycle-to-cycle variation in the gross indicated power and, accordingly, the instability of HCCI engine operation. Chapter 3 showed that COV $IMEP_g$ is inversely proportional to $IMEP_g$ (the gross indicated mean effective pressure), a parameter that represents the power generation load of the engine. Even if BPR and Phi change, the engine load does not change substantially because the flow rate of the fuel components (H_2 and CO) of the engine intake gas is not varied. Therefore, as shown in figure 4.10 a), the instability of HCCI engine operation does not vary substantially with variations in BPR and Phi. Additionally, stable HCCI combustion is achieved under all conditions in this section since the values of COV $IMEP_g$ are less than 5%, which set as the upper limit of stable combustion in chapter 3.[23, 33-35]

The second factor is the temperature gradient inside the SOFC cell. When the maximum temperature difference inside the SOFC cell increases, the thermal stress in the SOFC cell increases. An increase in the thermal stress can cause SOFC cell failure, which adversely affects the stability of system operation. Figure 4.10 b) shows the maximum temperature difference inside the SOFC as BPR and Phi vary. The maximum temperature difference decreases as BPR decreases because the lower BPR is, the higher the total external reforming rate, the higher the voltage of the SOFC cell, the

greater the proportion of the chemical energy of the fuel that can be used to produce power, and the smaller the portion of the fuel chemical energy released in the form of heat. Therefore, it is desirable to minimize BPR. Meanwhile, when Phi is less than 0.9 at the same BPR, the maximum temperature difference increases due to the decreasing total external reforming rate. However, the closer BPR is to zero, the smaller the difference.

The third factor is the pressure difference between the SOFC anode and the SOFC cathode or the outside of the SOFC. In the SOFC–HCCI engine hybrid system, the inlet part of the HCCI engine is connected to the anode side of the SOFC; therefore, the intake pressure of the HCCI engine is directly transferred to the SOFC anode (for reference, in practical system operation, the differential pressure between the SOFC anode and the HCCI engine may be within several kPa, but the differential pressure is not considered in this chapter). Therefore, as the HCCI engine intake pressure drops below atmospheric pressure, the pressure of the SOFC anode decreases, which increases the pressure difference between the SOFC anode and the SOFC cathode or the outside of the SOFC. This increase in pressure difference generates mechanical stress in the SOFC cell and sealing parts, and these mechanical stresses adversely affect the operation stability since they can break the cell or the sealing part and cause leakage. The specific value of the pressure difference that can cause these problems depends on the characteristics of the cell or stack, but it is best to minimize this pressure difference. Figure 4.10 c) shows the HCCI engine intake pressure. As shown in the graph, as BPR and Phi decrease, the intake pressure approaches atmospheric pressure. Therefore, it is generally recommended to fully open the throttle to lower Phi to keep the pressure close to atmospheric pressure to reduce the stress due to the pressure difference.

Therefore, the preferred BPR and Phi when other control parameters are fixed are

summarized as follows. First, maintaining a low BPR and reducing the flow rate bypassed to the steam separator increase the total external reforming rate, the cell voltage and the produced power of the SOFC; reduce the NO_x emissions from the HCCI engine; and decrease the maximum temperature difference inside the SOFC and the pressure difference between the SOFC anode and the SOFC cathode. Therefore, maintaining a low BPR is better for overall system operation. However, when BPR decreases, CO emissions increase. In particular, at a BPR of 0, CO emissions are approximately 800 ppm (O_2 15%). However, chapter 3 showed that the CO combustion efficiency is greater than 95%, even in this situation; therefore, there is no major problem with the combustion efficiency.

In the case of Phi, it is better to maintain a value of less than 0.9 because the emission of CO suddenly increases beyond 0.9. When Phi is less than 0.9, the external reforming rate decreases as Phi decreases; accordingly, the SOFC performance decreases. However, as Phi decreases, the HCCI engine intake pressure increases, and the HCCI engine net power increases. Therefore, when Phi is 0.9 or less, the total system power remains almost the same. However, maintaining a low Phi and reducing the pressure difference between the SOFC anode and the SOFC cathode or the outside of the SOFC is preferable for stable system operation because this can reduce the mechanical stress of the cell.

Therefore, if CO is reduced through after-treatment at the engine exhaust manifold, then minimizing BPR and Phi is beneficial for the system performance under the operation conditions considered in this section. In other words, supplying a large amount of steam and air diluent in the engine intake gas is advantageous for system operation. Considering that the amount of diluent cannot be large when spark ignition is used in an internal combustion engine, this result can be considered to be a

quantitative demonstration of the suitability of HCCI as the combustion strategy of an internal combustion engine as the bottoming cycle of the SOFC. This subject is covered in more detail in the discussion section.

4.3.2.2. Fuel utilization factor of SOFC variations

Util (fuel utilization factor of the SOFC) is a parameter representing the ratio of the amount of fuel used in the SOFC to the amount of fuel supplied to the SOFC. In this dissertation, Util is defined as follows. In the equation (4.6), the states of SOFC anode off-gas and reformed gas are calculated with the assumption that SOFC anode off-gas and reformed gas are in the equilibrium at 750 ℃ (for more details of the calculation process, refer to the appendix B.1).

$$Utilization\ factor(Util) = 1 - \frac{LHV\ of\ SOFC\ anode\ off-gas}{LHV\ of\ reformed\ gas} \quad (4.6)$$

When the amount of fuel input into the system is constant, Util is a direct representation of the amount of current or the power generation load of the SOFC. Specifically, when Util increases, both the current of the SOFC and the amount of power generated increase. Meanwhile, the change in Util varies the amount of fuel components (H_2 and CO) in the SOFC anode off-gas; accordingly, it also affects the power generation load of the HCCI engine. For example, if Util increases from 0.5 to 0.7 and uses more fuel in the SOFC, the amount of fuel in the anode off-gas is reduced by 40%, resulting in an approximately 40% reduction in the HCCI engine load. Therefore, Util affects not only the SOFC load but also the HCCI engine load; thus, Util can be regarded as the control parameter affecting the load distribution of the two power generation devices in the hybrid system. In this section, we therefore investigate how the system performance changes when Util changes and accordingly the load distribution changes for the two power generation devices. To this end, the system analysis is performed while Util and Phi are changed from 0.55 to 0.8 and from 0.55 to 1, respectively, whereas BPR is fixed as 0. Although the system analysis is also performed with varying Phi, the trend of the operation results as a function of Phi is not substantially different from the trend described in section 4.3.2.1, and thus the discussion will be focused on

the effect of Util in this section.

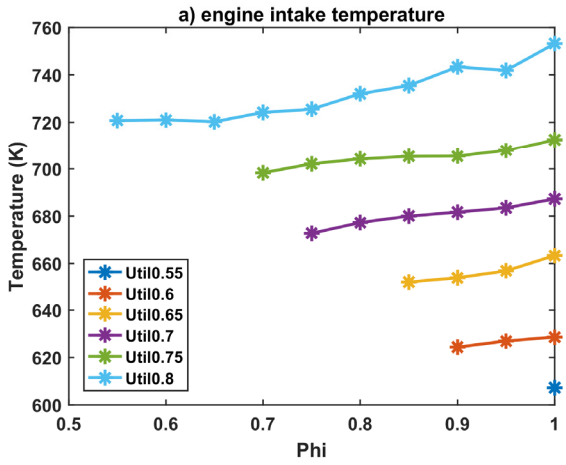

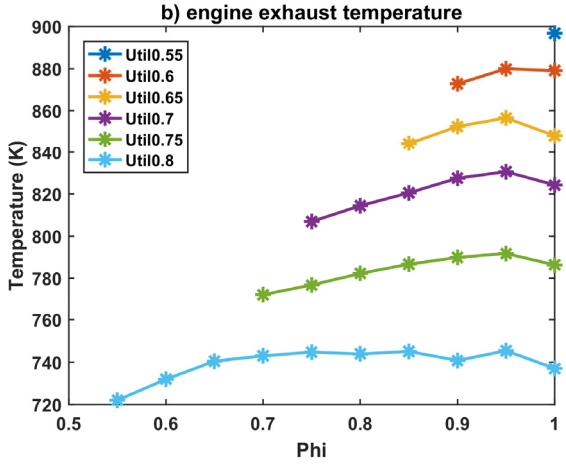

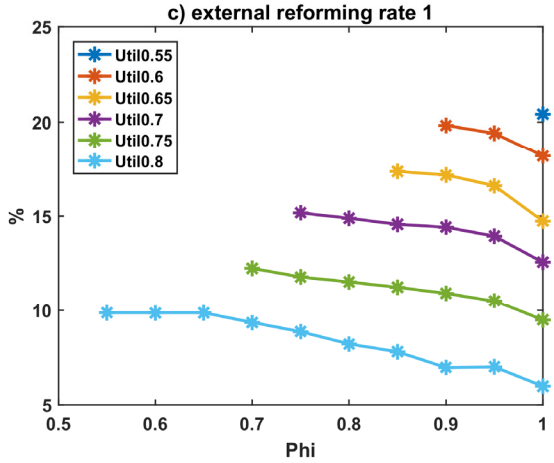

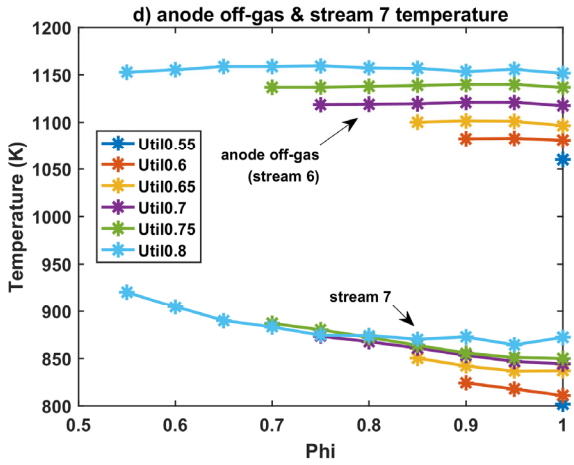
d) anode off-gas & stream 7 temperature
Temperature (K)
Phi
Util0.55
Util0.6
Util0.65
Util0.7
Util0.75
Util0.8
anode off-gas
(stream 6)
stream 7

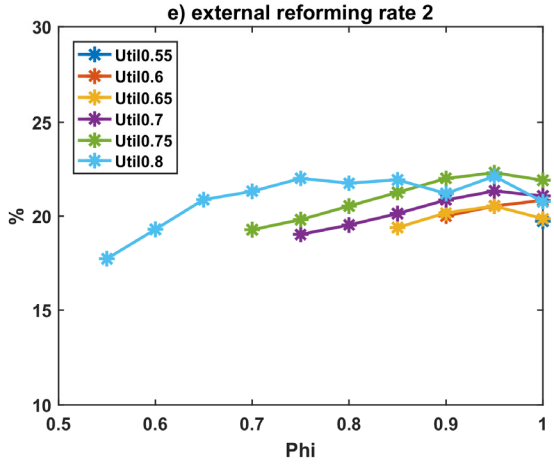
e) external reforming rate 2
%
Phi
Util0.55
Util0.6
Util0.65
Util0.7
Util0.75
Util0.8

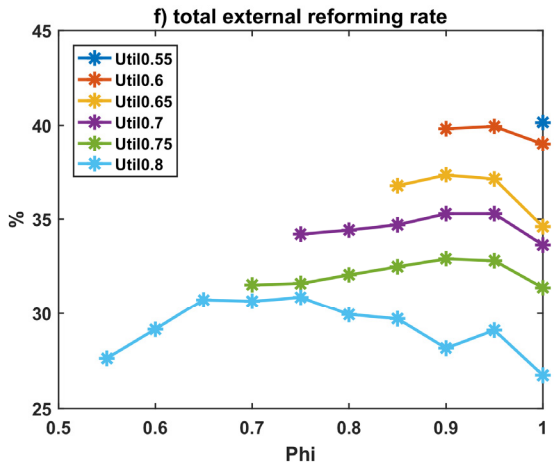
f) total external reforming rate
%
Phi
Util0.55
Util0.6
Util0.65
Util0.7
Util0.75
Util0.8

Figure 4.12. Temperatures and external reforming rates:
a) engine intake gas temperature; b) engine exhaust gas temperature;
c) external reforming rate 1; d) anode off-gas and stream 7 temperature;
e) external reforming rate 2; f) total external reforming rate

Figures 4.11 a) and b) show the intake and exhaust gas temperatures of the HCCI engine as functions of Util and Phi. As mentioned before, it was confirmed in chapter 3 that the predominant factor determining the required engine intake temperature is the specific heat ratio of the engine intake gas. When Util increases, the amount of diluent (H_2O and CO_2) in the engine intake gas increases, and the amount of fuel (H_2 and CO) decreases. Therefore, as Util increases, the specific heat ratio of the intake gas decreases. Accordingly, the required engine intake temperature increases. Chapter 3 reports that the exhaust gas temperature decreases as the amount of diluent relative to the amount of fuel in the engine intake gas increases. Therefore, when Util increases, the exhaust gas temperature decreases.

As explained in section 4.3.2.1, the temperatures and flow rates of the HCCI engine intake and exhaust gas affect the external reforming rate. In external reformer 1, the heat required for reforming is supplied by the engine exhaust gas; therefore, the temperature and flow rate of the exhaust gas strongly influence external reforming rate 1. When Util increases, both the temperature and the flow rate of the exhaust gas decrease at the same Phi. Therefore, external reforming rate 1 decreases as Util increases, as shown in figure 4.11 c).

In external reformer 2, the heat required for reforming is provided by the SOFC anode off-gas; therefore, the temperature and flow rate of the SOFC anode off-gas strongly affect external reforming rate 2. The temperature and flow rate of the SOFC anode off-gas increase as Util increases because a higher Util results in a larger amount of heat

generated from the electrochemical reaction and a greater amount of O_2 transmitted from the SOFC cathode. On the other hand, the required temperature of stream 7 (in figure 4.1) to achieve the necessary HCCI engine intake gas temperature under the given conditions is shown in figure 4.11 d). As shown in the graph, as Util increases, the required temperature of stream 7 increases due to the increase in the required engine intake temperature. However, figure 4.11 d) shows that the increase in anode off-gas temperature with increasing Util is larger than the increase in the temperature of stream 7. Therefore, an increase in Util increases the temperature difference between stream 7 and the SOFC anode off-gas, resulting in an increase in external reforming rate 2.

Figure 4.11 f) shows the total external reforming rate, which represents the sum of external reforming rates 1 and 2. As Util increases, the total external reforming rate generally decreases because with increasing Util, the decreasing effect on external reforming rate 1 is more dominant than the increasing effect on external reforming rate 2.

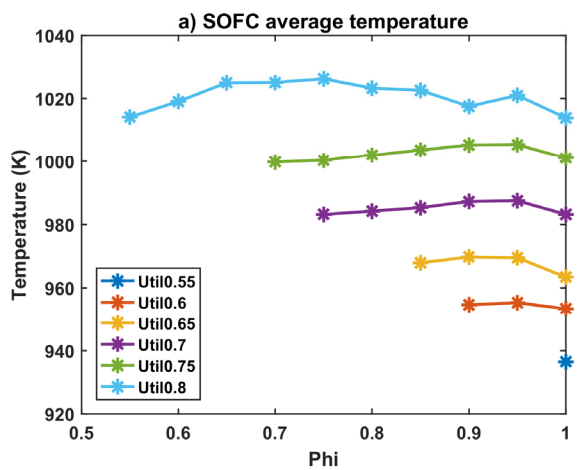

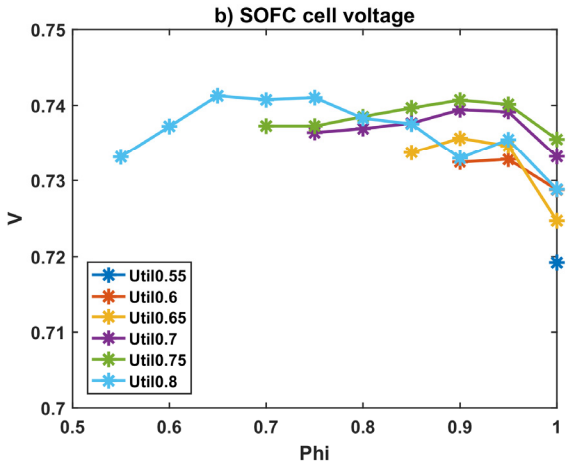
b) SOFC cell voltage
V
Phi
Util0.55
Util0.6
Util0.65
Util0.7
Util0.75
Util0.8

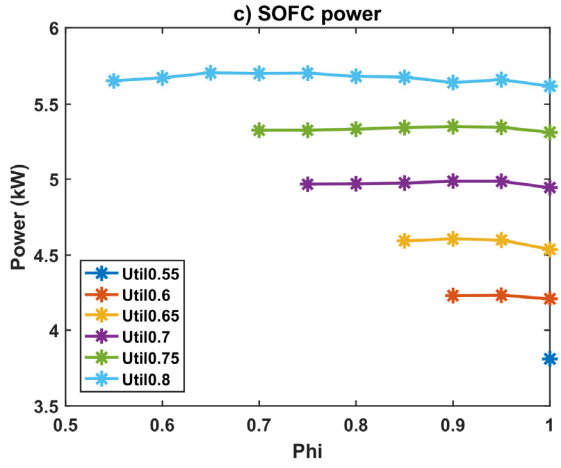
c) SOFC power
Power (kW)
Phi
Util0.55
Util0.6
Util0.65
Util0.7
Util0.75
Util0.8

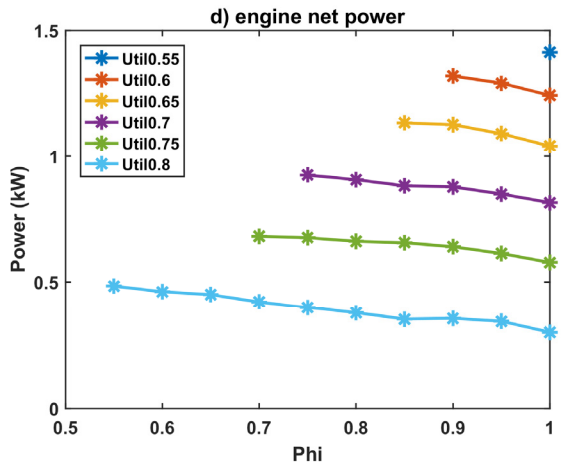
d) engine net power
Power (kW)
Phi
Util0.55
Util0.6
Util0.65
Util0.7
Util0.75
Util0.8

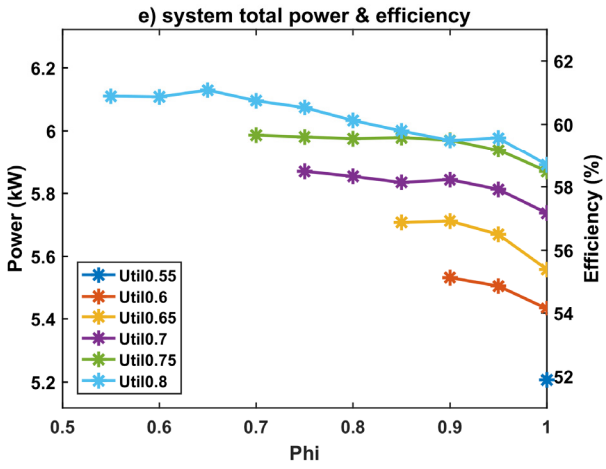
e) system total power & efficiency
Power (kW)
Efficiency (%)
Phi
Util0.55
Util0.6
Util0.65
Util0.7
Util0.75
Util0.8

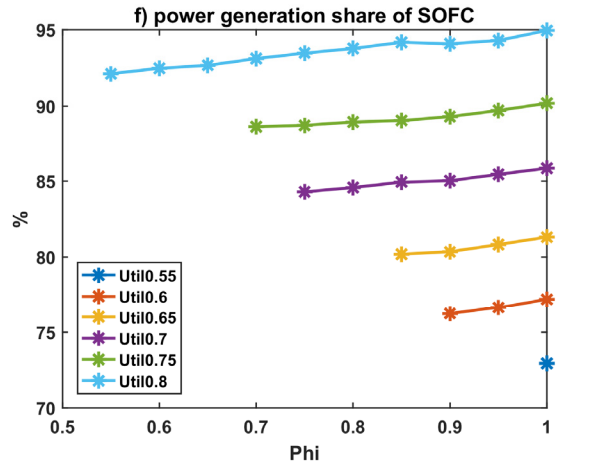
f) power generation share of SOFC
%
Phi
Util0.55
Util0.6
Util0.65
Util0.7
Util0.75
Util0.8

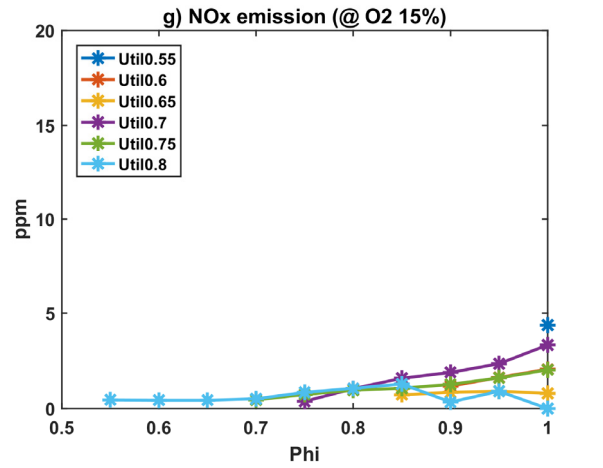
g) NOx emission (@ O2 15%)
ppm
Phi
Util0.55
Util0.6
Util0.65
Util0.7
Util0.75
Util0.8

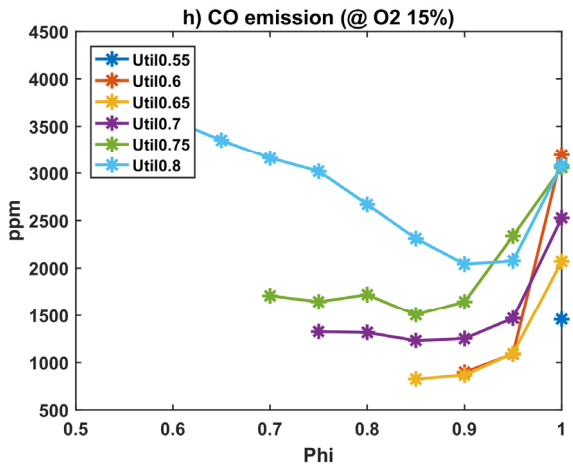

Figure 4.13. System performance: a) SOFC average temperature; b) SOFC cell voltage; c) SOFC power; d) engine net power; e) system total power and efficiency; f) g) NO_x emission (@ O_2 15%); h) CO emission (@ O_2 15%)

Figure 4.12 shows the system performances as Util changes. Figure 4.12 a) shows the average temperature of the SOFC body, which increases as Util increases because, as mentioned before, the amount of heat generated from the electrochemical reaction in the SOFC increases when Util increases. Furthermore, the trend of the average temperature at the same Util is similar to the trend of the total external reforming rate shown in figure 4.11 f) because when the amount of heat generated from electrochemical reactions is maintained by fixing the value of Util, the total external reforming rate mainly affects the average temperature.

Figure 4.12 b) shows the voltage of the SOFC cell. The change in average temperature described above creates an interesting cell voltage trend. Although, in general, the cell voltage decreases as the current increases, in the case of this system, the cell voltage does not change substantially as Util increases. Specifically, when Util increases, the cell voltage increases overall, and when Util increases beyond 0.75, the

cell voltage drops at certain points. The reason for this phenomenon is as follows. The increase in Util produces an increase in current, and the increase in current produces a decrease in cell voltage. However, simultaneously, the increase in Util increases the cell voltage by raising the average operating temperature. Therefore, when Util increases from 0.55 to 0.75, the effect of increasing cell voltage due to increasing temperature is more dominant than the effect of decreasing cell voltage due to the increase in current. In addition, when Util increases from 0.75 to 0.8, there are points where the decrease in cell voltage due to the increase in current is larger, and the opposite tendency is exhibited.

Results similar to the above results can be found in the literature, including an experimental study on an anode-supported intermediate-temperature direct internal reforming SOFC.[55] According to this study, as the external reforming rate decreases, the rate of decreasing voltage with respect to an increase in Util decreases. In particular, in this chapter, the cell voltage decreases by only ~ 0.01 V and remains constant as Util is increased from 60% to 80% in the cases with external reforming rates of 30% and 40%. Therefore, the cell voltage of the SOFC in the hybrid system is not expected to decrease substantially with increasing current even in the experiment.

Figure 4.12 c) shows the power produced by the SOFC, which is calculated based on the cell voltage. As shown in the graph, as Util increases, the SOFC power increases. This is attributed to the fact that as Util increases, the cell voltage does not change meaningfully, but the current increases substantially. Figure 4.12 d) shows the power produced by the HCCI engine. The figure shows that the HCCI engine power decreases as Util increases. Therefore, by summing the two devices' power, the total system power is calculated, as shown figure 4.12 e). The graph shows that when Util increases, the system total power increases because when Util increases, the power generation share

of the SOFC increases and the efficiency of the SOFC is higher than that of the HCCI engine. Figure 4.12 f) shows that when Util is 0.8, the power generation share of the SOFC reaches 90 ~ 95%.

Figures 4.12 g) and h) show the pollutant emission characteristics. First, as shown in figure 4.12 g), the amount of NOx emissions is maintained at a very low level (<5 ppm) at any Util in the SOFC–HCCI engine hybrid system because when BPR is kept at zero, the combustion temperature in the HCCI engine is sufficiently low at any Util. On the other hand, as shown in figure 4.12 h), the amount of CO emissions is increased as Util increases because, as stated in chapter 3, the increase in Util results in an increase in the amount of diluent in the intake gas, which reduces the combustion temperature and the CO combustion efficiency. As a result, when Util increases to 0.8, the amount of CO generated is approximately 2000 ~ 4000 ppm.

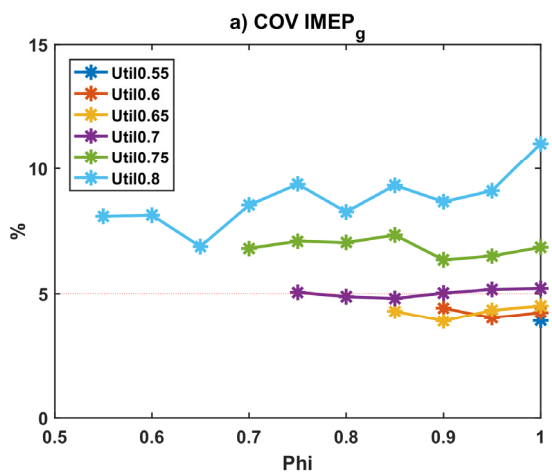

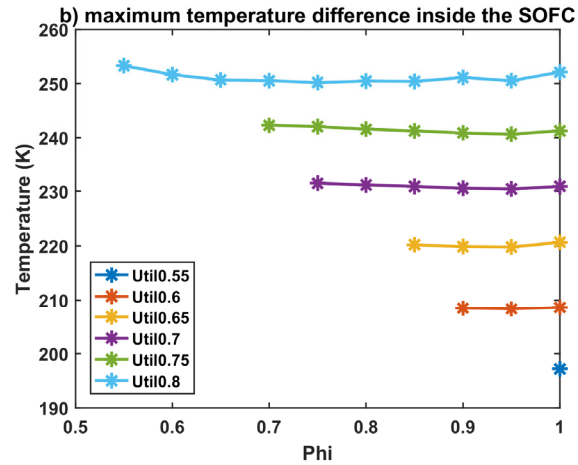

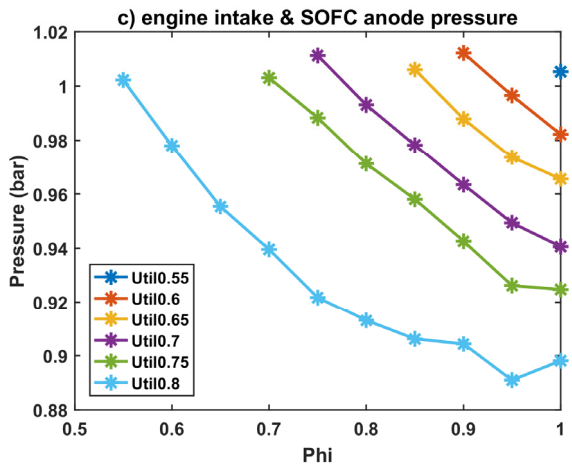

Figure 4.14. Constraints on system operation:

a) COV $IMEP_g$; b) maximum temperature difference inside SOFC;

c) engine intake and SOFC anode pressure

Figure 4.13 shows three factors that can affect the stability of system operation. The first factor is the combustion stability of the HCCI engine. As shown in figure 4.13 a), COV $IMEP_g$, which represents the instability of engine operation, increases when Util increases. The experimental results of chapter 3 have shown that the HCCI engine load ($IMEP_g$) and combustion instability (COV $IMEP_g$) are inversely proportional. Therefore, when Util increases, the engine load decreases and the COV $IMEP_g$

increases. Specifically, when Util is greater than 0.75, the value of COV $IMEP_g$ increases to greater than 5%, which is the upper limit of stable operation, and stable operation becomes difficult.

The second factor is the temperature gradient inside the SOFC. Figure 4.13 b) shows the maximum temperature difference inside the SOFC, and it is observed that the maximum temperature difference increases as Util increases. This is attributed to the fact that when Util increases, the amount of heat generated from the electrochemical reaction inside the SOFC increases. As mentioned before, this temperature difference produces thermal stress, which can cause cell failure. Therefore, the increase in Util has a negative effect on stable SOFC operation.

The third factor is the pressure difference between the SOFC anode and both the SOFC cathode and the outside of the SOFC. As mentioned before, the HCCI engine intake pressure is transmitted to the anode side of the SOFC; therefore, there can be a pressure difference between the SOFC anode and the SOFC cathode or the outside of the SOFC. This pressure difference produces mechanical stresses that can cause cell failure. It is therefore advisable to minimize this pressure difference by decreasing Phi to the maximum allowable for each Util. However, if Util is at least 0.8, decreasing Phi too much to match atmospheric pressure may undermine the CO combustion efficiency of the HCCI engine and increase the CO emissions, which may adversely affect system performance. Therefore, increases in Util at this point face a problem in that it is possible to increase the pressure difference between the anode and the cathode.

Therefore, when the other control parameters are fixed, as Util increases, the system total power and system efficiency generally increase, but system operation stability tends to decrease. Therefore, it is not preferable to increase Util over a certain standard.

4.3.2.3. System operation results at the design point

Based on the results of sections 4.3.2.1 and 4.3.2.2, the design point of system operation is selected as follows. First, BPR is set to 0; therefore, there is no stream separation. Then, Util is set to 0.7 in consideration of the stability of system operation. For Phi, 0.75, which is the value indicating full throttle, is selected. The following conditions are therefore selected as the design point: Util of 0.7, a BPR of 0, Phi of 0.75, a Fuel rate of 10.0 kW, CAD_{peak} of 372 CAD, $Util_{air}$ of 0.3, an SCR of 2.5, and RPM of 1800 rpm. Under these conditions, the SOFC produces 4.97 kW of power, and the HCCI engine produces 0.93 kW of power. Accordingly, the system efficiency reaches approximately 58.5%. Moreover, under these conditions, less than 1 ppm of NO_x is emitted and approximately 1300 ppm of CO is emitted. These results can be regarded as very promising considering that the size of the system currently being analysed is approximately 5 kW, which is relatively small for achieving high efficiency. The system operation results at this design point are summarized in detail in table 4.6.

Table 4.6. System operation results at the design point

Operating conditions		**Performance**	
Control parameters		**SOFC**	
Fuel rate (System fuel input)	10.0 kW	Average cell current density	0.382 A/cm^2
Util (SOFC fuel utilization factor)	0.7	Cell voltage	0.736 V
BPR (Bypass ratio to steam separator)	0	SOFC power	4.97 kW
Phi (Engine equivalence ratio)	0.75	SOFC efficiency	45.8%
CAD_{peak} (Engine combustion timing)	372 CAD	Power generation share of SOFC	84.3%
$Util_{air}$ (SOFC air utilization factor)	0.3	Temperature difference (Max)	231 K
SCR (Steam-to-carbon ratio)	2.5	**HCCI engine**	
RPM (Engine rpm)	1800 rpm	Engine net power	0.93 kW
Temperatures		Engine efficiency	25.1%
Anode inlet (stream 5)	774 K	Power generation share of HCCI	15.7%
Cathode inlet (stream 16)	970 K	NO_x emission (@ O_2 15%)	< 1 ppm
Anode outlet (stream 6)	1119 K	CO emission (@ O_2 15%)	1326 ppm
Cathode outlet (stream 17)	1131 K	COV $IMEP_g$	5.06%
Engine intake (stream 10)	673 K	**Total System**	
Engine exhaust (stream 11)	807 K	Total power (SOFC + HCCI)	5.89 kW
Pressures		Blower power	0.02 kW
Anode side (Engine intake)	1.01 bar	Total system net power	5.87 kW
Cathode side	1.01 bar	Total system net efficiency	58.5%
External reforming rates			
External reforming rate 1	15.2%		
External reforming rate 2	19.0%		
Total external reforming rate	34.2%		
External reformer 1 effectiveness	0.62		
External reformer 2 effectiveness	0.57		

4.4. Discussion

In section 4.3, we describe how the SOFC–HCCI engine hybrid system operates under varying control parameters. The results of the parametric study confirmed that when the system does not perform steam separation, that is, when BPR is 0, the overall system operation result is better. With respect to the engine equivalence ratio (Phi), it was confirmed that it should be less than 0.9 to decrease CO emissions and should be kept as low as possible to minimize the pressure difference between the SOFC anode and the SOFC cathode or the outside of the SOFC. For the fuel utilization factor of the SOFC, it was found that as it increases, the system efficiency tends to increase. Therefore, it was recommended that the fuel utilization factor of the SOFC (Util) should be as high as possible in a range that does not cause problems (e.g., concerning engine combustion efficiency, combustion stability, and temperature gradients inside the SOFC)

These tendencies can be summarized as system operation becomes more efficient as the dilution level of the engine intake gas increases unless the combustion efficiency of the engine is seriously deteriorated. This tendency illustrates the strength of the HCCI combustion strategy as the combustion strategy of the internal combustion engine used in the SOFC–HCCI engine hybrid system. In other words, the use of the HCCI combustion strategy has a very positive effect on the hybrid system efficiency because the HCCI engine can produce power successfully, even from intake gas with a large quantity of diluent.

The composition of the engine intake gas at the determined design point is shown in table 4.7. As shown in the table, the percentage of fuel components (H_2 and CO) in the engine intake gas is only 12.8%. According to other studies that have measured the flame speed of the H_2 and CO mixture with varying dilution levels, under the conditions shown in the table, the laminar flame propagation speed is expected to be only several

cm/s or nearly non-flammable.[56] Therefore, under these conditions, using spark ignition (SI) as the combustion strategy is expected to be very difficult. To use the spark ignition strategy, steam should be separated, and Phi would have to be maintained close to 1 by controlling the throttle. Because such control is thought to reduce system efficiency, the HCCI combustion strategy in the ICE as an SOFC bottoming cycle is more efficient in terms of system efficiency than the SI strategy.

Table 4.7. Composition of the HCCI engine intake gas (@ the design point)

H_2	10.8%	Fuel	12.8%
CO	2.0%		
H_2O	37.5%		
CO_2	8.9%	Diluent	78.6%
N_2	32.2%		
O_2	8.6%	Oxidant	8.6%

4.5. Conclusions

In this chapter, the operation of an SOFC-HCCI engine hybrid system was analysed by combining the experimental results from an HCCI engine with the simulation models of other components. Using the results of the analysis, the effects of HCCI engine operation on the operation of the hybrid system, especially the SOFC, were investigated. It was found that the SOFC in the hybrid system generally has an SOFC anode inlet gas characterized by a low external reforming rate (e.g., 30 ~ 40%) and low temperature (e.g., 750 ~ 800 K). Thus, the operating temperature of the SOFC is relatively low (e.g., ~ 900 K near the entrance of the SOFC). Therefore, it was confirmed that using an anode-supported type of SOFC is suitable for the hybrid system since this type can reduce the ohmic losses of the electrolyte, which would increase rapidly if the operating temperature were to be low. Additionally, due to these operation characteristics of the SOFC, values of control parameters should be determined while considering maximizing the external reforming rate.

Various system analyses were performed while varying three control parameters (Util, BPR, and Phi). Based on these results, the effects of each parameter were investigated, and the values of control parameters needed to achieve not only good performances but also the stability of system operation were confirmed. First, maintaining a low BPR, i.e., reducing the flow rate bypassed to the steam separator, enhances almost all system operation results such as the efficiencies of the SOFC and HCCI engine. In the case of Phi, maintaining a value of below 0.9 is better because the emission of CO rapidly increases beyond 0.9. When Phi is 0.9 or less, the total system power remains almost the same. However, maintaining a low Phi is preferable for stable system operation because it can reduce the mechanical stress of the cell, which is caused by the pressure difference between the anode and the cathode or the outside of the SOFC. In the case

of Util, it was found that when Util increases, the system efficiency generally increases, but the stability of system operation tends to decrease. Therefore, it is not desirable to increase Util beyond a certain point.

Based on these analyses, the design point of 5 kW-class SOFC–HCCI engine hybrid system was determined in considering system performance as well as operational stability. The determined point is as follows: Util of 0.7, BPR of 0, and Phi of 0.75. At this operating point, the SOFC and HCCI engine produce 4.97 kW and 0.93 kW of power, respectively, while generating less than 1 ppm of NO_x (@ O_2 15%). Consequently, the system efficiency reaches approximately 58.5%. However, approximately 1300 ppm of CO (@ O_2 15%) is emitted. Considering that the system being analysed is relatively small, approximately 5 kW, these results can be considered as promising results. From these results, the potential of the SOFC–HCCI engine hybrid system was validated. Additionally, at the design point, fuel components (H_2 and CO) represent only 12.8% of the engine intake gas, and the remaining 87.2% of the engine intake gas is filled with diluents and oxidants. This shows the strength of the HCCI strategy in the SOFC–ICE hybrid system because combusting this type of gas successfully by spark ignition is difficult due to the slow flame propagation speed.

Chapter 5
Experimental study of SOFC–HCCI engine hybrid system

5.1. Introduction

In chapter 4, the operation of the entire SOFC–HCCI engine hybrid system was analysed by combining the experimental results of HCCI engine and the simulation models of other components, including the SOFC. The significance of chapter 4 can be summarized as follows. First, chapter 4 investigated the operation characteristics of the SOFC under the hybrid system. Particularly, whether the SOFC can be operated successfully in the hybrid system was analysed. Second, system operations were analysed while varying the control parameters. Third, the ranges of the control parameters not only achieving successful performance but also enabling stable system operation. Based on the results of analyses, the design point of system operation was determined in the last part of chapter 4

However, the experiment of the entire system should be conducted to fully prove the feasibility of the SOFC–HCCI engine hybrid system. Therefore, in this chapter, the experiment of the entire SOFC–HCCI engine hybrid system is conducted to fully prove the feasibility of system concept. In the experiment, the experimental condition was chosen based on the design point of system operation determined in chapter 4.

The objectives of this chapter can be summarized as follows. The first objective is to analyse the feasibility of the system operation experimentally. Specifically, whether the HCCI engine can be operated by SOFC anode off-gas and whether the SOFC can be operated with having HCCI engine in the downstream are investigated experimentally. The second objective is to find out the problems in real operation, which cannot be

found in the simulation model. The system design and operation strategy to solve the problems, which are found in this chapter, are analysed in chapter 6 with more details. The third objective is to check the validity of assumption that made in the analyses conducted in chapters 3 and 4.

The main body of this chapter consists of three parts: experiment, results, and discussion. In section 5.2 (Experiment), the experimental setup and how the experiment was conducted are described in detail. Additionally, the experimental conditions of this chapter are explained in section 5.2. In section 5.3 (Results), first of all, a general overview of the 200-hour continuous operation results is provided. Also, the system operation results of major operating points in the 200-hour continuous operation are introduced. These results are compared with the result of chapter 4 to determine the difference between the simulation and experiment. In section 5.4 (Discussions), the problems of current system were identified based on the results of section 5.3. Therefore, problems to be solved for improving the system performance are summarized in the discussions.

5.2. Experiment

To prove the feasibility of the hybrid system, the experiment was conducted continuously over 200 hours. The HCCI engine used in the experiment was same as the HCCI engine experimented in chapter 3. The SOFC utilized in the experiment was 5 kW-class SOFC of MiCo corporation. The one-dimensional SOFC model mentioned in chapter 4 was validated with the experiment data of this SOFC. The external reformer developed by Chungnam National University for the hybrid system was used in the experiment.[49] These experimental apparatus are installed and combined to each other in Korea Institute of Machinery and Materials (KIMM). Therefore, the experiments were performed in KIMM. It should be noted that the experiments were conducted with researchers from the KIMM, Seoul National University, and MiCo corporation.

5.2.1. Experimental setup

5.2.1.1. Outline of experimental setup

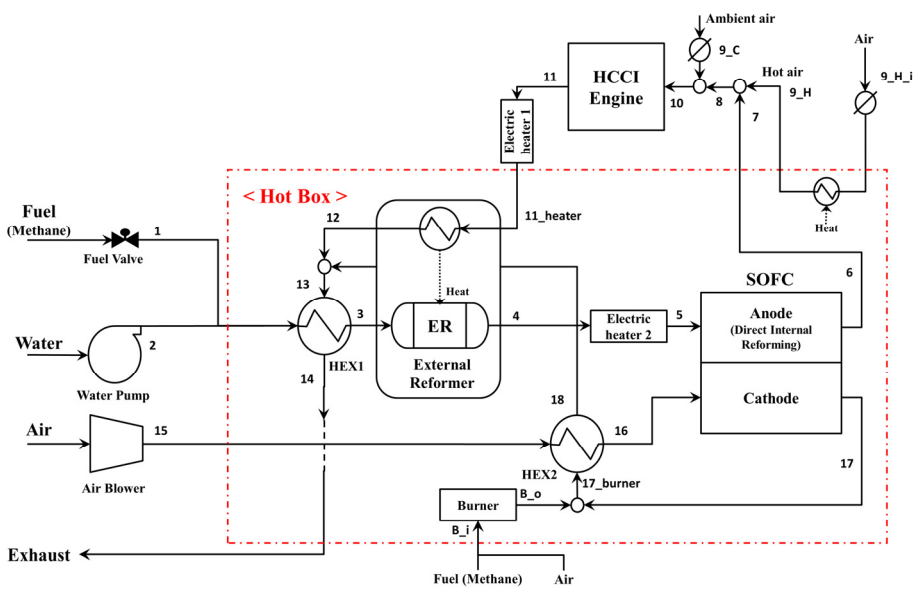

Figure 5.1. Schematic of the hybrid system conducted for the experiment

Figure 5.1 shows the schematic of the hybrid system which were constructed for the

experiment. The schematic shown in figure 5.1 is different from the schematic analysed in the above chapters for the following points.

First, the steam separator was eliminated based on the results of chapter 4, which show that system performance generally improves when BPR (bypass ratio to the steam separator) decreases.

Second, considering that there can be considerable amount of the heat loss in the experiment, the external reformer 2 was also eliminated. In chapters 2~ 4, the external reformer 2 utilized the excess heat of the SOFC anode off-gas to increase the external reforming rate. Because the first goal of the experiment in chapter 5 is to show the feasibility of system operation rather than achieving the maximum efficiency, to avoid the misfire inside the HCCI engine and to stably provide enough heat to achieve the HCCI combustion, it was decided to eliminate the external reformer 2 and to maintain the temperature of SOFC anode off-gas as much as possible. For a similar reason, electric heaters and a burner was added to provide the additional heat to make the operation of system stable.

Third, as shown in figure 5.1, all the system components except the HCCI engine and peripherals are installed in the hot box. Therefore, the hot box and the HCCI engine exchanges the gases.

Fourth, producing hot air part was added in the schematic considered in this chapter. Because of this part, air entrained into the HCCI engine is composed of ambient air and hot air. The hot air (200 ~ 300 ℃) was made from passing through the outer part of the hot box. This hot air is utilized to provide the necessary heat to achieve the HCCI combustion. Additionally, by changing the ratio of hot and ambient air, it was possible to control the combustion timing to the desired value.

Finally, to reduce the complexity of the experiment, methane instead of natural gas

was used for the fuel of the system, and MFCs instead of the fuel valve, the air blowers, and the throttles were utilized to supply the methane and air. Only air supplying for the burner was performed by the blower.

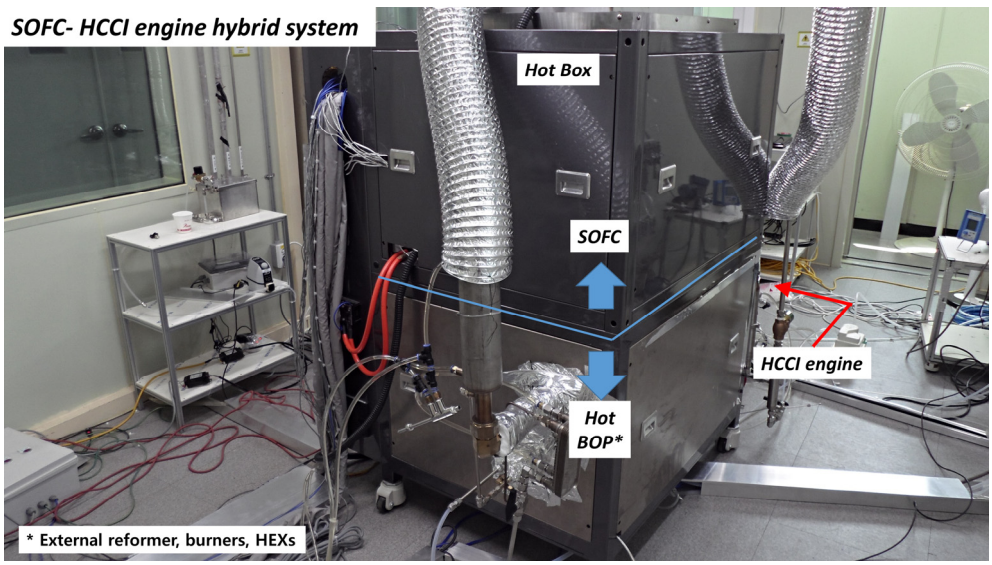

Figure 5.2. SOFC–HCCI engine hybrid system constructed for the experiment

Figure 5.2 shows the SOFC–HCCI engine hybrid system constructed in KIMM. As mentioned above, the system consists of the hot box and the HCCI engine. The hot box is divided into upper and lower parts. In the upper part, the SOFC is positioned and the hot BOP (balance of plant), such as the external reformer, the burner, and heat exchangers, are located in the lower part of the hot box. Therefore, the system inlet fuel and air are first supplied to the lower part, and then entered into the upper part (the SOFC). The outlet gases of the SOFC are supplied to the HCCI engine through passing the lower part of the hot box.

5.2.1.2. SOFC

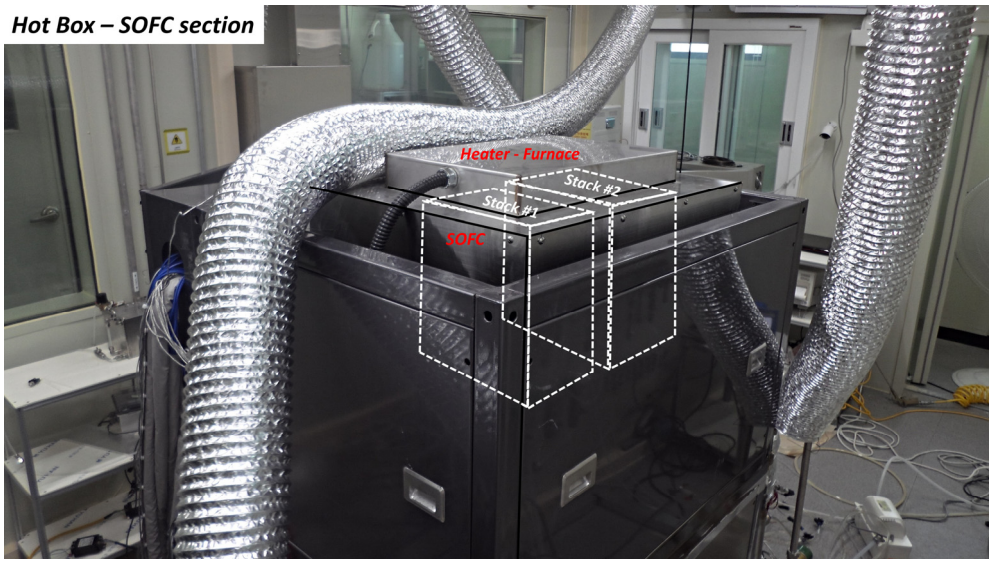

Figure 5.3. SOFC in the upper part of the hot box

Figure 5.3 shows the closer look of the upper part of the hot box. The upper part consists of two parts: the place for the SOFC stacks, and the electric heater (furnace) at the top of the SOFC.

For the SOFC, 5 kW-class SOFC of MiCo corporation, which consists of two parallelly-connected 2.5 kW-class SOFC stacks, was utilized. Each SOFC stack consists of serially-connected 80 cells. The electric heater was mainly used to raise the temperature of the SOFC during the start-up process, and was operated for stability of the stack if the situation requires heat even during the regular operation.

5.2.1.3. HCCI engine

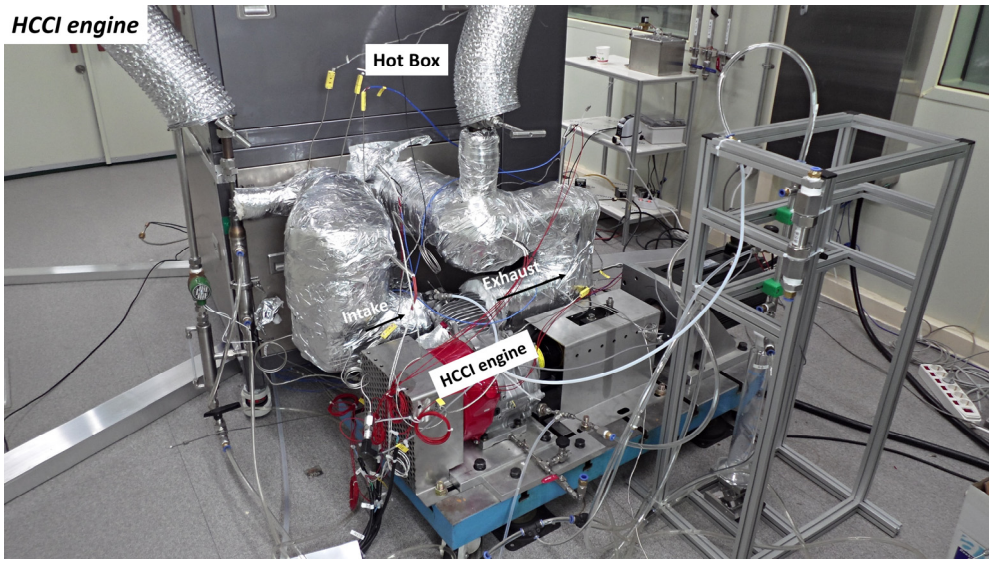

Figure 5.4. HCCI engine in the SOFC–HCCI engine hybrid system

Figure 5.4 shows the HCCI engine part of the hybrid system. As shown in the figure, HCCI engine was located in the outside of the hot box. Therefore, heat loss is generated from exchanging high temperature engine intake gas comes out of the hot box as well as high temperature engine exhaust gas entering the hot box. It can be seen that the lines between the hot box and the HCCI engine are insulated by the cerak-wool to the maximum to minimize the heat loss. The diameter of the cerak-wool was 200 ~ 250 mm.

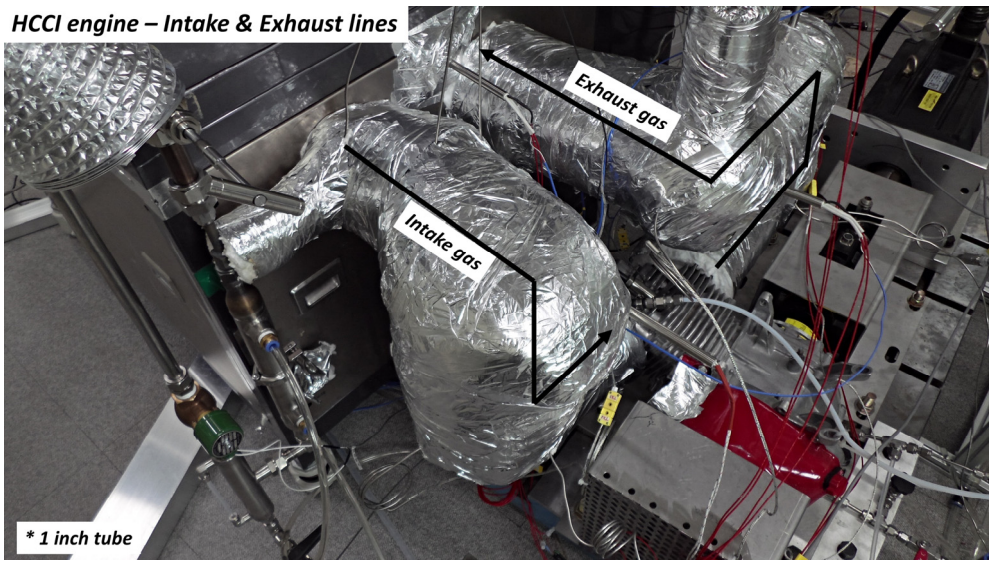

Figure 5.5. Intake and exhaust lines

Figure 5.5 shows the closer look of HCCI engine intake and exhaust gas lines. The black line indicated in figure 5.5 shows the gas line insulated by the cerak-wool. These gas lines were made of 1-inch lok type tubes.

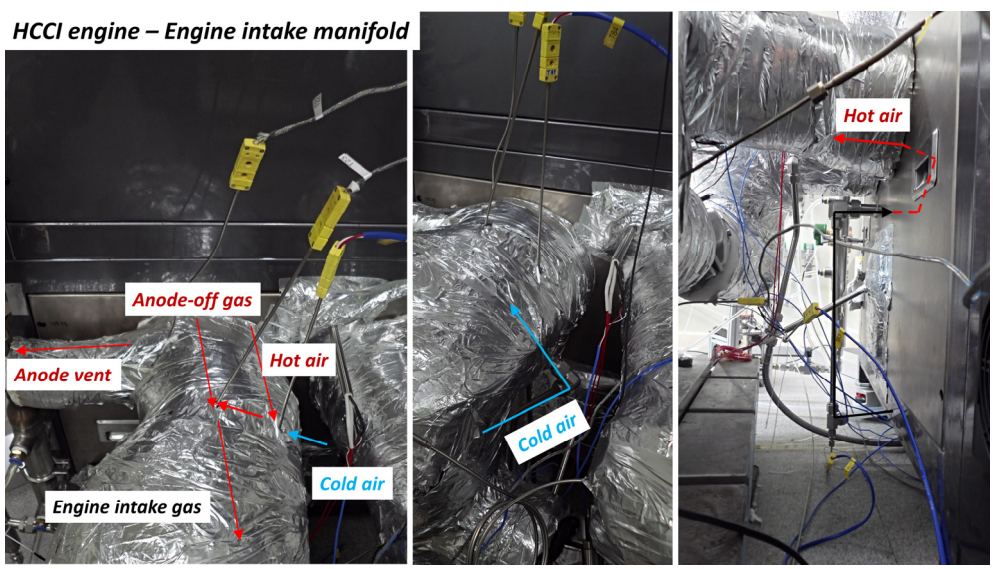

Figure 5.6. Intake part of the HCCI engine

Figure 5.6 shows the closer look of the intake part of the HCCI engine. As mentioned above engine intake gas is made of mixing the SOFC anode off-gas with the hot and

ambient air. The hot air is created by taking the outside air with the ambient temperature into the hot box for a while and then extracting the remaining heat from the hot box. Since the temperature of the intake gas has a significant influence on the combustion of the HCCI engine, the use of the hot and ambient air simultaneously greatly facilitates control of the combustion of the HCCI engine. The patent for this concept is in preparation because this is important idea in the control of the SOFC–HCCI engine hybrid system.

5.2.2. Experimental approach

The central goal of the experiment was to verify the feasibility of the SOFC–HCCI engine hybrid system. To accomplish this goal, the stable continuous operation of the hybrid system for over 200 hours was set as the first objective of the experiment.

The operating condition was determined based on the results of chapter 4. In particular, BPR is set as 0 and Phi is set as the lowest value in the possible range. According to chapter 4, increasing Util is helpful to increase the system efficiency, but to increase Util beyond 0.7 may make the stability of the operation worse. Therefore, Util was selected as 0.7 at the design point determined in chapter 4. Contrary to the result of chapter 4, Util is set as ~ 0.55 for the continuous operation presented in this chapter.

This was to achieve the stability of SOFC operation. When Util increases, the temperature gradient inside the SOFC cell increases, and accordingly, the thermal stress in the SOFC cell increases. To reduce the possibility of failure caused by this thermal stress, Util is set as lower value. Additionally, because the cells inside the stacks cannot be completely uniform and the manifolds cannot divide the inlet gases to completely the same amount for each cell, the voltage of each cell is different. For reference, table

5.1 shows the experimental results for the voltage of each module, which consists of 20 serially-connected cells (A stack is made of 4 modules), in the steady-state operation point. As shown in the table, the voltages of modules are different. The difference of the cell voltages is increased when the current increase. The difference between the cell voltages can induce the situation that some cell is in operation with higher Util than the set value, and this can cause the cell failure. Because of these reasons, the Util is set as ~ 0.55.

Table 5.1. Differences in voltages of SOFC modules

	Voltage [V]
Module 1	16.7
Module 2	17.3
Module 3	17.3
Module 4	16.8

However, to see the feasibility of operation with high Util, the experiment with high Util was also conducted in the very last part of experiment.

5.3. Results

5.3.1. 200-hour continuous operation

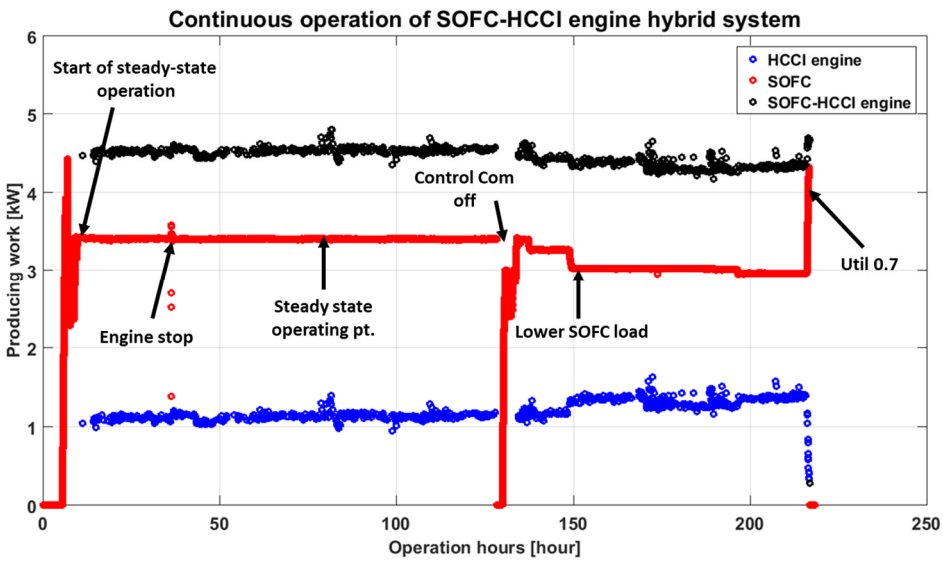

Figure 5.7. 200-hour continuous operation of SOFC–HCCI engine hybrid system

Figure 5.7 shows the result of 200-hour continuous operation of SOFC–HCCI engine hybrid system. Even though, there were two times of operation stop caused by malfunction of experimental apparatus, system operation was successfully performed over 200 hours. More specifically, for the first 120 ~ 130 hours, the system operated very stably. However, because of malfunction of control computers, the system was shut down suddenly near the 120 ~ 130 hours. Due to this event, the stack was suspected to be damaged, and the current of the SOFC was lowered approximately 6 A.

Though there was sudden stop, system operation results show that stable operation of the hybrid system was successfully achieved. From these results, it can be said that the feasibility of the SOFC–HCCI engine hybrid system was verified experimentally.

5.3.2. Steady- state operation results

In this section, the operation result at the steady-state operation point are described in detail. The detailed operation condition is summarized in table 5.2. As mentioned above, control parameter is chosen based on the results of chapter 4. However, the values of some control parameters are different from those of chapter 4. This can be attributed to the fact that the experiment in chapter 5 is not focused on maximizing system efficiency, unlike the values in chapter 4, but is focused on identifying the feasibility of the system operation for the first time. The values of the changed parameters are as follows.

First, the value of Fuel rate was 10.0 kW in chapter 4, but in the experiment in this chapter, 7.8 kW, which is about 22% lower than 10.0 kW, was chosen. This is for lowering the current of the SOFC to reduce the heat generated in the SOFC. When the amount of heat generated in the SOFC decreases, the temperature difference inside the SOFC cell decreases, and accordingly, the possibility of cell failure caused by thermal stress can be reduced.

SCR was also increased from 2.5 to 3. This was to prevent carbon coking problems that might occur in external reformers. However, this change is not good for system efficiency because it uses energy to make more water to steam. $Util_{air}$ was changed from 0.3 to 0.21. This change was also for reducing the temperature difference inside the SOFC cell. It is noted that CAD_{peak} was finely tuned to 371 CAD from 372 CAD.

Table 5.2. Operating conditions and performance at steady-state operation

Operating conditions		Performance	
Control parameters		**SOFC**	
Fuel rate (System fuel input)	7.8 kW	Average cell current density	0.227 A/cm^2
Util (SOFC fuel utilization factor)	0.54	Cell voltage	0.849 V
BPR (Bypass ratio to steam separator)	0	SOFC power	3.40 kW
Phi (Engine equivalence ratio)	0.71	Power generation share	74.3%
CAD_{peak} (Engine combustion timing)	371 CAD	**HCCI engine**	
$Util_{air}$ (SOFC air utilization factor)	0.21	Engine net power	1.18 kW
SCR (Steam-to-carbon ratio)	3.15	Engine efficiency	26.1%
RPM (Engine rpm)	1800 rpm	Power generation share	25.7%
Temperatures		NO_x emission (@ O_2 15%)	1 ppm
Anode inlet (stream 5)	986 K	CO emission (@ O_2 15%)	577 ppm
Reformer outlet (stream 4)	796 K	**Total System**	
Cathode inlet (stream 16)	992 K	Total power (SOFC + HCCI)	4.58 kW
Anode outlet (stream 6)	1010 K	System efficiency	59.0%
Cathode outlet (stream 17)	1014 K	Power of electric heater 1	1.07 kW
Engine intake (stream 10)	673 K	Power of electric heater 2	0.35 kW
Heater out (stream 11_heater)	807 K	Total power of electric heaters	1.42 kW
Pressures		LHV of burner fuel	3.04 kW
Anode side	1.03 bar		
Cathode side	1.04 bar		
External reforming rates			
External reforming rate	50.1%		

Table 5.2 shows the results of system operation. First, the HCCI engine was operated properly under the given condition. The LHV of the HCCI engine intake gas was 4.52 kW, and the HCCI engine produced a net indicated power of about 1.15 kW. Therefore, it can be confirmed that the gross and net efficiency of the engine is approximately 30.7%

and 26.7%, respectively. At this time, it was confirmed that NOx and CO was generated approximately 1 ppm (O_2 15%) and 577 ppm, respectively. Overall, the experimental results of HCCI engine does not differ significantly from the engine performance in chapters 3 and 4. Figures 5.8 and 5.9 show the in-cylinder pressure profile and pressure-volume profile, and it can be confirmed that HCCI combustion was achieved successfully.

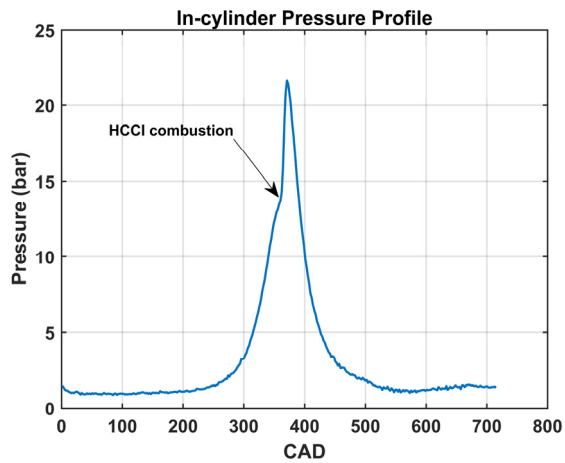

Figure 5.8. In-cylinder pressure profile of HCCI engine operation

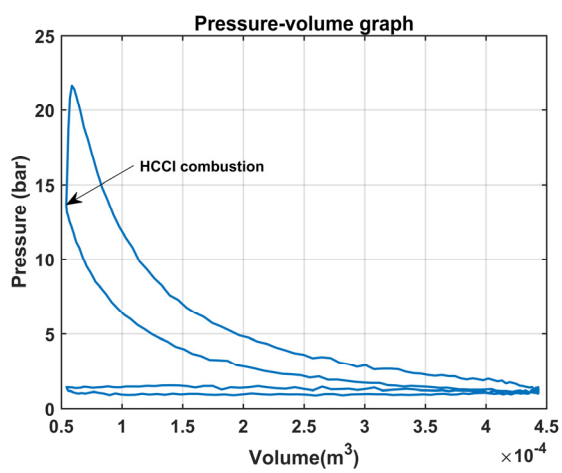

Figure 5.9. Pressure-volume graph of HCCI engine operation

As mentioned above, various points were considered for enabling stable operation of the SOFC. First, electric heaters were used in order to increase the temperature of engine exhaust gas and to adjust the external reforming rate to about 50% because the external reforming rate would be too low when reforming was performed by utilizing only the temperature of the engine exhaust gas. In addition, an additional electric heater was operated on the anode inlet side to further increase the temperature of the gas discharged from the external reformer. Similarly, a methane burner was operated on the cathode side to increase the temperature of the cathode inlet gas. All of the electric power consumed in electric heaters is about 1.42 kW, and the energy amount of CH_4 burned in burner reaches about 3.04 kW on LHV basis.

This additional heat supply helped the SOFC operation, resulting in about 3.4 kW of power production in the SOFC. The current, the voltage, the average current density, and the cell voltage were 50.1 A, 68.0 V, 0.227 A / cm^2, and 0.849 V, respectively.

In this operating point, the integrated operation of SOFC and HCCI engine was confirmed to be stable. At this time, it was confirmed that total produced power from the SOFC and the HCCI engine is ~ 4.58 kW and achieves about 59.0% efficiency, if the efficiency is calculated based on the amount of CH_4 fuel (7.8 kW) supplied to produce power in both devices.

Taking the power consumption in electric heaters and the amount of energy of the addition of CH_4 in the burner into account, the system efficiency is significantly decreased. However, considering that this experiment was conducted not to maximize the efficiency but to prove the feasibility of the system operation, and considering that the experiment was made through the prototype rather than the optimized product, it is expected that the changes in the system design and system control can improve the system performance.

5.3.3. Oscillation caused by the HCCI engine

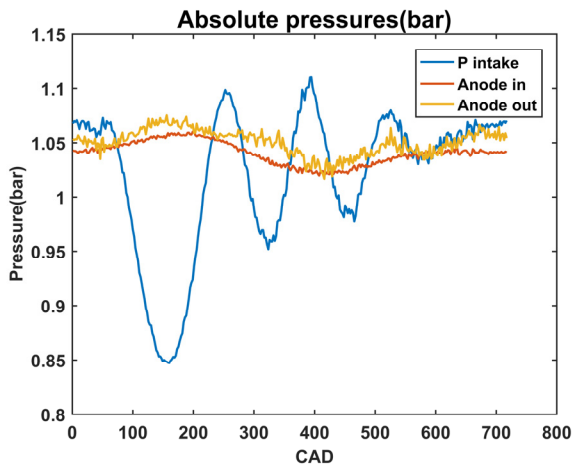

Figure 5.10. Pressures at the engine intake and the anode side of the SOFC

The internal combustion engine does not make steady continuous flow but has a batch process that sucks and burns gas at every cycle. This creates a pressure oscillation in the HCCI engine intake side. Therefore, it was worried that this pressure oscillation may harm the SOFC operation.

However, as shown in figure 5.11, it was confirmed that the pressure oscillation at the HCCI engine intake manifold resulting from the intake process of the HCCI engine is not transferred to the SOFC anode side dominantly. This is because the flow paths between the HCCI engine intake manifold and the SOFC anode side act as a damper to this oscillation and reduce the oscillation.

Therefore, the pressure oscillation caused by the HCCI engine operation can be considered not to cause significant problems in the operation of the SOFC. In addition, if the RPM increases further and the time it takes for one engine cycle is further reduced, this oscillation is expected to be further reduced.

5.3.4. Measurements of the compositions of anode inlet, anode outlet, and engine exhaust gases

To further analyze the state of system operation, the compositions of the anode inlet, anode outlet (anode off), and engine exhaust gases were measured by the gas chromatography. Through these measurements, the state of system operation was identified further, and the validities of assumptions made in chapters 3 and 4 to estimate the compositions of anode inlet, anode outlet, engine exhaust gases, were investigated.

Table 5.3. Measured composition of anode inlet gas (dry basis)

H_2	67.8%
CO	3.4%
CO_2	14.3%
CH_4	14.5%

First, the composition of the anode inlet gas was measured in dry basis, and the measured values are shown in table 5.3. To identify the temperature of equilibrium that makes similar composition of anode inlet gas, the compositions of equilibrium while varying the temperature are shown in figure 5.12.

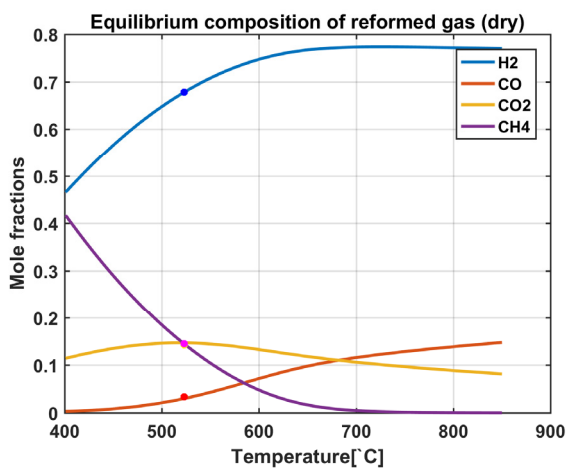

Figure 5.11. Composition of the reformed gas with variation of temperature

In the figure, the dots are the measured value and the line shows the equilibrium composition at each temperature. It is shown that the lines are in very good agreement with the dots (measured value) when the temperature is 523 ℃ (external reforming rate 50.1%). At this time, the measured temperature of the cold gas side outlet gas of the external reformer was 540 ℃, so that, as assumed in chapters 3 and 4, the reformer outlet gas was emitted in the equilibrium of almost similar temperature to the temperature of the reformer outlet gas. This is because, the reformer is filled with a sufficient amount of catalyst, and the gas hourly space velocities of the external reformers are small enough. Therefore, the assumptions that made for estimating the compositions of anode inlet gas is confirmed to be valid.

Table 5.4. Measured composition of anode outlet gas (dry basis)

	Measured	Estimated
H_2	61.8%	61.8%
CO	10.2%	10.0%
CO_2	28.0%	28.2%
CH_4	0.0%	0.0%

Table 5.4 shows the compositions of anode outlet gas. In chapters 3 and 4, when estimating the anode outlet gas (or anode off-gas), which is the fuel of engine, it was assumed that all the CH_4 in the SOFC is reformed and there is no CH_4 in the anode off-gas. Additionally, it is assumed that the anode off-gas is discharged in equilibrium composition of 750 ℃. The temperature of equilibrium, which makes similar composition of anode off-gas to the measured composition on the left side of table 5.4, is calculated as 765 ℃, which is very similar to 750 ℃. Therefore, it can be confirmed that assumptions made in chapters 3 and 4 when determining the anode off-gas composition were valid.

Table 5.5. Measured composition of engine exhaust gas (dry basis)

	Measured	Estimated*
H_2	-	0.0%
CO	-	0.0%
CO_2	13.3%	13.9%
N_2	67.2%	68.0%
O_2	19.5%**	18.1%

* Estimated composition is calculated from the assumption of complete combustion

** O_2 composition was inversely calculated from measured values of other components

Table 5.5 shows the composition of engine exhaust gas. In chapters 3 and 4, it was assumed that H_2 is not left but all combusted in the HCCI engine. As shown in the left side of table 5.5, H_2 was not measured at all in the engine exhaust gas. Therefore, the assumptions made in chapters 3 and 4 can be regarded as reasonable. Also, the measured exhaust gas composition was very similar to the composition calculated by assuming complete combustion from the amount of system inlet fuel, steam and air. Therefore, it can be confirmed that the measurement was performed reliably.

5.4. Discussion

The biggest difference between the experimental results of entire SOFC–HCCI engine hybrid system and the results of the system analysis conducted in chapter 4 is the amount of heat loss from the various system components, including the SOFC.

In particular, the heat loss from the SOFC was calculated to be approximately 1.56 kW at the steady-state operation point, which is about a half of the produced power (~3.4 kW) from the SOFC. Considering that this experiment is performed by using the prototype rather than the optimized product, it is expected that the heat loss from the SOFC and the other system components can be simply further reduced by optimizing the insulation of inside and outside of the hot box.

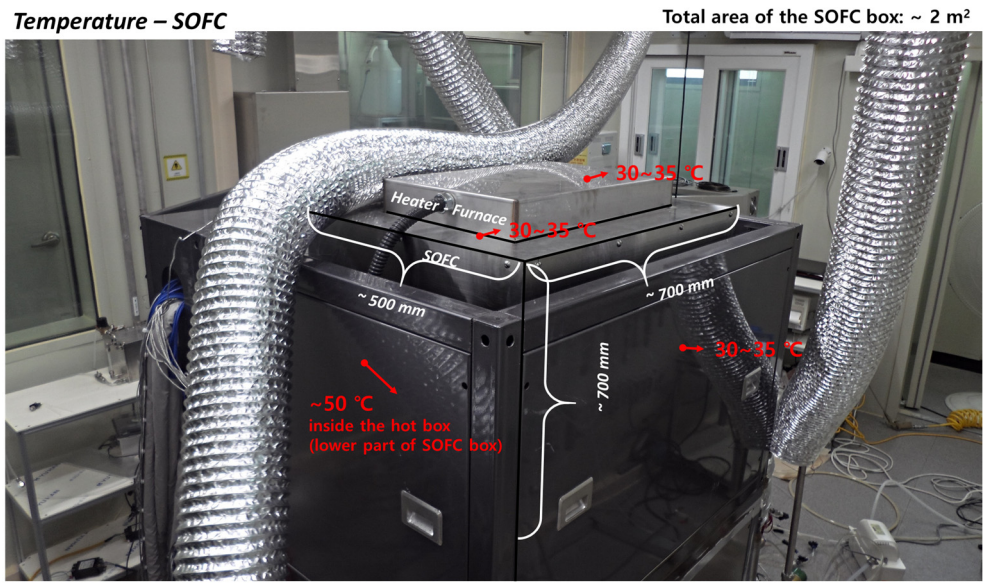

Figure 5.12. Temperatures of points at the surface of the SOFC box.

Figure 5.12 shows the temperatures of points at the surface of the SOFC box. As shown in the figure, the surface temperatures are approximately 30 ~ 50 ℃. Total area of the surface that faces the convection by the air is approximately 2 m^2. Because the temperature of the SOFC is the highest in the system, and the area of the surface to the power generation capacity is relatively large, much of the heat loss is expected to be

generated from this part.

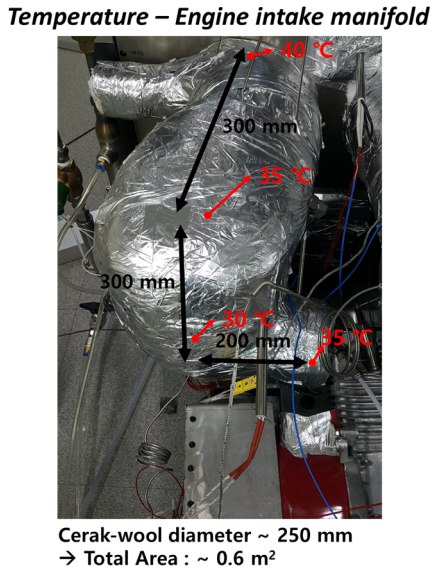

Figure 5.13. Temperatures of points at the surface of the engine intake manifold

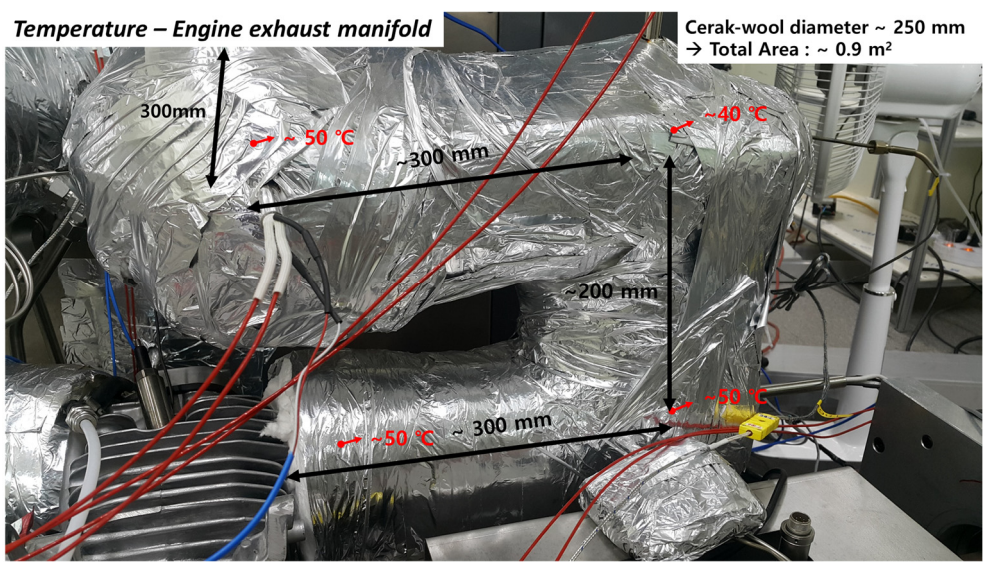

Figure 5.14. Temperatures of points at the surface of the engine exhaust manifold

Meanwhile, figures 5.13 and 5.14 show the temperatures of points at the surfaces of engine intake and exhaust manifold. As shown in the figures, the temperatures of the

surfaces of engine intake and exhaust manifolds are also 30 ~ 50 ℃. In particular, the temperatures of exhaust manifold are approximately 40 ~ 50 ℃, and the temperatures of intake manifold are approximately 30 ~ 40 ℃. The area of the surfaces of intake and exhaust manifolds are approximately 0.6 m^2 and 0.9 m^2, respectively. Therefore, the it can be expected that there is a similar amount of heat loss in engine intake and exhaust manifolds to the case of the SOFC box. Therefore, reducing the heat loss from exchanging gases between the hot box and the HCCI engine is also important. Reducing heat loss can be acquired simply by increasing the insulation thickness. More fundamentally, lowering the temperatures of engine intake and exhaust gases by increasing the compression ratio of the HCCI engine can be considered as the option to reduce the heat loss from this area. This method is analysed in detail in chapter 6.

Finally, it is interesting to note that for reducing the heat loss and increasing the system efficiency, the SOFC must be designed to sustain the temperature difference inside the SOFC cell because the decrease in the heat loss from the SOFC may increase the temperature difference inside the SOFC cell. Therefore, it can be said that the ability to sustain the bigger temperature difference inside the SOFC is essential to increase the system efficiency in the SOFC–HCCI engine hybrid system. Additionally, if this is possible, the system efficiency can be expected to increase further through control such as additionally increasing Util as well as $Util_{air}$.

5.5. Conclusions

In chapter 5, the experimental results of the entire SOFC-HCCI engine hybrid system are presented. Especially, the first 200-hour continuous operation of SOFC-HCCI engine hybrid system was performed, and the feasibility of the hybrid system was verified. Experimental results show that the system can operate relatively constantly during 200 hours of operation. As a result of the steady-state operation, it was found that the SOFC and HCCI engines produced power approximately 3.40 kW and 1.18 kW, respectively. Total system power was 4.58 kW; the system efficiency reaches to 59.0% when calculated from dividing this amount of power by the amount of system fuel input (7.8 kW).

The effect of pressure oscillation caused by HCCI engine on the anode side of the SOFC was analysed also in this chapter. It was confirmed that the pressure oscillation caused by the HCCI engine is canceled much when it comes to the SOFC anode because the flow path between the engine intake and the SOFC acts as a damper. This confirms that the adverse effect of pressure oscillation on SOFC is negligible.

Additionally, the compositions of the anode inlet, the anode outlet (anode off), and engine exhaust gases were measured by gas chromatography and it was confirmed that the assumptions made in chapters 3 and 4 to estimate the compositions of anode inlet, anode outlet, and engine exhaust gases were valid.

However, in the experiment of the hybrid system described in this chapter, electric heaters were used at the engine exhaust gas side and the anode inlet side to raise the temperature of the anode inlet gas and a burner was utilized to increase the temperature of cathode inlet gas for the stability of SOFC operation. Considering both the amount of power consumed in the electric heaters used and the amount of fuel injected into the burner, the system efficiency is significantly reduced. The major reason to decrease the

efficiency to this extent is the large amount of heat loss from the SOFC and the hot box.

Because the experiment of this chapter was conducted not to achieve the highest efficiency but to investigate whether the operation of the SOFC-HCCI engine hybrid system was possible and the experiment was conducted with the prototype rather than the optimized product, the amount of heat loss can be reduced much more by optimizing the system design as well as the system operating conditions. The methods and the system design to reduce the heat loss and to increase the efficiency are analysed in more details in chapter 6.

Chapter 6
Numerical study for the optimization of system design

6.1. Introduction

According to the results of chapters 3 ~ 5, following three issues should be considered to improve the system performance.

Issues

1. Increasing the amount of heat supplied to the SOFC by decreasing the heat loss.
2. Eliminating the CO emission for the system with near-zero pollutant emission.
3. Achieving the stability of operation while increasing the fuel utilization factor of the SOFC.

In this chapter, the system designs and the methods to resolve above issues and to improve the system performance are introduced. Additionally, each system design or method is analysed quantitively to expect the effect of the change. Among the various methods, following three methods are proposed in this chapter.

Methods

1. Additional catalytic oxidizer
2. Heat recovery from engine coolant
3. Variations of the compression ratio of the HCCI engine

It is noted that these three methods are all related to the HCCI engine part of the system. The changes of design related with the SOFC for the further improvements of system performance are remained as the future work of this dissertation. Figure 6.1

shows the three methods with the system schematic.

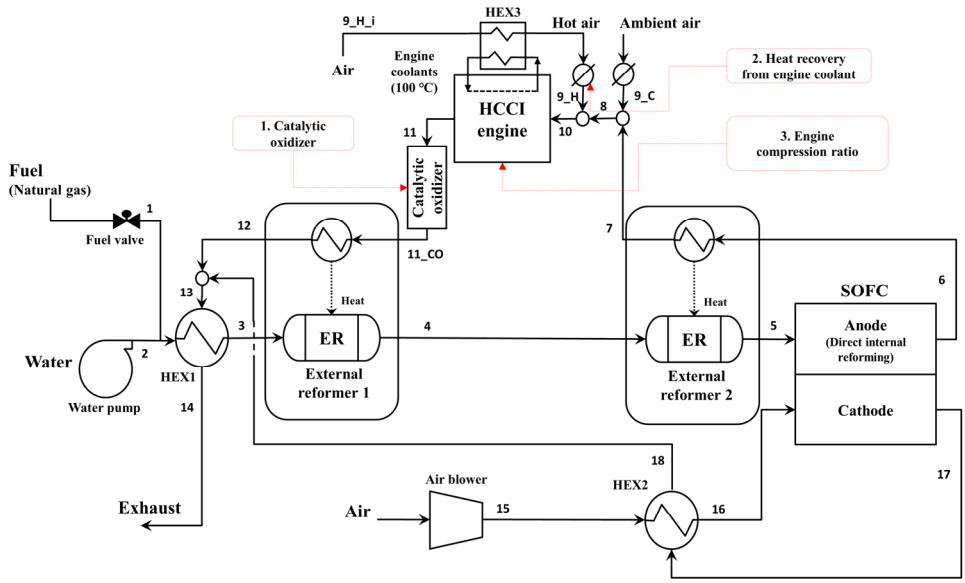

Figure 6.1. System design to improve the system performance

In order to confirm the effects of the methods 1 and 2, the methodology used in chapter 4 was used because the effect of methods 1 and 2 can be analysed without the changes in the HCCI engine; thus, the experimental results of the HCCI engine can be utilized in these cases.

On the other hand, the effect of the method 3 was investigated with the simulation results of the HCCI engine because it is difficult to experiment the HCCI engine while varying the engine geometry freely. The simulation model of the HCCI engine, which is well validated with the experimental results of the HCCI engine, was constructed for this purpose.

For these purposes, the main body of this chapter consists of three parts: methodology, results, and discussion. In section 6.2 (Methodology), the methodologies to assess the effect of each method to improve the system performance are introduced. Additionally, the simulation model of the HCCI engine to assess the effect of compression ratio variations is described. In section 6.3 (Results), the results of analysis on the effect of

each method to improve the system performance are introduced. From the results of the analyses, the final design to achieve the best performance is determined. In section 6.4 (Discussion), implicit implications of increment in compression ratio are discussed.

6.2. Methodology

6.2.1. Outline of the methodology

As mentioned above, the effects of methods 1 and 2 were analysed by the methodology described in chapter 4. The experimental results of the HCCI engine was integrated with the simulation models of other components to expect the system operation. Therefore, it is encouraged to refer to section 4.2 to know the methodology.

The effect of method 3 was analysed by utilizing the simulation model of HCCI engine. Zero-dimensional simulation model was constructed for the HCCI engine. MATLAB, developed by Mathworks, was used to construct the simulation model. Additionally, the Cantera thermodynamic toolbox and the GRI 3.0 mechanism were used with MATLAB.[39, 45] The simulation model of HCCI engine is described in detail in section 6.2.2.

For assessing the system operation results with this HCCI engine simulation model, the algorithm explained in figure 4.5 was utilized similarly. The simulation results of the HCCI engine instead of the experimental results of the HCCI engine was used in the algorithm.

6.2.2. Simulation model of HCCI engine

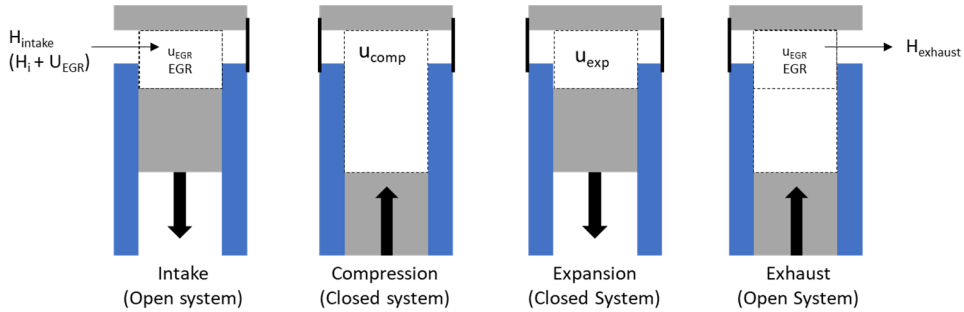

Figure 6.2. HCCI engine simulation model description

Figure 6.2 shows the description of HCCI engine simulation model. For the modelling, the literature [57] was primarily referred to. Four processes (intake, compression, expansion, and exhaust) of the engine cycle was modelled. For compression and expansion processes, in-cylinder gas is modelled as closed system and a series of ordinary differential equations (ODEs) described below were employed for the modelling.

$$\dot{\theta} = n \quad (6.1)$$

First, the crank angle degree (θ) is calculated from pre-determined engine rpm (n).

$$\dot{V} = \frac{\pi}{4}\mathrm{B}^2 a\dot{\theta}\left(\sin\theta + \frac{a\sin\theta\cos\theta}{\sqrt{l^2 - a^2\sin^2\theta}}\right) \quad (6.2)$$

The in-cylinder volume (V) is calculated from crank angle degree and engine geometry.[23] For reference, B, a, and l indicate the bore, the crank radius, and the connecting rod length, respectively.

$$\dot{\mathrm{U}} = \dot{Q} - \mathrm{P}\dot{V} \quad (6.3)$$

$$\mathrm{m}C_V\dot{T} + \sum_i \dot{m}_i u_i - \dot{Q} + \mathrm{P}\dot{V} = 0 \quad (6.4)$$

$$\dot{T} = \frac{1}{mC_V}\left(\dot{Q} - \mathrm{P}\dot{V} - \sum_i \dot{m}_i u_i\right) \quad (6.5)$$

Form the first law of thermodynamics, the in-cylinder temperature can be calculated. For calculating the change in mass of each molecule, which is caused by chemical reaction, in in-cylinder gas, the GRI 3.0 mechanism is utilized.

For the heat transfer to the outside ($\dot{Q}$), Woschni's correlation is employed.[23] A scaling factor is also employed to validate the simulation model with experimental results.

$$\mathrm{P} = \frac{mRT}{V} \quad (6.7)$$

Lastly, the in-cylinder pressure is calculated from the equation of state for ideal gas.

For gas exchanging processes, which are intake and exhaust processes, lumped heat transfer model and the pumping loss was calculated. For calculation of heat transfer, Woschni's correlation was employed again. In addition, as shown in the figure 6.2, the effect of internal exhaust gas recirculation (or residual gas) is also considered in the model. Through these considerations, it was attempted to predict the temperature of engine intake and exhaust gas more precisely, which are important parameters in assessing the system operation results.

The simulation model was validated with the engine experimental results of chapter 3. The following figures show validation, which confirms that the engine model can simulate the experimental conditions well. For reference, in the following graphs, the lines show the results of simulation, and the dots show the results of experiment. However, it should be noted that it is difficult to simulate the pressure rise rate or CO emission similar to experimental result since the engine model is zero-dimensional model. For these reasons, the simulation model has limitation in simulating extremely diluted cases, which cause large difference in the combustion efficiency between simulation and experiment. In addition, it should be also noted that this model has a limitation in simulating cycle-to-cycle variations.

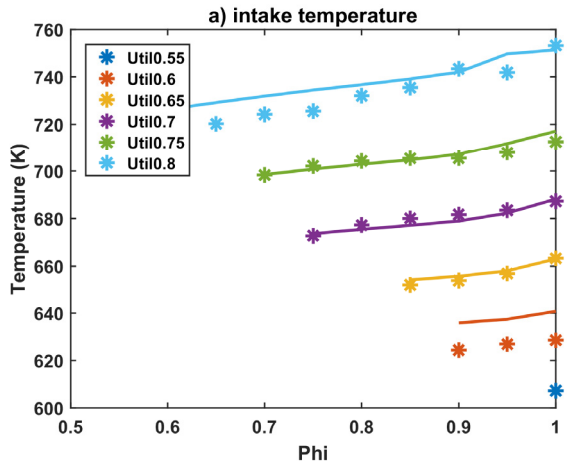
a) intake temperature
Util0.55
Util0.6
Util0.65
Util0.7
Util0.75
Util0.8
Temperature (K)
760
740
720
700
680
660
640
620
600
0.5
0.6
0.7
0.8
0.9
1
Phi

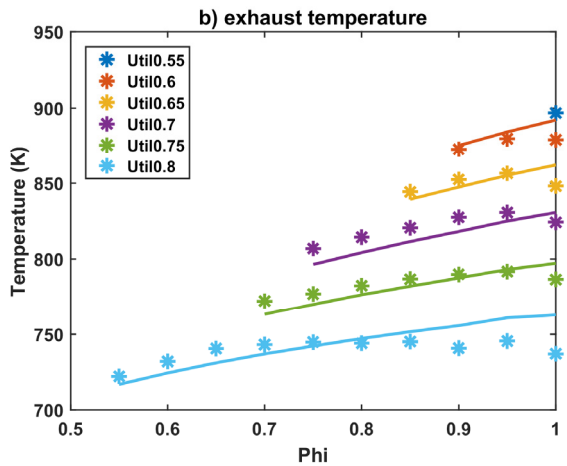
b) exhaust temperature
Util0.55
Util0.6
Util0.65
Util0.7
Util0.75
Util0.8
Temperature (K)
950
900
850
800
750
700
0.5
0.6
0.7
0.8
0.9
1
Phi

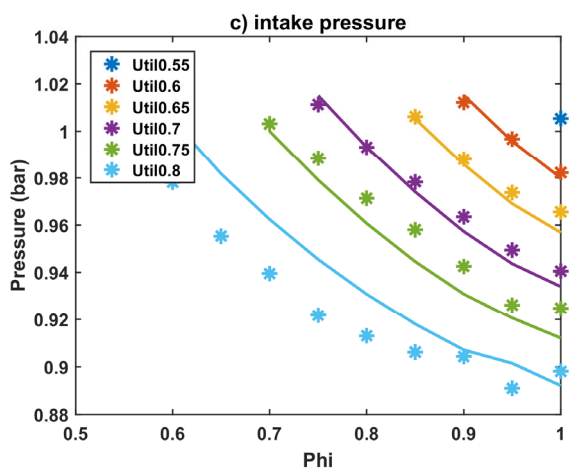
c) intake pressure
Util0.55
Util0.6
Util0.65
Util0.7
Util0.75
Util0.8
Pressure (bar)
1.04
1.02
1
0.98
0.96
0.94
0.92
0.9
0.88
0.5
0.6
0.7
0.8
0.9
1
Phi

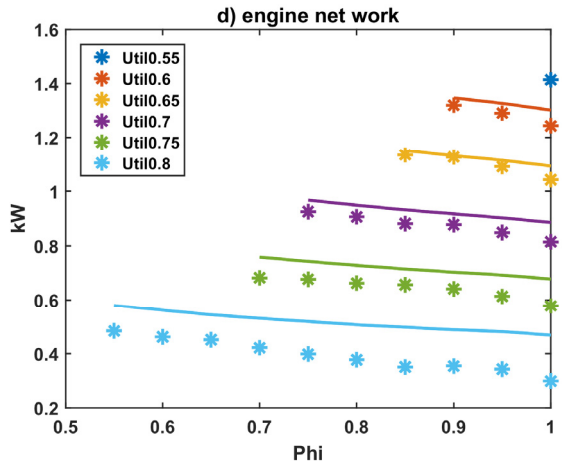

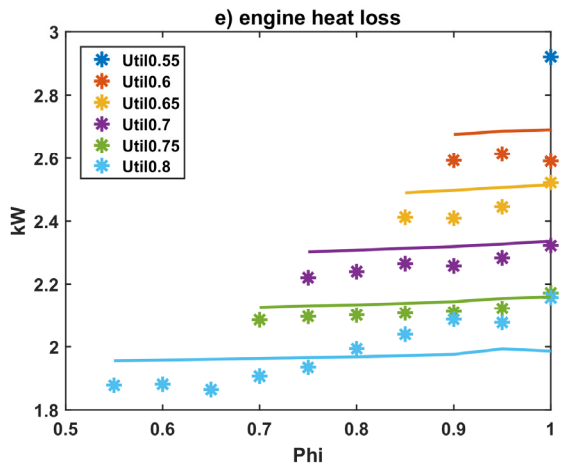

Figure 6.3. Validation results of engine simulation model: a) intake temperature; b) exhaust temperature; c) intake pressure; d) engine net power; e) engine heat loss

6.3. Results

6.3.1. Additional catalytic oxidizer

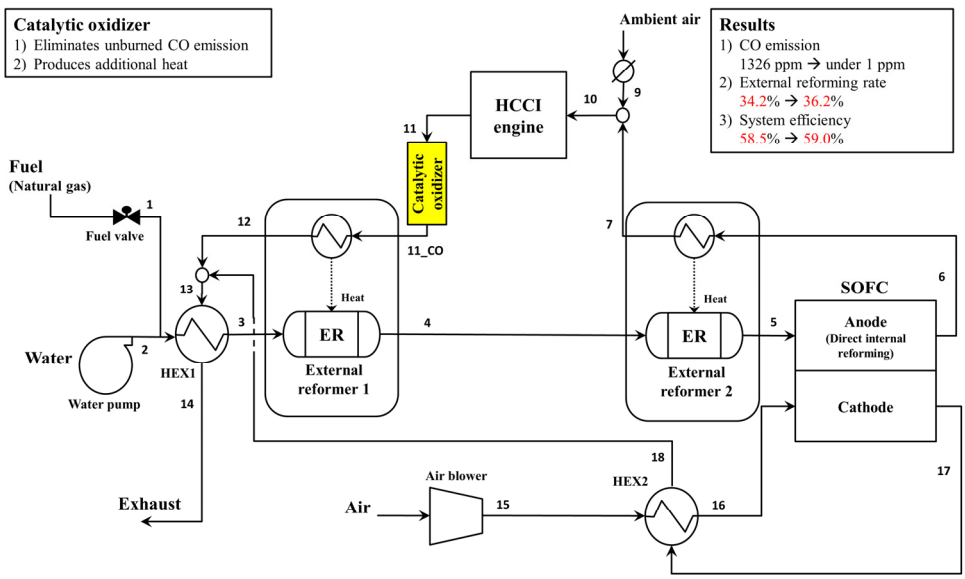

Figure 6.4. Schematic of the hybrid system (method 1)

Figure 6.4 shows the schematic of the hybrid system with an additional catalytic oxidizer. The additional catalytic oxidizer in the downstream of the HCCI engine helps to resolve the issues 1 and 2, which are listed in section 6.1. Through oxidizing the CO emission by installing the simple catalytic oxidizer, the SOFC–HCCI engine hybrid system can become the system that generates near-zero pollutant emission because there is no other pollutant emission, such as NO_x, in the engine exhaust gas. Additionally, from the oxidation of CO, the additional heat can be generated and supplied to the external reformer. Therefore, the external reforming rate can be increased, and accordingly, the system efficiency can be improved further.

Table 6.1 shows the results of system operation with an additional catalytic oxidizer at the design point determined in chapter 4. For reference, the design point is as follows: Fuel rate of 10.0 kW, SCR of 2.5, $Util_{air}$ of 0.3, Util of 0.7, BPR of 0, Phi of 0.75, CAD_{peak} of 372 CAD, and RPM of 1800 rpm.

Table 6.1. Changes in results of system operation (method 1)

System operating		Performance	
Temperatures		**SOFC**	
Anode inlet (stream 5)	781 K (+7)	Average cell current density	0.382 A/cm^2
Cathode inlet (stream 16)	973 K (+3)	Cell voltage	0.743 V (+0.007)
Anode outlet (stream 6)	1123 K (+5)	SOFC power	5.01 kW (+0.05)
Cathode outlet (stream 17)	1134 K (+3)	SOFC efficiency	46.0% (+0.2)
Engine intake (stream 10)	673 K	Power generation share of SOFC	84.4% (+0.1)
Engine exhaust (stream 11_{CO})	820 K (+13)	Temperature difference (Max)	231 K
		Temperature of SOFC body	903 K (+4)
		HCCI engine	
		CO emission (@ O_2 15%)	< 1 ppm
		NO_x emission (@ O_2 15%)	< 1 ppm
External reforming rates		Net power	0.925 kW
External reforming rate 1	16.6% (+1.4)	**Total System**	
External reforming rate 2	19.6% (+0.6)	Total power (SOFC + HCCI)	5.94 kW (+0.05)
Total external reforming rate	36.2% (+2.0)	Blower power	0.02 kW
External reformer 1	0.65 (+0.03)	Total system net power	5.92 kW (+0.05)
External reformer 2	0.59 (+0.02)	Total system net efficiency	59.0% (+0.5)

In the table, the changes in the results of system operation are indicated in parentheses. As shown in the table, CO emission is expected to be reduced to under 1 ppm. Because the conversion efficiency of CO for the catalytic oxidizer generally reaches over 90% when the temperature is 300 ℃ or more, almost all of the CO is expected to be eliminated at the current engine exhaust temperature (~ 540 ℃).[23] Therefore, the pollutant emissions of the system can be at near-zero as shown in the table. For reference, the remaining amount of CO was calculated as the equilibrium composition

of the engine exhaust gas.

Because of the heat generated from the oxidation of CO, the engine exhaust temperature increases. Accordingly, the total external reforming rate also increases approximately 2.0%. The increase in external reforming rate also raise the temperature of the SOFC and improve the performance of the SOFC. As shown in the table, the cell voltage and produced power of the SOFC are expected to be raised approximately 0.007 V and 0.05 kW, respectively. Overall, the system efficiency can be reached to 59.0% by the increase of 0.5%.

6.3.2. Heat recovery of engine coolant

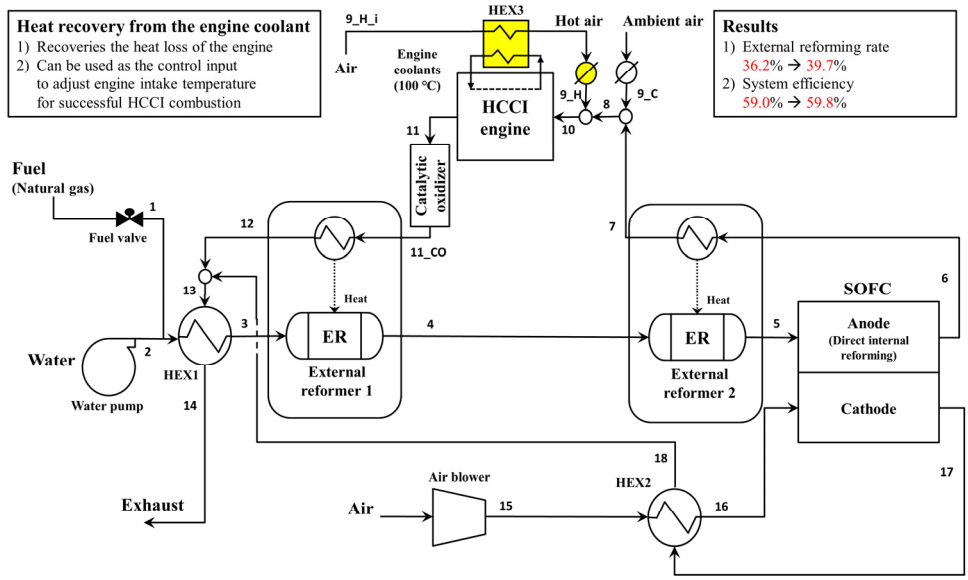

Figure 6.5. Schematic of the hybrid system (methods 1 and 2)

Figure 6.5 shows the schematic of the hybrid system with an additional catalytic oxidizer as well as the heat recovering part. The excess heat of engine coolant is recovered in this heat recovering part. By heat exchanging the air with the engine coolant, the hot air (~ 80 ℃) can be made. For reference, the effectiveness of the HEX3 (in figure 6.5) is assumed to be 0.85. The temperature of engine coolant is set as 100 ℃ because the temperature of oil was maintained near 100 ℃ in every experiment conducted in chapters 3 and 5.

The heat of SOFC anode off-gas could be more utilized for external reforming in the external reformer 2 if the temperature of air increases. Therefore, this heat recovering part can increase the external reforming rate, and accordingly, the system efficiency. Therefore, it can be said that this part helps to resolve the issue 1 listed in section 6.1. Additionally, this kind of double throttle system is considered to be valuable because it helps to control the HCCI combustion by changing the temperature of engine intake gas as shown in chapter 5.

Table 6.2. Changes in results of system operation (methods 1 and 2)

System operating		Performance	
Temperatures		**SOFC**	
Anode inlet (stream 5)	794 K (+13)	Average cell current density	0.382 A/cm^2
Cathode inlet (stream 16)	978 K (+5)	Cell voltage	0.755 V (+0.012)
Anode outlet (stream 6)	1130 K (+7)	SOFC power	5.09 kW (+0.08)
Cathode outlet (stream 17)	1140 K (+6)	SOFC efficiency	46.4% (+0.04)
Engine intake (stream 10)	673 K	Power generation share of SOFC	84.6% (+0.2)
Engine exhaust (stream 11_{CO})	820 K	Temperature difference (Max)	230 K (-1)
		Temperature of SOFC body	910 K (+7)
		HCCI engine	
		CO emission (@ O_2 15%)	< 1 ppm
		NO_x emission (@ O_2 15%)	< 1 ppm
External reforming rates		Net power	0.925 kW
External reforming rate 1	16.9% (+0.3)	**Total System**	
External reforming rate 2	22.9% (+3.3)	Total power (SOFC + HCCI)	6.02 kW (+0.08)
Total external reforming rate	39.7% (+3.5)	Blower power	0.02 kW
External reformer 1	0.66 (+0.01)	Total system net power	6.00 kW (+0.08)
External reformer 2	0.67 (+0.08)	Total system net efficiency	59.8% (+0.8)

Table 6.2 shows the operational results of the system shown in figure 6.5 at the design point determined in chapter 4. Similar to section 6.3.1, the changes in operational results are shown in parentheses. Here, the changes indicate the difference between the operational results of the systems in section 6.3.2 and section 6.3.3, in order to show the effect of addition of heat recovering part.

As shown in the table, the total external reforming rate is increased approximately 3.5% and the amount of power generated in the SOFC increases approximately 0.08

kW. Overall, total system power and the system efficiency can be reached to 6.00kW and 59.8%, respectively.

It should be noted that the amount of heat transferred to the air from the engine coolant is approximately 0.09 kW. 0.09 kW is about 4% of total heat loss of HCCI engine (~ 2.22 kW). According to the literature, about 80 ~ 90 % of the energy of the heat loss is transferred to the cooling medium and about 10 ~ 20 % of the energy of the heat loss is transferred to oil and radiation from the engine's external surfaces.[23]

Therefore, even for the case of the engine experimented in chapters 3 and 5, which is air and oil-cooled engine, it is expected that 4% of the heat loss can be recovered from engine oil. If the size of the engine increases and the method of engine cooling is changed to water-cooled, the larger amount of the energy is expected to be increased, and the efficiency of the system can be further increased.

6.3.3. Compression ratio of HCCI engine

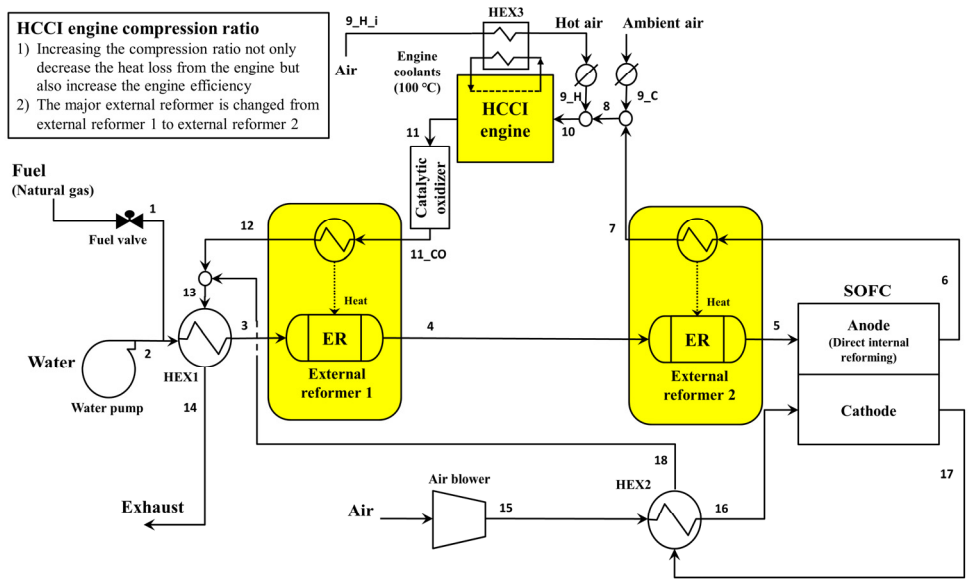

Figure 6.6. Schematic of the hybrid system (methods 1, 2, and 3)

In section 6.3.3, the performance of the hybrid system is investigated while increasing the compression ratio of the HCCI engine. Increasing the compression ratio generally increases the engine efficiency and leads to lower the required engine intake temperature to achieve the HCCI combustion. Simultaneously, the engine exhaust temperature also decreases. The decrease in intake and exhaust gas temperatures reduces the heat transfer in the HCCI engine, so an increase in the compression ratio can be considered to be a solution to the issue 1.

Similar to sections 6.3.1 and 6.3.2, the system performance at the design point determined in chapter 4 are analysed in this section. When the engine intake temperature decreases as the compression ratio increases, the volume flow rate of the gas delivered from the SOFC to the HCCI engine decreases. Therefore, if there is no other change, this will reduce the engine intake pressure. As discussed in chapter 4, reducing the engine intake pressure primarily increases the pumping loss and reduces engine power. Additionally, this also reduces the pressure on the SOFC anode side and

increases the pressure difference between the anode and cathode of the SOFC; thus, this makes a bad influence on the stability of SOFC operation.

The easiest method to keep the intake pressure close to atmospheric pressure is to lower the value of Phi when the system operation condition is determined. However, as shown in chapter 3, if Phi decreases excessively, the engine peak temperature decreases too much, which can adversely affect combustion efficiency and engine efficiency.

Another way to keep intake pressure close to atmospheric pressure is to reduce the displacement of the engine as increasing the compression ratio. Because the purpose of this chapter is to find a system design for increasing the efficiency of the system, this method is more fitted to this purpose. Therefore, the simulation analysis for the variations of the compression ratio was carried out with varying the engine displacement to maintain the engine intake pressure as 1 atm.

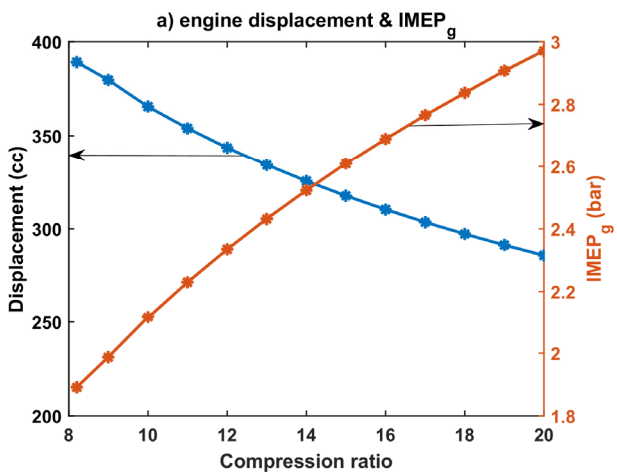

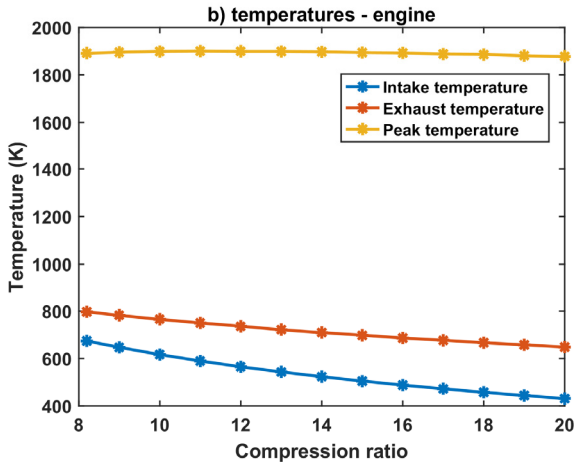
b) temperatures - engine
Intake temperature
Exhaust temperature
Peak temperature
Temperature (K)
Compression ratio

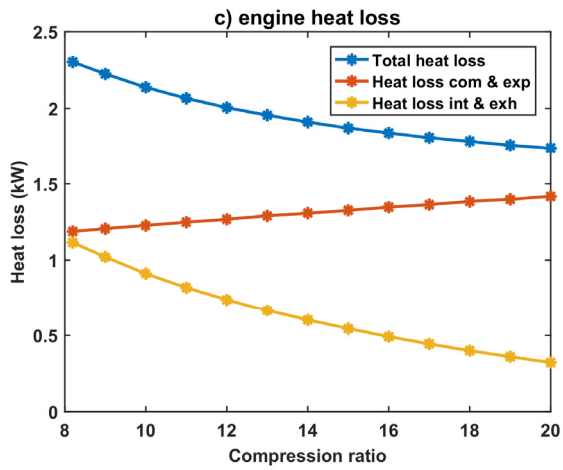
c) engine heat loss
Total heat loss
Heat loss com & exp
Heat loss int & exh
Heat loss (kW)
Compression ratio

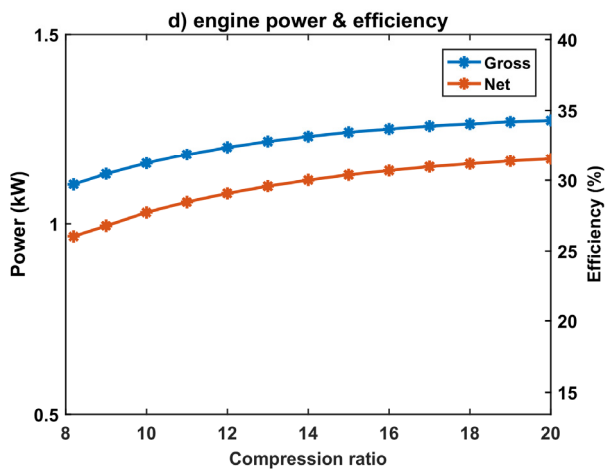
d) engine power & efficiency
Gross
Net
Power (kW)
Efficiency (%)
Compression ratio

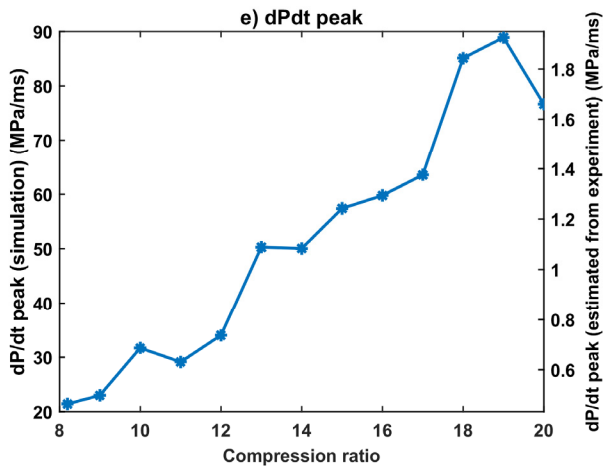

Figure 6.7. HCCI engine performance with the variations of engine compression ratio: a) engine displacement & $IMEP_g$; b) temperatures – engine; c) engine heat loss; d) engine power and efficiency; e) dP/dt peak.

Figure 6.7 shows the engine performance with the variations of engine compression ratio. First, figure 6.7.a) shows the engine displacement which decreases with increasing compression ratio as mentioned above. Specifically, displacement is reduced by about 26.5% from about 389 cc (compression ratio 8.2) to 286 cc (compression ratio 20). In general, the price of an engine is known to be proportional to the displacement.[28] Therefore, this reduction in engine displacement is also useful to reduce the system prices through engine downsizing.

Figure 6.7.b) shows the changes in temperatures while varying the compression ratio. As a result, the engine intake and exhaust gas temperatures decrease simultaneously as compression ratio increases. Meanwhile, the engine peak temperature hardly changes. Therefore, the CO combustion efficiency is expected to change little. This decrease in intake and exhaust temperature reduces the amount of engine heat loss. Figure 6.7.c) shows the heat loss from the engine. First, the total heat loss decreases significantly with increasing compression ratio. Figure 6.7.c) also shows this heat loss by dividing to the

heat loss in the intake & exhaust processes and the heat loss in the compression & expansion processes among the four strokes of the engine. It is interesting to note that the heat loss in the compression and expansion processes increases as the compression ratio increases. This is due to the reduced engine displacement. As the engine displacement decreases, the surface to volume ratio increases, which increases the engine heat loss if other conditions are similar. However, it can be seen that as the compression ratio increases the heat loss in the intake and exhaust process is reduced substantially to decrease the overall heat loss.

Figure 6.7.d) shows the change in power with increasing compression ratio. As is well known, the increase in compression ratio leads an increase in efficiency.

On the other hand, the pressure rise rate (dP/dt) increases due to the increase of the compression ratio, which may adversely affect the stable operation. Because the HCCI simulation model is a zero-dimensional model, it is difficult to predict the pressure rise rate correctly, but simulation results show that the pressure rise rate increases by about 4 to 4.5 times at a compression ratio of 20 compared to a compression ratio of 8.2. As shown in figure 3.7 of chapter 3, the experimental value of the dP/dt peak at a given operating condition is approximately 0.5 MPa/ms. Assuming that the value of dP/dt peak increases at an increasing rate in the simulation model, it is expected to be approximately 2 MPa/ms. Therefore, it can be predicted that the operation is not in trouble, considering that 5 MPa/ms is generally the lower limit that makes the problem of the engine durability.

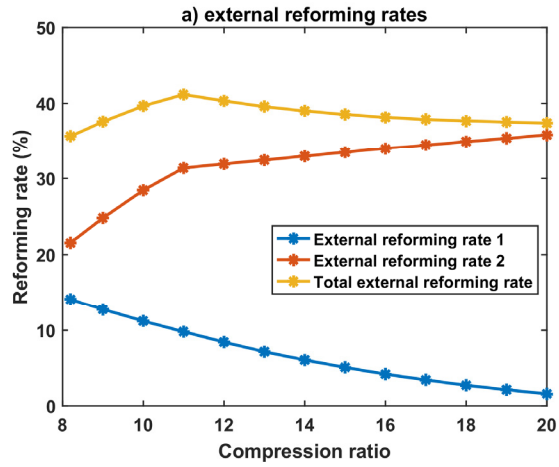
a) external reforming rates
Reforming rate (%)
Compression ratio
External reforming rate 1
External reforming rate 2
Total external reforming rate

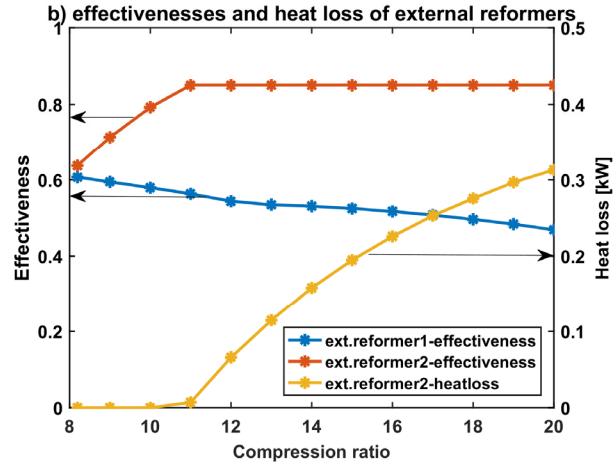
b) effectivenesses and heat loss of external reformers
Effectiveness
Heat loss [kW]
Compression ratio
ext.reformer1-effectiveness
ext.reformer2-effectiveness
ext.reformer2-heatloss

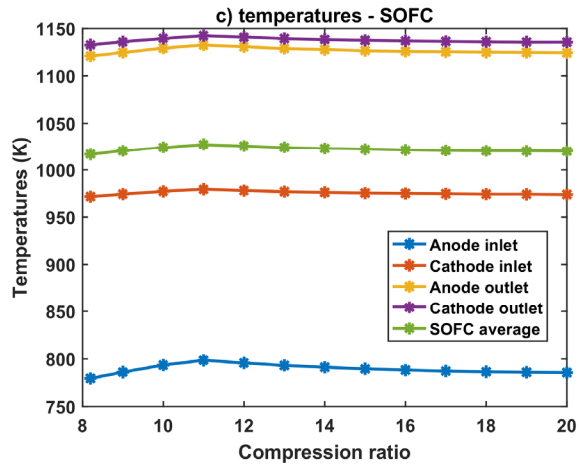
c) temperatures - SOFC
Temperatures (K)
Compression ratio
Anode inlet
Cathode inlet
Anode outlet
Cathode outlet
SOFC average

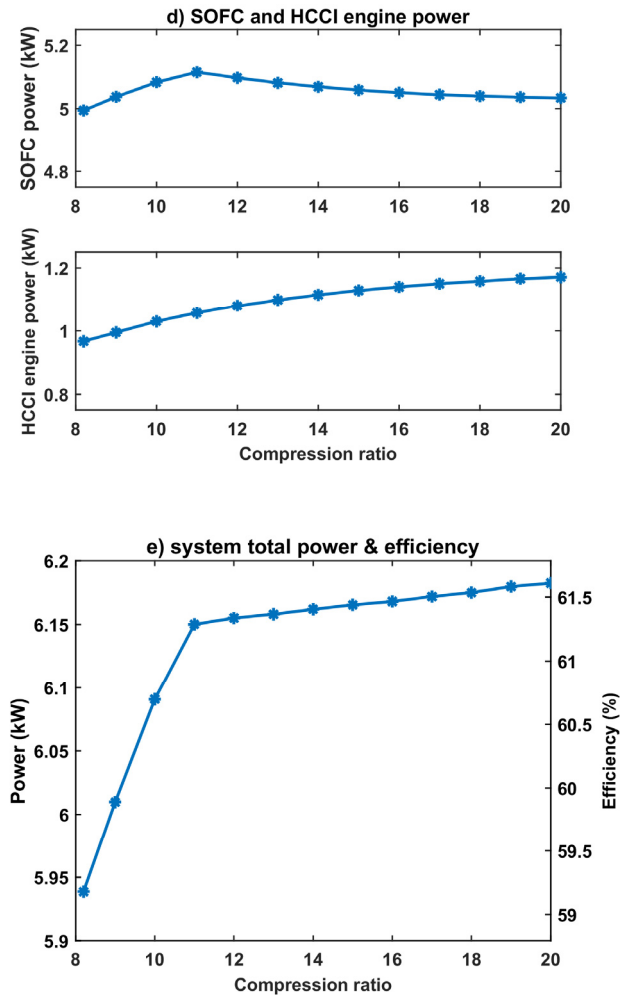

Figure 6.8. System performance with the variations of engine compression ratio: a) external reforming rates; b) effectiveness and heat loss of external reformers; c) temperatures – SOFC; d) SOFC and HCCI engine power; e) system total power and efficiency

Figure 6.8. shows the system performance with the variations of engine compression ratio. First, Figure 6.8.a) shows the external reforming rates. As the compression ratio increases, the intake and exhaust temperatures decrease; thus, the external reforming rate 1 decreases and the external reforming rate 2 increases. In particular, when the compression ratio is 8.2, the reforming rates of the two external reformers are not

significantly different. However, when the compression ratio is 20, almost no reforming takes place in the external reformer 1 and external reformer 2 becomes the major external reformer. Meanwhile, the increasing rate of external reforming rate 2 while increasing the engine compression ratio is decreased from the point of compression ratio 11. This phenomenon occurs because the required engine intake temperature is so lowered as the compression ratio increases that the heat exchanging in the external reformer 2 cannot be performed until this intake temperature is reached. As shown in figure 6.8.b), the effectiveness of the external reformer 2 reached 0.85 from the point of compression ratio 11. Generally, it is difficult to design a heat exchanger that is more effective than this. From this point, it is difficult to transfer the entire amount of excess heat remaining in the SOFC anode off-gas to be utilized for reforming. Therefore, in order to make the temperature lowered to the required intake temperature, there should be a heat loss in the external reformer 2. This amount of heat loss increases as the compression ratio increases as shown in figure 6.8 b).

Because of this, the total external reforming rate is maximized at a compression ratio of 11. For this reason, as shown in figure 6.8.c), all of the temperatures related with the SOFC are maximized at the point of compression ratio 11, and as shown in figure 6.8.d), the efficiency of the SOFC is maximized at the point of compression ratio 11 as well.

Figure 6.8.e) shows the system total power and efficiency calculated from summing the SOFC power and the HCCI engine power. From the above, it can be seen that the power of SOFC is maximized at the point of the compression ratio 11, but the engine power increases even after the point of the compression ratio 11. Therefore, as the compression ratio increases the system power increases overall, but the increase is not large after the point of compression ratio 11. Nonetheless, increasing the compression ratio to 20 is more beneficial not only in terms of system efficiency, but also in various

aspects of operating the system. These are discussed in more detail in section 6.4 (Discussions).

In chapter 3, the stability of the HCCI engine operation is known to be inversely proportional to the value of $IMEP_g$. This point was one of the main causes of not increasing Util beyond 0.7. however, as seen in figure 6.7.a), the increase in compression ratio increases the $IMEP_g$ by increasing the produced power as well as reducing the engine displacement. This increases the stability of the HCCI engine operation, and accordingly, it makes the system possible to operate at higher Util. Therefore, in the case of higher compression ratio, the system efficiency can be improved further by increasing the Util; thus, the method of increasing compression ratio can resolve the issue 3 listed in section 6.1. The detailed system operation results of this point are described in section 6.3.4.

6.3.4. Operation results of the optimized hybrid system

Table 6.3. Operation results of the optimized hybrid system

Operating conditions		**Performance**	
Control parameters		**SOFC**	
Fuel rate (System fuel input)	10.0 kW	Average cell current density	0.409 A/cm^2 (+0.027)
Util (SOFC fuel utilization factor)	0.75 (+0.05)	Cell voltage	0.761 V (+0.025)
BPR (Bypass ratio to steam separator)	0	SOFC power	5.49 kW (+0.53)
Phi (Engine equivalence ratio)	0.7 (-0.05)	SOFC efficiency	50.0%(+4.2)
CAD_{peak} (Engine combustion timing)	372 CAD	Power generation share of SOFC	85.4%(+1.1)
$Util_{air}$ (SOFC air utilization factor)	0.3	Temperature difference (Max)	239 K(+8)
SCR (Steam-to-carbon ratio)	2.5	**HCCI engine**	
RPM (Engine rpm)	1800 rpm	Compression ratio	20 (+11.8)
Temperatures		Displacement	281 cc (-108)
Anode inlet (stream 5)	793 K (+19)	Engine net power	0.94 kW(+0.02)
Cathode inlet (stream 16)	996 K (+26)	Engine efficiency	30.4%(+5.3)
Anode outlet (stream 6)	1154 K(+36)	Power generation share of HCCI	14.6%(-1.1)
Cathode outlet (stream 17)	1163 K(+32)	NO_x emission (@ O_2 15%)	< 1 ppm
Engine intake (stream 10)	450 K(-223)	CO emission (@ O_2 15%)	< 1 ppm (-1325)
Engine exhaust (stream 11)	625 K(-182)	$IMEP_g$	2.5 bar(+0.7)
Pressures		**Total System**	
Anode side (Engine intake)	1.01 bar	Total power (SOFC + HCCI)	6.43 kW (+0.54)
Cathode side	1.01 bar	Blower power	0.02 kW
External reforming rates		Total system net power	6.41 kW (+0.54)
External reforming rate 1	1.1%(-14.1)	Total system net efficiency	63.8% (+4.8)
External reforming rate 2	38.3%(+19.3)	**Heat loss**	
Total external reforming rate	39.4%(+5.2)	Engine heat loss	1.53 kW(-0.69)
External reformer 1 effectiveness	0.50 (-0.12)	Reformer 2 heat loss	0.25 kW(+0.25)
External reformer 2 effectiveness	0.85 (+0.28)	Total heat loss	1.78 kW(-0.44)

Table 6.3 shows the operation results of the final optimized system. For reference,

the changes in the results of system operation are indicated in parentheses. The changes are calculated from the results of section 4.3.2.3. The final system operation results show that the SOFC power is increased about 0.525 kW and the engine power is raised about 0.015 kW from the results of section 4.3.2.3, which is the system operation results before the optimization. As a result, the system power and the system efficiency are increased by approximately 0.54 kW and 4.8%, respectively. Therefore, the efficiency of the system reached 63.8%; the pollutant emission was near-zero.

6.4. Discussion

In this section, the advantages of increasing the compression ratio even beyond 11 are discussed. Although, the increases in the system efficiency is not large with increasing the compression ratio beyond 11, there are four reasons to prefer the higher compression ratio than 11.

First, as mentioned above, the engine can be downsized if the compression ratio is increased. Because there are a large amount of diluents in the engine intake gas, the required engine displacement is relatively large compared to engine power, and this makes the cost of the hybrid system to increase. Therefore, increasing the compression ratio and decreasing the displacement can help to reduce the cost of the hybrid system.

Second, since the intake and exhaust gas temperatures decrease as the compression ratio increases, it is possible to reduce the heat loss that may be occurred during the gas exchanging process between the hot box and the HCCI engine in the experimental operation. As mentioned in section 5.4, a large amount of heat loss is caused by the gas exchanging process between the hot box and HCCI engine, and therefore, decreasing the heat loss from this part can help to improve the system performance in actual system operation.

Third, the system schematic can be simplified by eliminating external reformer 1 from the system schematic in the case of high compression ratio because the external reforming rate 1 is almost negligible.

Fourth, in actual system operation, heat loss occurs in hot box or SOFC unlike simulation. In this case, unlike simulation analysis, it is expected that heat loss is not necessarily occurred in external reformer 2. Therefore, the increase in system efficiency will be more pronounced as increasing the compression ratio.

6.5. Conclusions

From the results of chapters 3 to 5, it was confirmed that the hybrid system has three following issues regarding its operation: CO emissions, a large amount of heat loss, and low Util. In this chapter, three different modifications in system design are applied as an effort to resolve such operational issues. The entire hybrid system model including the HCCI engine has been utilized for analyzing the effect of the three design modifications, and the results of simulation indicate that after applying these methods, the hybrid system can achieve efficiency of ~ 64% while yielding near-zero pollutant emissions. The final layout of the SOFC–HCCI engine hybrid system is presented in figure 6.9.

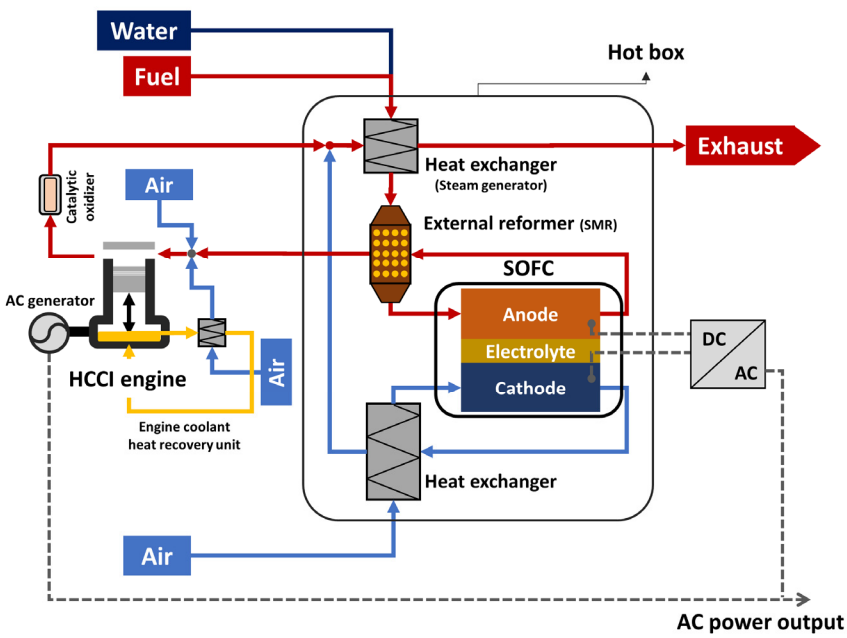

Figure 6. 9. The optimized configuration of the SOFC–HCCI engine hybrid system

Firstly, an additional catalytic oxidizer is installed in the downstream of HCCI engine for eliminating CO emissions as well as supplying additional heat to the SOFC.

Secondly, a heat recovery unit of the engine is added to the system. This unit can recover a certain amount of heat loss caused in the engine. Consisting of dual throttles, this unit can also assist in controlling the HCCI combustion.

Lastly, the compression ratio is changed. By increasing the compression ratio of the engine, it was able to substantially reduce the temperatures of the gases exchanged between the HCCI engine and the hot box; thus, the amount of heat loss of the HCCI engine is reduced. In addition, a simpler configuration of the system can be utilized because the external reformer 1 is not essential with elevated compression ratio. The increase of the compression ratio also increases the $IMEP_g$ as it increases the efficiency of the engine and decrease the required engine displacement. The increment in $IMEP_g$ helps to stably operate HCCI engine with higher Util.

Chapter 7
Performance of a scaled-up SOFC–HCCI engine hybrid system

7.1. Introduction

In chapters 3 to 6, the design point of system operation and the optimized system design for the best performance and stability were determined by conducting simulation and experiment of the SOFC–HCCI engine hybrid system. The final design of the system is proposed in figure 6.9.

The analyses in chapters 3 to 6 were performed with 5 kW-class SOFC–HCCI engine hybrid system. Although this power generation capacity was suitable for performing various analyses on the system at the lab-scale, the real-world products are often larger than this power generation capacity. Therefore, this chapter conducts an evaluation on performance of an enlarged system. While scaling up the system, system configuration is fixed as the final design determined in chapter 6, and the operating point is also fixed at the design point determined in chapters 4 and 6.

The main body of this chapter consists of two parts: methodology and results. In section 7.2 (Methodology), the methodologies for scaling up the system are introduced. In section 7.3 (Results), the results of analysis on the effect of scaling up are introduced. From the results of this analyses, the performance of 100 kW-class SOFC–HCCI engine hybrid system is predicted.

7.2. Methodology

For predicting the performance of scaled-up hybrid system, a simulation of the entire system is performed. The size of the system is increased from 5 kW-class to 100 kW-class. The same simulation model and system simulation method are used as those mentioned in section 6.2.

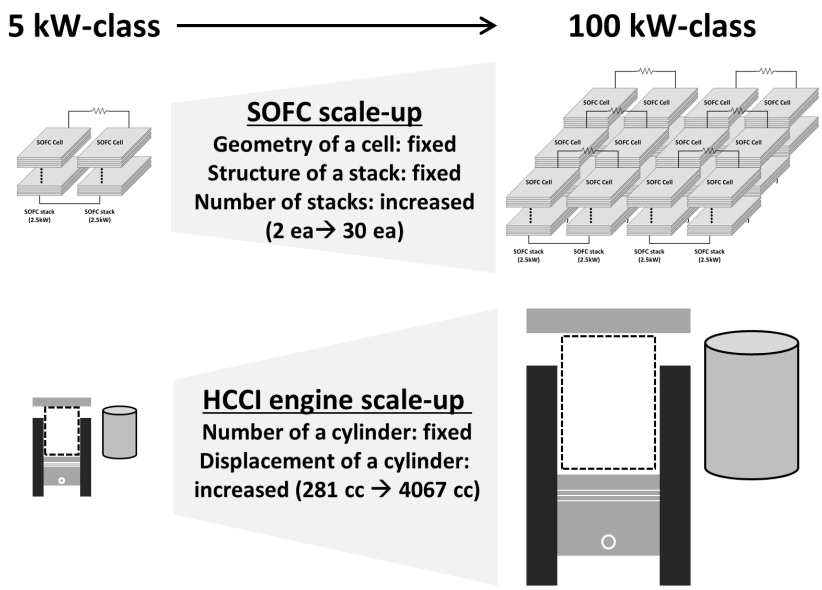

Figure 7. 1. Methodologies for scaling up SOFC and HCCI engine

The methodology employed for scaling up the hybrid system is shown in figure 7.1. As shown in the figure, increasing the number of modularized stacks is selected as the scaling up methodology for the SOFC. This methodology is the strategy used by SOFC manufacturers, such as Bloom Energy, for scaling up the system.[58] As a stack is modularized, the design of a cell and the structure of a stack do not change while scaling up the system.

On the other hand, for scaling up the HCCI engine, enlarging the displacement of a cylinder of HCCI engine is selected as the methodology. This methodology is adopted

because the base size of the cylinder is relatively small for achieving several hundred-kW power generation.[59]

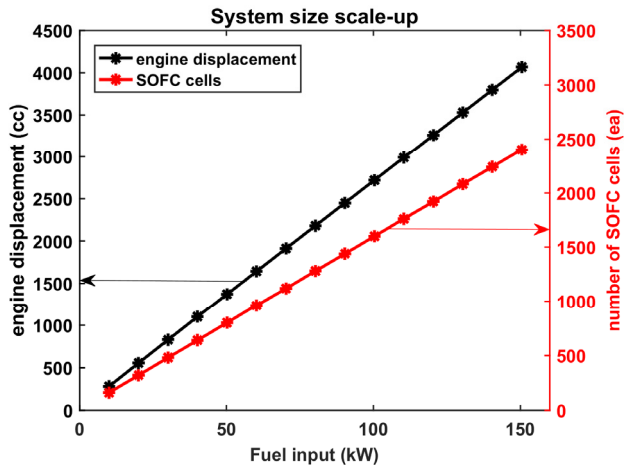

Figure 7. 2. System size scale-up

Figure 7.2 indicates the results of scaling-up the system; number of total SOFC cells and the displacement of a cylinder are shown in the figure.

As increasing the size of a cylinder decrease the surface-to-volume ratio of a cylinder, it has advantages for decreasing the heat loss and improving engine performance. As seen in chapter 6, one of the major concerns restraining a successful system operation is the large amount of heat loss. Therefore, decreasing the amount of heat loss of HCCI engine can help to improve not only the HCCI engine operation but also the entire system operation. As a result of increasing the system size, the displacement of a cylinder is increased from ~ 280 cc to 4000 cc. Note that although the displacement of 4000 cc is within the typical range of internal combustion engine for power generation, it is hard for such large-displacement system to use a single cylinder engine due to the difficulty in maintaining the balance of the engine. However, this aspect is not considered in this study.

7.3. Results

In this section, the simulation results of scaling up are presented. System simulation is conducted while varying the amount of fuel input from 10.0 kW to 150.0 kW. As a result, the system size is increased from 5 kW-class to 100 kW-class, and finally the performance of 100 kW-class SOFC–HCCI engine hybrid system is predicted.

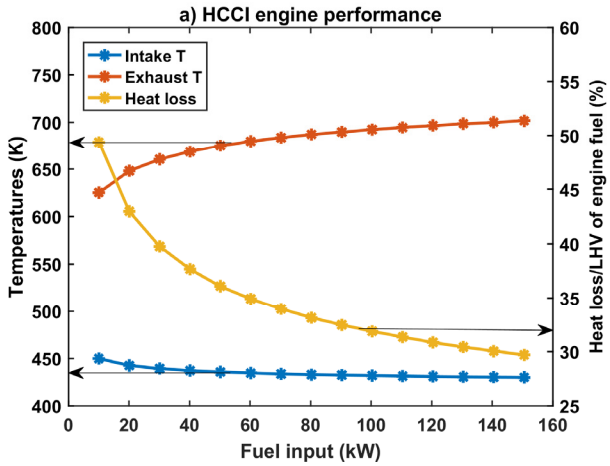

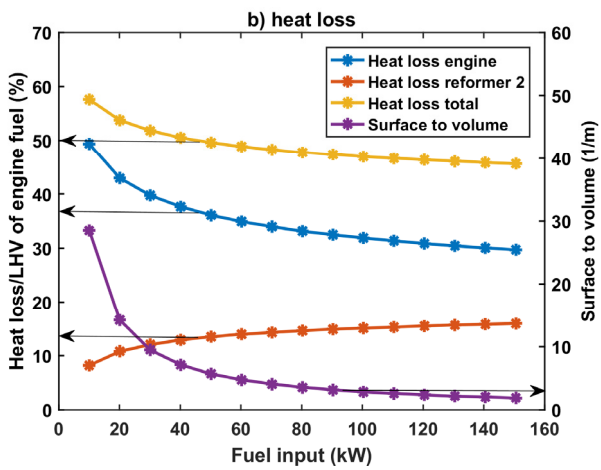

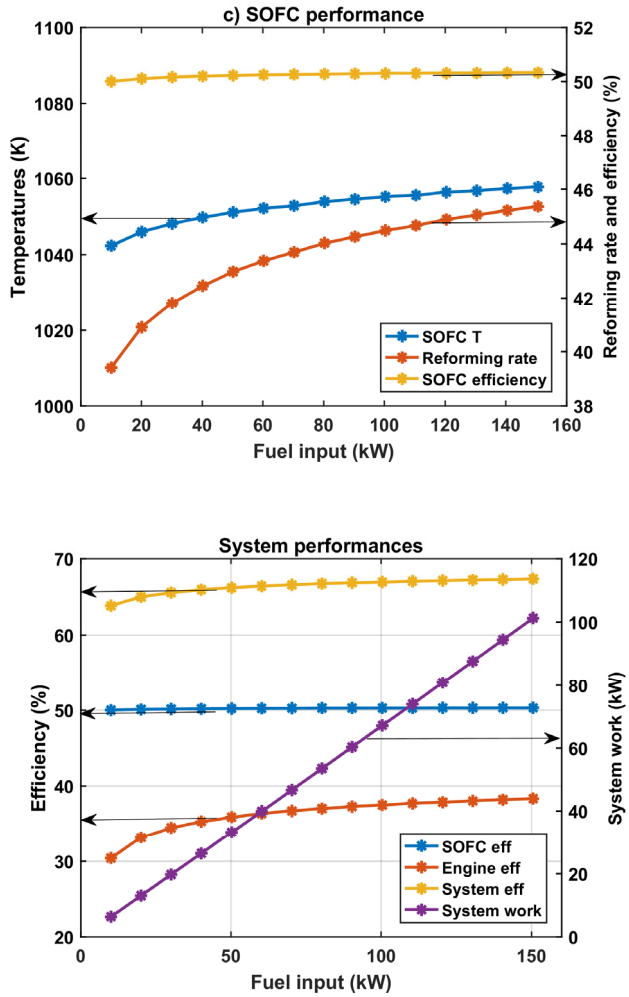

Figure 7. 3. System performance with the variations of the system size: a) HCCI engine performance; b) SOFC performance; c) heat loss; d) system performance

Figure 7.3 a) summarizes the performance of HCCI engine with increasing size of the system. As shown in the figure, as system size increases the amount of heat loss from HCCI engine is decreased due to the decrease in surface to volume ratio of HCCI engine. Figure 7.3 b) shows that the trend of engine heat loss is very similar to the trend of surface to volume ratio; thus, it is confirmed that the decrease in the surface to volume ratio reduces the engine heat loss. For this reason, as system size increases, the required

intake temperature of HCCI engine for achieving stable combustion decreases and the exhaust temperature increases. In addition, the decrease in heat loss of HCCI engine improves the HCCI engine performance. Figure 7.3 d) shows that as system size increases the engine efficiency increases.

The decrease in engine intake gas temperature increases the heat loss from external reformer 2 because the effectiveness is limited to 0.85. Despite of the increase in heat loss from external reformer 2, the total heat loss of the system is decreased due to the decrease in engine heat loss. Therefore, enlarging system size is also helpful to supply sufficient heat to the SOFC, and increase the efficiency of the SOFC because it increases the external reforming rate. Figure 7.3 c) shows the performance of the SOFC while increasing system size. As shown in the figure, the increment of the external reforming rate causes the increase in SOFC operating temperature; thus, it increases the efficiency of the SOFC. Therefore, it can be concluded that increasing system size improves not only the HCCI engine performance but also the SOFC performance. Accordingly, combining the effects of the enlarged system size on HCCI engine and SOFC, the efficiency of 100 kW-class system is predicted as 67.4% which is 3.6% higher than 63.8%, the efficiency of 5 kW-class system.

Chapter 8
Conclusions

A SOFC–HCCI engine hybrid system is a new concept of a SOFC hybrid system. In an effort to investigate the operating characteristics and verify the feasibility of the system, computational and experimental studies were performed in this dissertation.

Four following guiding questions were proposed in chapter 1 and five studies were conducted in chapters 3 to 7 for answering these questions.

Guiding questions

1. Does an HCCI engine fuelled by SOFC anode off-gas successfully operate?
2. Can an SOFC successfully operate under a combined operation with an HCCI engine?
3. What is the best approach to controlling the system for achieving the best performance and a stable operation?
4. What is the best design of the system to maximize the system performance?

Studies

1. Experimental study of HCCI engine operation fuelled by SOFC anode off-gas
2. Numerical and experimental study on operating characteristics of the SOFC under the hybrid system and design point performance of the hybrid system
3. Experimental study of SOFC–HCCI engine hybrid system
4. Numerical study for the optimization of system design
5. Numerical study for predicting the performance of 100 kW-class hybrid system

As a result of these studies, the feasibility of the system was verified, and the design point of operation and the optimized system design were determined. In following paragraphs, the results and implications of each study are summarized.

(1) Experimental study of HCCI engine operation fuelled by SOFC anode off-gas

Guiding question 1 was answered in study (1). From the experimental results, the feasibility of HCCI engine as the bottoming cycle of the SOFC was verified. The experimental results indicated that HCCI engine operation can produce significant amount of power (w/ 25-30% gross indicated efficiency) while emitting very small amount of NOx (<5 ppm @ O_2 15%). In addition, the ranges of system control parameters for achieving successful HCCI engine operation were identified. It was concluded that HCCI engine operation with an exceedingly low engine load ($IMEP_g$ < 1.8 bar) or an excessively diluted engine intake gas (fuel molar fraction < 0.125) should be avoided. Additionally, the most important factor determining the engine intake and exhaust temperatures were identified. These results are important because engine intake and exhaust temperatures affect the external reforming rate and the operation of the SOFC. The most dominant factor determining the required engine intake temperature for achieving HCCI combustion was found to be the specific heat ratio of the engine intake gas. On the other hand, the most dominant factor in determining the engine exhaust temperature was found to be the peak temperature of the in-cylinder gas in an engine cycle.

(2) Numerical and experimental study on operating characteristics of the SOFC under the hybrid system and design point performance of the hybrid system

Guiding questions 2 and 3 were answered in study (2). The operation of an SOFC-

HCCI engine hybrid system was investigated by integrating the experimental results of the HCCI engine with the simulation models of other components. From the results of the investigation, the operating characteristics of the SOFC in the hybrid system were identified. The most important characteristic of the SOFC operation is that the SOFC should operate with an SOFC anode inlet gas that has a low external reforming rate (e.g., 30 ~ 40%) and low temperature (e.g., 750 ~ 800 K). This makes the operating temperature of the SOFC as relatively low (e.g., ~ 900 K near the entrance of the SOFC). From these findings, it was concluded that using an anode-supported type of SOFC is suitable for the hybrid system because this type can decrease the ohmic losses of the electrolyte, which would be large in the low temperature. The design point of system operation was determined by conducting parametric study on system operation. System analyses were performed while varying three control parameters (Util, BPR, and Phi); the effects of each parameter were investigated. In case of BPR, maintaining a low BPR, that is, decreasing the flow rate bypassed to the steam separator, is found to be better for achieving higher efficiency. In the case of Phi, maintaining a value of below 0.9 is suitable for decreasing the CO emissions. Additionally, maintaining a low Phi is recommended for the stability of system operation as it would decrease the mechanical stress of the cell. For Util, it was confirmed that increment of Util increases the system efficiency but decreases the stability of system operation. Therefore, it was concluded that maintaining Util below a certain point is desirable. Finally, the design point of 5 kW-class SOFC–HCCI engine hybrid system was determined as follows: Util of 0.7, BPR of 0, and Phi of 0.75. The results of system operation are evaluated as follows. SOFC and HCCI engine produce 4.97 kW and 0.93 kW of power, respectively, while yielding less than 1 ppm of NO_x (@ O_2 15%) and ~ 1300 ppm CO (@ O_2 15%). The total system efficiency is evaluated as ~ 58.5%.

(3) Experimental study of SOFC–HCCI engine hybrid system

Guiding questions 1 and 2 were answered more directly in study (3) by conducting the experiment of entire system. From the results of first 200-hour continuous operation of SOFC-HCCI engine hybrid system, the feasibility of the hybrid system was directly verified. The operating point in this 200-hour continuous operation was determined based on the system analysis conducted in study (2). The experimental results indicated that SOFC and HCCI engine produced power approximately 3.40 kW and 1.18 kW, respectively; overall, 4.58 kW of power was produced by the system. In addition, the influence of pressure oscillation caused by HCCI engine on the anode side of the SOFC was investigated. The pressure oscillation caused by the HCCI engine was found to be canceled much when it comes to the SOFC anode due to the flow path between the engine intake and the SOFC. From dividing total system power by the amount of system fuel input (7.8kW), 59.0% was calculated as the system efficiency. However, electric heaters and additional burner were used in the experiment due to the unexpected large amount of heat loss from the system. Therefore, it was found that decreasing the amount of heat loss is essential for better system operation.

(4) Numerical study for the optimization of system design

Guiding question 4 was answered in study (4). As an effort to resolve three major issues regarding its operation (CO emissions, a large amount of heat loss, and a low Util), three different modifications to system design (additional catalytic oxidizer, heat recovery from the engine coolant, and increasing the compression ratio of the engine) are applied and the effects of each modification are analysed. For this, the simulation model of the entire hybrid system has been constructed and utilized.

The results of simulation indicate that through applying these modifications to the

system, the hybrid system can achieve efficiency of ~ 63.8% while producing near-zero pollutant emissions. Firstly, an additional catalytic oxidizer eliminates CO emissions as well as supplies additional heat to the SOFC. Secondly, a heat recovery unit is added to the engine part and this unit can decrease a certain amount of heat loss and increase the system performance. Lastly, increasing the compression ratio of the engine reduces the temperatures of engine intake and exhaust gases, and accordingly, the amount of heat loss of the HCCI engine is reduced; it also increases the $IMEP_g$ as it increases the efficiency of the engine. The increment of $IMEP_g$ helps to stably operate HCCI engine with higher Util.

(5) Numerical study for predicting the performance of 100 kW-class hybrid system

Numerical study on the system performance was conducted while scaling up the system from 5 kW-class to 100 kW-class whereas maintaining the design of system determined in study (4). Simulation model used in study (4) was utilized in study (5). Increasing the size of system was performed by increasing the number of modularized SOFC stacks and enlarging the size of a cylinder of the HCCI engine. Because the surface to volume ratio of the engine was decreased as the system size was increased, the engine heat loss was decreased. Due to this fact, the efficiencies of HCCI engine, SOFC, and the entire system were raised. From the simulation, it was evaluated that the efficiency of ~ 67.4% could be achieved when the system was scaled up to 100-kW. These results show the possibility of SOFC-HCCI engine hybrid systems being used as ultra-high efficiency power generation systems.

Summary

The feasibility of the SOFC–HCCI engine hybrid system was verified by the studies conducted in this dissertation. Based on the investigations of the system operation characteristics, the system design for the best performance and stable operation was determined as shown in the following figure. The design point of system operation was also determined. Therefore, it can be concluded that the design of the system for the actual operation was determined. When the scale of the system with this design is increased to 100 kW-class, the efficiency of the system is predicted as ~ 67.4% while yielding near-zero pollutant emissions.

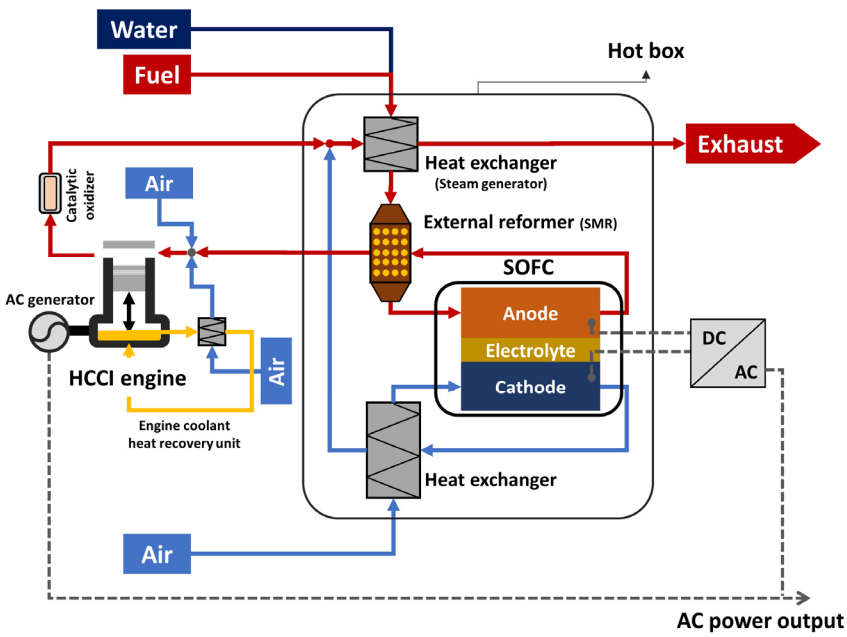

Figure 8. 1. The optimized configuration of the SOFC–HCCI engine hybrid system

Future work

The development of a practical system based on the final system design proposed by this dissertation is required for the commercialization of this system. For the development of the system, it is necessary to study and develop the control strategies to stably operate the system in various situations. Therefore, the study on transient behaviour of the system is required for the future work.

Appendix A
Experimental setup of HCCI engine experiment

The appendix A presents detailed description of experimental setup of HCCI engine that supplements chapter 3. Various photographs of experimental apparatus, which are installed in the building 313 of Seoul National University, are shown with the description.

A.1. Outline of experimental setup

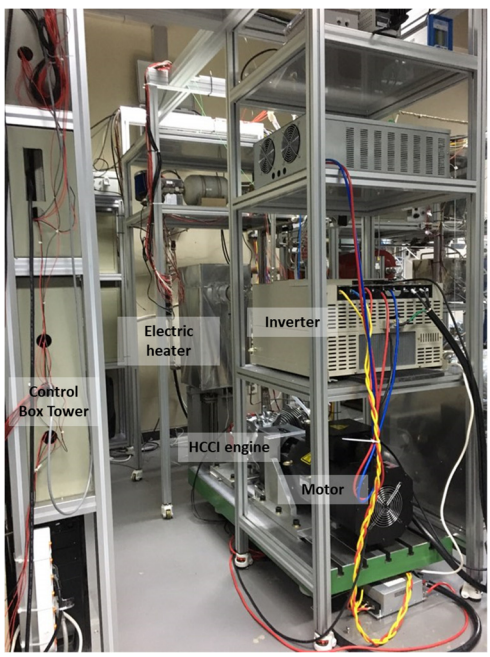

Figure A1. Side view of experimental setup

Figure A1 shows the outline of experimental setup. Various experimental apparatuses are arranged and combined as shown in figure 3.1 of main text. As mentioned in section 3.2.1, the SOFC anode off-gas is emulated by utilizing MFCs, a water pump, a static mixer, an electric heater and an electric boiler. The emulated SOFC anode off-gas is input into the HCCI engine to experiment HCCI engine operation fuelled by SOFC anode off-gas.

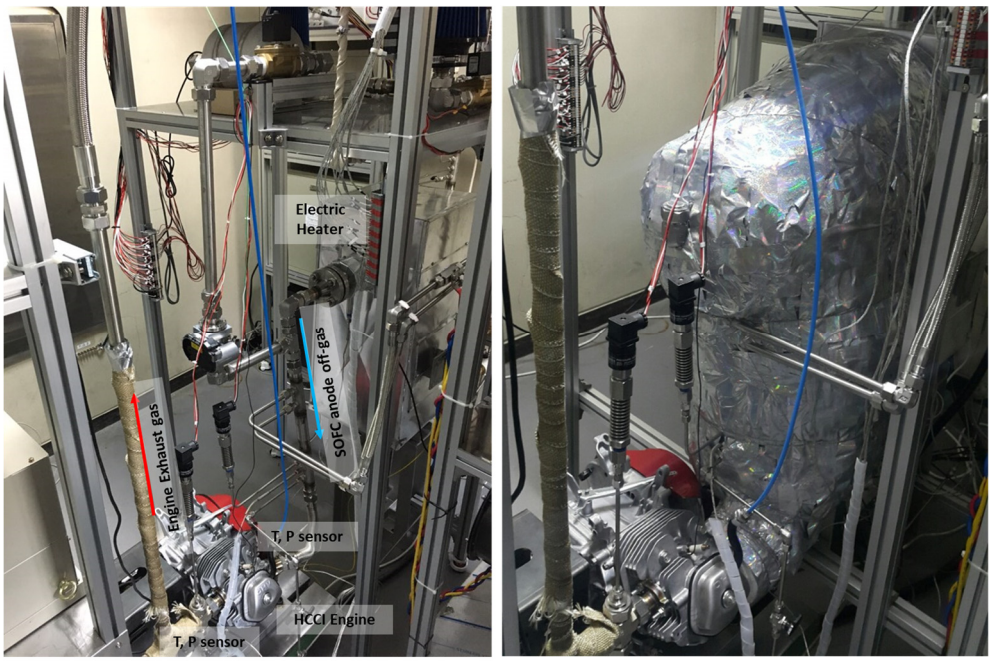

Figure A2. Front view of experimental setup

Figure A2 shows the engine intake and exhaust part of experimental setup. As shown in figure A2, the emulated SOFC anode off-gas is input into the HCCI engine. The right-side of the figure shows that the flow path between the electric heater and HCCI engine is insulated by Cerak-Wool. Since the temperature of SOFC anode off-gas is high, the thickness (or radius) of Cerak-Wool is relatively thick, about 200 ~ 250 mm, to prevent the heat loss.

A.2. HCCI engine

For the experiment, the commercial Honda GX390 model was modified to HCCI engine. This engine is single-cylinder engine and the displacement is about 389 cc. This engine is selected to match the 5 kW-class SOFC. The spark plug is replaced by in-cylinder pressure sensor to enable HCCI operation. The intake and exhaust manifolds are re-fabricated for the experiment of HCCI engine fuelled by SOFC anode off-gas.

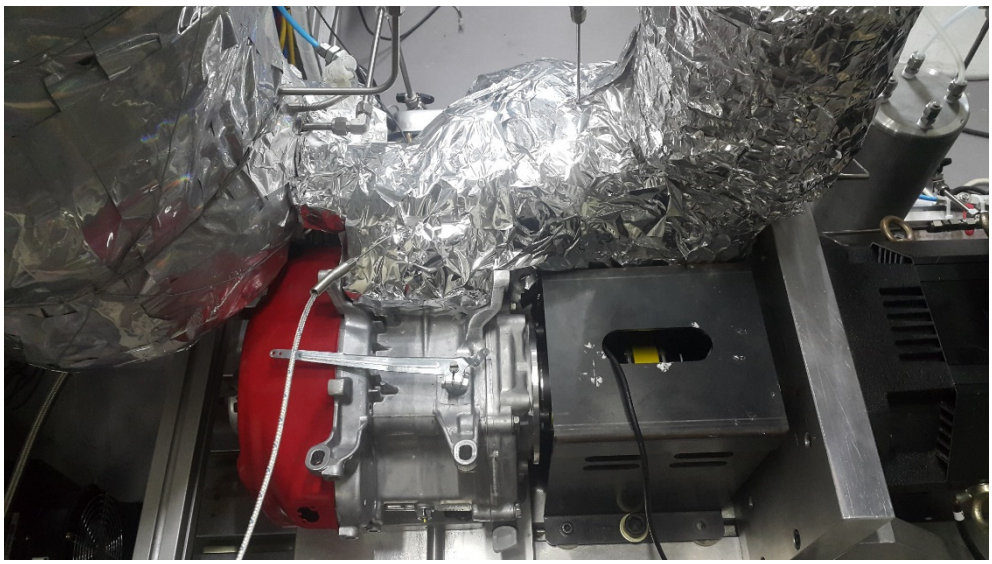

Figure A3. Top view of HCCI engine

As shown in figure A3, not only the manifolds but also the part of engine surface are insulated by Cerak-Wool to reduce the heat loss from the HCCI engine. In the SOFC–HCCI engine hybrid system, the engine exhaust gas is utilized as the heat source of the external reformer. Therefore, reducing the heat loss of the HCCI engine can directly increase the external reforming rate, and accordingly, the SOFC performance.

The thickness of Cerak-Wool which covers the engine surface is about 100 mm. The thickness (or radius) of Cerak-Wool which covers engine intake and exhaust manifold is about 150 ~ 200 mm. To prevent overheating of HCCI engine, which can be caused by the insulation of engine surface, the temperatures of engine surface and engine oil are monitored. Additionally, to maintain the similar engine cooling condition while varying the experiment conditions, the temperature of engine oil is maintained near 110 ℃ using an external oil conditioner.

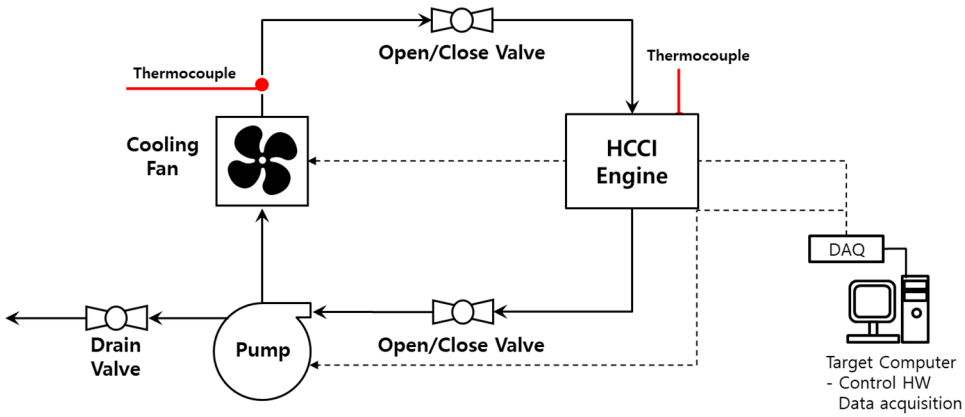

Figure A4. Schematic of oil external cooling circuit

Figure A4 shows the schematic of oil external conditioner. The oil conditioner consists of an oil pump, a cooling fan and valves. The temperatures of engine oil in the HCCI engine and the outlet of the cooling fan are monitored, and the oil pump and the cooling fan are turned on remotely by the target computer, depending on the temperature of oil.

A.3. Dynamometer

The dynamometer of HCCI engine consists of an inverter and a motor. The motor shaft is connected to the crankshaft of HCCI engine. The rotational speed of motor is controlled by the inverter. The inverter is controlled by target and host computers with utilizing DAQs. As a result, the rotational speed of the motor is maintained as the selected value (usually 1800 rpm), independent of combustion inside the HCCI engine.

HIGEN TN 300 model (30 kW-class) was used for the motor. HIGEN FDA 7000 model was used for the inverter. Because the capacity of the motor and inverter is large, there was a lot of noise which disturbs the acquisition of accurate experimental data. Therefore, two noise filters are installed to reduce the noise. One noise filter was installed before the inverter and the other noise filter was installed after the inverter.

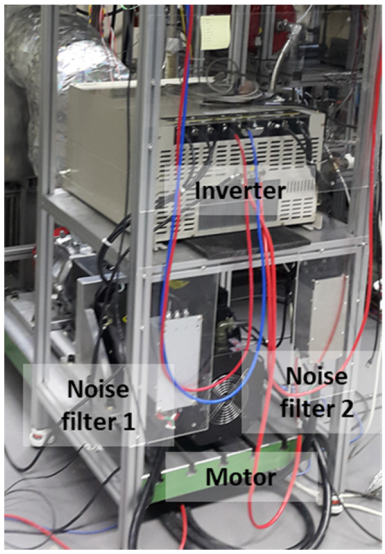

Figure A5. Dynamometer

A.4. Emulator of the SOFC anode off-gas

A.4.1. MFCs and a water pump

Emulator of the SOFC anode off-gas consists of MFCs, a water pump, a static mixer, and an electric heater.

Four MFCs (CO_2, CO, H_2, Air) were used to supplies the gases. Bronkhost MFCs were used for supplying CO_2 and Air, and Brooks MFCs were used for supplying H_2 and CO. KNF Simdos 10 model was used as the water pump. The range of flow rate of this water pump was from 1 to 100 ml/min. The flow rates of MFCs and a water pump were controlled by computers and DAQs. The MFCs and the water pump were calibrated before the experiment to improve the accuracy.

A.4.2. Electric heater

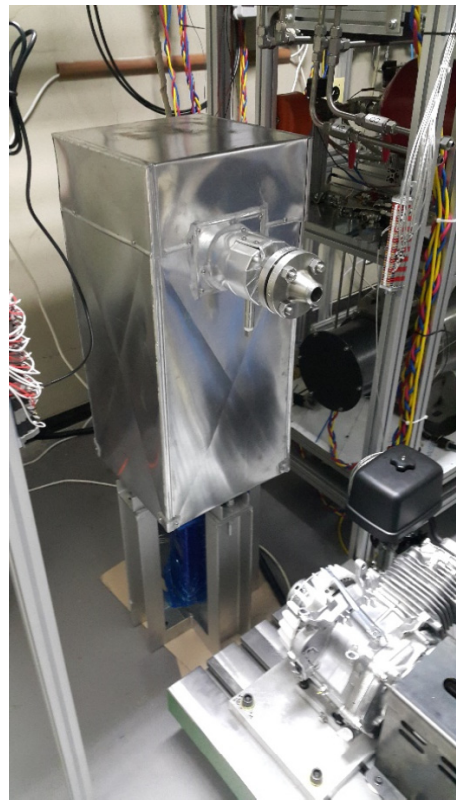

Figure A6. Electric heater (WATLOW 12 kW-class)

WATLOW 12 kW-class electric heater was used for emulating the temperature of SOFC anode off-gas. The heater was manufactured to be able to increase the temperature of gas to ~ 850 ℃ because the temperature of SOFC anode off-gas is as high as 700 ~ 800 ℃. Alloy 600 is selected as the material for the shell, nozzle, and baffle of the electric heater. The heating element of the electric heater was made of alloy 840.

A.5. Exhaust gas analyser

Figure A7. Exhaust gas analyzer (Eurotron GreenLine MK2)

Figure A7 shows the exhaust gas analyzer used in the experiments. The exhaust gas analyzer measured the CO and NO_x emission of engine exhaust gas. The engine exhaust gas is dried out before entering the exhaust gas analyzer. For drying out the engine exhaust gas, the exhaust gas was heat-exchanged with ambient air and condensed as shown in figure A8. The condensed exhaust gas passed through a moisture absorbent (DRIERITE absorbent) to absolutely dry out H_2O in the exhaust gas.

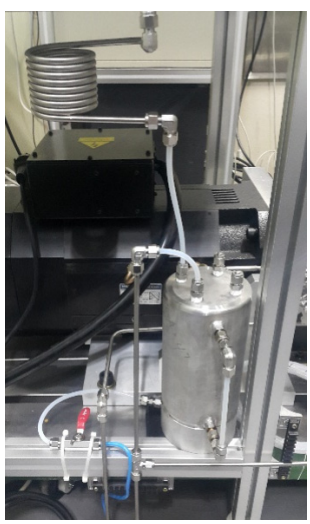

Figure A8. Condensation of water in the engine exhaust gas

A.6. Control room

Figure A9. Engine control room

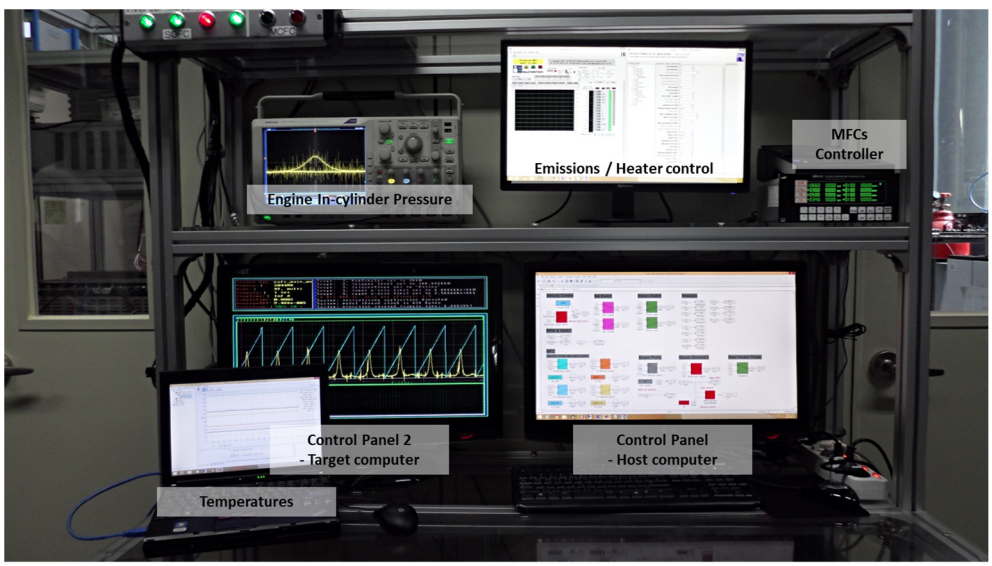

Host Computer: Mathworks MATLAB Simulink/Real-Time Workshop
Target Computer: Mathworks xPC operating system

Figure A10. Control panels

Figures A9 and A10 show the engine control room. There are six control panels in the control room.

Three computers were utilized to control and monitor the engine experiment. The

first one was used for the host computer and the second one was used for the target computer. The host computer was equipped with intel i7 CPU and 8 GB RAM. The host computer communicated with an exhaust gas analyzer and a heater controller by using RS-232 communication.

The target computer was equipped with intel i3 CPU and 4 GB RAM. The target computer was also equipped with NI DAQ 6259 board and MCC PCI QUAD 04 encoder board for enabling real-time signal sensing and actuating via computers.

The third one was dedicated for acquisition of temperatures. NI 9211 was connected to this computer to acquire the data of temperatures. The oscilloscope was used for monitoring the combustion phase of the HCCI engine.

Appendix B
Calculation methods related with HCCI engine experiment

The appendix B presents detailed calculations that supplements chapter 3. It is noted that MATLAB (Mathworks corporation) and the Cantera thermodynamic toolbox were used for the calculations.

B.1. Composition and flow rate of HCCI engine intake gas

In this dissertation, the flow rate and composition of the HCCI engine intake gas are determined when the Fuel rate, Util, BPR, and Phi values are given. The HCCI engine experiments are performed using the emulated gas corresponding to the calculated flow rate and composition. The method for determining the flow rate and composition of the HCCI engine intake gas when control parameter values are given is as follows.

First, the composition of natural gas, which is used as the fuel of the hybrid system, is regarded as the average composition of natural gas in South Korea. The composition is as follows: 91.3% CH_4, 5.4% C_2H_6, 2.1% C_3H_8, 1% C_4H_{10}, and 0.2% N_2.[28, 60] To reduce the complexity of the calculation, it is assumed that there C_4H_{10} and N_2 are not present. Additionally, in this system, this natural gas is reformed via methane reforming, and the value of the steam to carbon ratio is fixed at 2.5.

In this system, the reforming reaction occurs in the external reformer and in the SOFC. It is assumed that the natural gas is completely reformed to H_2 and CO in the SOFC; thus, the final state of the reformed gas does not include any other component, such as CH_4, except for H_2, CO, H_2O, and CO_2. In addition, it is assumed that the reformed gas is in equilibrium with respect to the water-gas shift reaction at a potential SOFC operating temperature of 750 °C (1023 K) and 1 atm.

In this dissertation, Util (i.e., the fuel utilization factor of an SOFC) is defined as follows.

$$Utilization\ factor(Util) = 1 - \frac{LHV\ of\ SOFC\ anode\ off-gas}{LHV\ of\ reformed\ gas}$$

To simplify the calculation, it is assumed that H_2 and CO in the reformed gas are oxidized to H_2O and CO_2 according to the value of Util and that the final composition of the SOFC anode off-gas is determined by considering the compositional change of the SOFC anode off-gas due to the equilibrium of the water-gas shift reaction at 1 atm and 750 ℃ (1023 K). Finally, it is assumed that the steam in the SOFC anode off-gas is separated at 60 ℃ by the steam separator.

B.2. In-cylinder temperature

The temperature inside the engine cylinder is estimated using the ideal gas law: $PV = mRT$. The value of P, i.e., the in-cylinder pressure, is measured using an in-cylinder pressure transducer, and the value of V, i.e., the in-cylinder volume, is calculated based on the measured engine CAD and engine geometric information.

The value of m, i.e., the mass of the in-cylinder gas, is calculated as follows. The in-cylinder gas consists of fresh engine intake gas of this engine cycle and residual gas that is not discharged during the exhaust process of the previous engine cycle but remains in the clearance volume. The masses of these two gases are added to calculate the mass of the entire in-cylinder gas. First, the mass of the fresh engine intake gas is calculated from the flow rate information of the experimental equipment, i.e., the MFCs and water pump. Second, the amount of residual gas is calculated as follows. The temperature of the gas remaining in the clearance volume is assumed to be equal to the measured temperature of the exhaust gas, and the pressure of this gas is assumed to be equal to

the atmospheric pressure. In addition, the composition of this gas is assumed to be the completely combusted composition of the engine intake gas, except for some unburned CO. Therefore, the mass of the residual gas remaining in the clearance volume of the previous engine cycle is calculated using the ideal gas law with the temperature, pressure, volume (clearance volume) and composition computed above. The final mass inside the cylinder is determined by adding together these two masses.

Additionally, the composition of the in-cylinder gas, which affects the value of R (gas constant), before the occurrence of combustion is obtained by mixing the two gases together, similar to the mass calculation method mentioned above. From this composition, the value of R of the in-cylinder gas is calculated. After combustion, it is difficult to estimate the composition of the in-cylinder gas, which also makes it difficult to calculate the value of R of the in-cylinder gas. In this dissertation, to reduce the complexity of the analysis, it is assumed that the gas composition after the peak pressure is achieved is equal to the composition of the exhaust gas. To further simplify the calculation, it is assumed that the compositional change from the start of combustion (SOC) to the peak pressure is linear with respect to time.

B.3. SOC (start of combustion) timing

The SOC can be defined using various methods. In this dissertation, the SOC is determined using the in-cylinder pressure, which is the only value directly measured in the cylinder at the time of combustion. As shown in figure A11, the in-cylinder pressure rise rate (dP/dt) profile of the firing cycle, which indicates that HCCI combustion occurs in the cylinder, is different from that of a motoring cycle. In the case of a motoring cycle, the pressure rise rate increases during the compression process and decreases during the expansion process. However, in the case of a firing cycle with combustion after the top-

dead-center (TDC) considered in this study, the pressure rise rate rapidly increases again after decreasing around TDC. In this study, such starting point of the second increase is selected as the SOC.

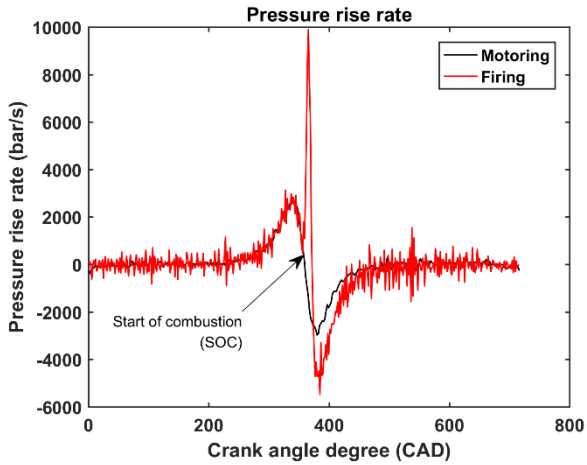

Figure A11. Pressure rise rate profiles of motoring and firing cycles

Appendix C
One-dimensional SOFC simulation model

In the appendix C, the one-dimensional SOFC simulation model is described in detail. The constants used in the model are as follows. R denotes the universal gas constant, 8.3145 J/mol·K; n_e denotes the number of electrons produced in the oxidation reaction of one H_2 molecule, 2; and F denotes the Faraday constant, 96,485 C/mol.

C.1. Electrochemical reaction model

The voltage of the SOFC cell is calculated from the Nernst potential and various voltage losses (activation, ohmic, and concentration losses). The Nernst potential is the potential difference between the anode and the cathode when the entire electrochemical reaction of the SOFC is in equilibrium. When the electrochemical reaction is out of equilibrium and the reaction occurs in one direction, irreversible voltage losses occur, and the cell voltage drops. Therefore, the voltage of the SOFC cell is modelled using equation (A1). The methods used to calculate the Nernst potential and each voltage loss are described in the following sections.

$$V_{cell} = V_{nerst} - V_{act} - V_{ohm} - V_{conc} \quad \text{(A1)}$$

For reference, two literatures [28, 61] are primarily referred for constructing electrochemical reaction model.

Nernst potential

The Nernst potential is calculated from equations (A2) and (A3).[1] In this dissertation, it is assumed that only H_2 participates in the oxidation reaction (i.e., electrochemical reaction) and that CO affects the electrochemical reaction only by participating in the water-gas shift (WGS) reaction. The oxidation reaction rate of CO

is known to be much lower than that of H_2; therefore, CO indirectly participates in the electrochemical reaction mainly through the WGS reaction rather than direct participation.[62, 63]

$$V_{nernst} = E_0 + \frac{RT}{n_e F} ln\left(\frac{(p_{an,H2}/p_{atm})(p_{ca,O2}/p_{atm})^{0.5}}{p_{an,H2O}/p_{atm}}\right) \quad (A2)$$

$$E_0 = -\frac{\Delta G_T^0}{n_e F} = -\frac{(G_{H2O,T} - G_{H2,T} - \frac{G_{O2,T}}{2})}{n_e F} \quad (A3)$$

Activation loss

Activation loss refers to the voltage that is sacrificed to lower the activation barrier of the forward reaction and cause the electrochemical potential of the anode and cathode to both be out of equilibrium and react in one direction. This voltage loss is calculated from the Butler-Volmer equation, which is given in equation (A4).[1]

$$j = j_0 \left\{exp\left(\alpha \frac{n_e F V_{act}}{RT}\right) - exp[-(1-\alpha)\frac{n_e F V_{act}}{RT}]\right\} \quad (A4)$$

In the equation, j denotes the current density (A/m^2), j_0 denotes the exchange current density (A/m^2), and α denotes the transfer coefficient, whose value is usually from 0.2 to 0.5.[1] In this dissertation, α is 0.5, which is a common value for SOFCs, and the Bulter-Volmer equation is simplified to the following equation (A5).[64, 65]

$$V_{act} = \frac{2RT}{n_e F} sinh^{-1}\left(\frac{j}{2j_0}\right) \quad (A5)$$

The value of the exchange current density depends on the materials and the operating conditions of the electrodes. In this dissertation, the values of the exchange current densities for the anode and cathode are calculated from equations (A6) and (A7).[66] According to the literature, $E_{act,an}$ and $E_{act,ca}$ (in equation A5 and A6) are typically

in the range of 120 ~ 160 kJ/mol.[46, 67, 68] Additionally, γ_{an} is usually smaller than γ_{ca}, and they are generally in the range of 10^8 ~ 10^{11} (A/m^2).[46, 66, 69] Table 4.1 in the main text shows the selected values of $E_{act,an}$, $E_{act,ca}$, γ_{an}, and γ_{ca}.

$$j_{0,an} = \gamma_{an} \times \left(\frac{p_{H_2}}{p_{atm}}\right) \times \left(\frac{p_{H_2O}}{p_{atm}}\right) \times exp\left(-\frac{E_{act,an}}{RT}\right) \quad \text{(A6)}$$

$$j_{0,ca} = \gamma_{ca} \times \left(\frac{p_{O_2}}{p_{atm}}\right)^{0.25} \times exp\left(-\frac{E_{act,ca}}{RT}\right) \quad \text{(A7)}$$

Ohmic loss

Ohmic loss refers to the voltage sacrificed to transmit an O^{2-} charge from the cathode side to the anode side in the electrolyte and to move electrons in the interconnect. The thicknesses and resistivity of each cell component are used to calculate the magnitude of the ohmic loss. Equations (A10) through (A12) are used to calculate the resistivity of the anode, cathode, and electrolyte.[70] We chose stainless steel based interconnect, and equation (A13) is used to calculate the resistivity of the interconnect. The equations show that the resistivity is a function of the operating temperature.[28, 71]

$$V_{ohm} = R_{ohm} \times j \quad \text{(A8)}$$

$$R_{ohm} = \rho_{an} \times d_{an} + \rho_{ca} \times d_{ca} + \rho_{el} \times d_{el} + \rho_{int} \times d_{int} \quad \text{(A9)}$$

$$\rho_{an} = 2.98 \times 10^{-5} \times exp\left(-\frac{1392}{T}\right) \quad \text{(A10)}$$

$$\rho_{ca} = 8.114 \times 10^{-5} \times exp\left(\frac{600}{T}\right) \quad \text{(A11)}$$

$$\rho_{el} = 2.94 \times 10^{-5} \times exp\left(\frac{10350}{T}\right) \quad \text{(A12)}$$

$$\rho_{int} = 1.68 \times 10^{-2} \times exp\left(\frac{-413.5}{T}\right) \quad \text{(A13)}$$

Concentration loss

Concentration loss is caused by the limited diffusion rates of the porous electrodes. The concentration loss of each electrode is calculated using equations (A14) and (A15).[72] Since the gas flowing in the cathode consists of only O_2 and N_2, the diffusion of O_2 to N_2 is considered for the case of the cathode. In the anode, H_2 is mainly diffused to H_2O and CO. In this dissertation, it is assumed that H_2 is diffused to H_2O because the amount of H_2O is the largest in the anode. This binary approximation is known to be relatively accurate since the molecular weights of H_2O and CO are similar, and H_2O and CO have similar collision integrals.[70]

$$V_{conc,an} = \frac{RT}{2F} ln\left[\frac{1 + \left(\frac{RT}{2F}\right)\left(\frac{d_{an}}{D_{an}^{eff} p_{an,H_2O}}\right) j}{1 - \left(\frac{RT}{2F}\right)\left(\frac{d_{an}}{D_{an}^{eff} p_{an,H_2}}\right) j}\right] \quad \text{(A14)}$$

$$V_{conc,ca} = -\frac{RT}{4F} ln\left[\frac{\frac{p_{ca}}{\alpha_{O_2}} - \left(\frac{p_{ca}}{\alpha_{O_2}} - p_{ca,O_2}\right) exp\left(\left(\frac{RT}{4F}\right)\left(\frac{\alpha_{O_2} d_{ca}}{p_{ca} D_{ca}^{eff}}\right) j\right)}{p_{ca,O_2}}\right] \quad \text{(A15)}$$

Each diffusion coefficient is calculated as follows. The ordinary diffusion coefficient and Knudsen diffusion coefficient are first calculated and then combined to calculate the effective diffusion coefficient. Each porosity and tortuosity is determined as the commonly used values found in the literature.[28, 72] Table 4.1 of the main text shows the values. The ordinary diffusion coefficient can be expressed as equations (A16) and (A17) based on kinetic theory.[1, 73]

$$p_{an} \times D_{O,H_2/H_2O} = 3.64 \times 10^{-4} \times \left(\frac{T}{\sqrt{T_{c,H_2}\, T_{c,H_2O}}}\right)^{2.334} \left(p_{c,H_2}\, p_{c,H_2O}\right)^{\frac{1}{3}} \left(T_{c,H_2}\, T_{c,H_2O}\right)^{\frac{5}{12}} \left(\frac{1}{M_{H_2}} + \frac{1}{M_{H_2O}}\right)^{\frac{1}{2}} \quad \text{(A16)}$$

$$p_{ca} \times D_{O,O_2/N_2} = 2.745 \times 10^{-4} \times \left(\frac{T}{\sqrt{T_{c,O_2}\, T_{c,N_2}}}\right)^{1.823} \left(p_{c,O_2}\, p_{c,N_2}\right)^{\frac{1}{3}} \left(T_{c,O_2}\, T_{c,N_2}\right)^{\frac{5}{12}} \left(\frac{1}{M_{O_2}} + \frac{1}{M_{N_2}}\right)^{\frac{1}{2}} \quad \text{(A17)}$$

T_c and p_c in equations (A16) and (A17) denote the temperature and pressure of each substance at the critical point. Temperatures of 33.3, 647.3, 154.4, and 126.2 K are used for the critical temperatures of H_2, H_2O, O_2, and N_2, respectively, and 12.8, 217.5, 49.7, and 33.5 atm are used for the critical pressures of H_2, H_2O, O_2, and N_2, respectively.[1, 73]

The Knudsen diffusion coefficient is calculated from the following equation (A18). r denotes the pore diameter, and M_i denotes the molecular weight of each substance. r is determined by referring to the literature. The values are shown in table 4.1 of the main text.[28, 72]

$$D_{K,i} = 97\, r \sqrt{\frac{T}{M_i}} \quad \text{(A18)}$$

The final values of the effective diffusion coefficients for the anode and cathode are calculated as follows.

$$D_{O,i(eff)} = D_{O,i}\left(\frac{\varepsilon}{\tau}\right) \quad \text{(A19)}$$

$$D_{K,i(eff)} = D_{K,i}\left(\frac{\varepsilon}{\tau}\right) \quad \text{(A20)}$$

$$\frac{1}{D_{i(eff)}} = \frac{1}{D_{o,i(eff)}} + \frac{1}{D_{K,i(eff)}} \quad \text{(A21)}$$

$$D_{an(eff)} = \left(\frac{p_{H_2O}}{p_{an}}\right) D_{H_2(eff)} + \left(\frac{p_{H_2}}{p_{an}}\right) D_{H_2O(eff)} \quad \text{(A22)}$$

$$D_{ca(eff)} = D_{O_2(eff)} \quad \text{(A23)}$$

α_{O_2}, which is used in equation (A15), is calculated as follows.

$$\alpha_{O_2} = \frac{D_{K,O_2(eff)}}{D_{K,O_2(eff)} + D_{O,O_2/N_2(eff)}} \quad \text{(A24)}$$

C.2. Mass balances

In SOFCs, fuel and air enter the fuel and air channels, respectively, and flow into the anode and cathode. Then, through an electrochemical reaction, H_2 and O_2 are consumed, and H_2O is produced. When the voltage of the SOFC cell is given, the current density distribution can be calculated from the electrochemical model, which is described in appendix C. 1, and the mass balance equation of each control volume can be expressed as equations (A25) through (A27). For reference, it is recommended to refer to figure 4.3 of the main text to better understand the following equations.

$Fuel\ channel$:

$$\dot{m}_{fuel}(x+dx) = \dot{m}_{fuel}(x) - \dot{m}_{H_2}(x) + \dot{m}_{H_2O}(x)$$
$$= \dot{m}_a(x) - \frac{1}{2F}(j(x)Ldx)M_{H_2} + \frac{1}{2F}(j(x)Ldx)M_{H_2O} \quad \text{(A25)}$$

$Air\ channel$:

$$\dot{m}_{air}(x+dx) = \dot{m}_{air}(x) - \dot{m}_{O_2}(x) = \dot{m}_{air}(x) - \frac{1}{4F}(j(x)Ldx)M_{O_2} \quad \text{(A26)}$$

$SOFC$:

$$\dot{m}_{H_2O}(x) = \dot{m}_{H_2}(x) + \dot{m}_{O_2}(x) \quad \text{(A27)}$$

The changes in mass flow rates in the fuel and air channels are calculated from equations (A25) and (A26).

C.3. Energy balances

In a direct internal reforming SOFC, an electrochemical reaction occurs to produce electric work and heat (sensible energy) from chemical energy, and the produced heat affects the temperature distribution. In addition, the temperature distribution simultaneously influences the internal reforming reaction and the electrochemical reaction. Therefore, the electrochemical reaction, internal reforming reaction, and temperature distribution are coupled. To model these physical phenomena, the energy balance formulas of three control volumes are established as follows. Again, it is recommended to refer to figure 4.3 of the main text to help understand the following equations.

$Fuel\ channel$:

$$\dot{m}_{fuel}(x+dx)h_{fuel}(x+dx) = \dot{m}_{fuel}(x)h_{fuel}(x) - \dot{m}_{H_2}(x)h_{H_2}(x) + \dot{m}_{H_2O}(x)h_{H_2O}(x) + \alpha_{conv,fuel}(x)Ldx\,(T_{SOFC}(x) - T_{fuel}(x)) \quad \text{(A28)}$$

$Air\ channel$:

$$\dot{m}_{air}(x+dx)h_{air}(x+dx) = \dot{m}_{air}(x)h_{air}(x) - \dot{m}_{O_2}(x)h_{O_2}(x) + \alpha_{conv,air}(x)Ldx\,(T_{SOFC}(x) - T_{air}(x)) \quad \text{(A29)}$$

$SOFC$:

$$Q_{cond}(x+dx) = Q_{cond}(x) + \dot{m}_{H_2}(x)h_{H_2}(x) + \dot{m}_{O_2}(x)h_{O_2}(x) - \dot{m}_{H_2O}(x)h_{H_2O}(x) - V \times j(x)Ldx - \alpha_{conv,air}(x)Ldx\left(T_{SOFC}(x) - T_{air}(x)\right) - \alpha_{conv,fuel}(x)Ldx\left(T_{SOFC}(x) - T_{fuel}(x)\right) \quad \text{(A30)}$$

In the model, an electrochemical reaction is considered to occur within the SOFC control volume. Therefore, in equations (A28) through (A30), $h_{H_2}(x)$, $h_{O_2}(x)$, and $h_{H_2O}(x)$ are calculated from the temperatures of the fuel channel control volume, air channel control volume, and SOFC control volume, respectively. Additionally, as shown in equations (A25) and (A26), $\dot{m}_{H_2}(x)$, $\dot{m}_{H_2O}(x)$, and $\dot{m}_{O_2}(x)$ are calculated from the current density.

For the heat transfer model, the convection between the SOFC body and the fuel and air gas, as well as the conduction inside the SOFC body, are modelled. It was assumed that there is no heat lost to the surroundings. The convection heat transfer coefficients ($\alpha_{conv,fuel}(x)$ and $\alpha_{conv,air}(x)$) are calculated from equations (A31) and (A32), assuming a constant Nusselt number of 3.09.[74, 75] Additionally, $k_{fuel}(x)$ and $k_{air}(x)$ denote the thermal conductivity of the fuel and air gas, and they are calculated by the Cantera thermodynamic toolbox and GRI 3.0 mechanism. $d_{h,fuel}$ and $d_{h,air}$ denote the hydraulic diameter of each channel and are calculated with equation (A33). $d_{channel}$, which denotes the height of the fuel and air channel, is set to 1.5 mm.

$$\alpha_{conv,fuel}(x) = \mathrm{Nu}\,\frac{k_{fuel}(x)}{d_{h,channel}} \quad \text{(A31)}$$

$$\alpha_{conv,air}(x) = \mathrm{Nu}\,\frac{k_{air}(x)}{d_{h,channel}} \quad \text{(A32)}$$

$$d_{h,fuel} = d_{h,air} = \frac{2Ld_{channel}}{L + d_{channel}} \quad \text{(A33)}$$

The conduction in the SOFC is assumed to occur only in the x direction, and the conductive heat transfer is calculated using equation (A34). d_{SOFC} is the sum of the thicknesses of the anode, cathode, and electrolyte. Additionally, the thermal conductivity of the SOFC body is determined to be 10 W/(m K) according to various

values in the literature.[46, 70, 71]

$$Q_{cond}(x+dx) = -k_{SOFC}\,\frac{T_{SOFC}(x+dx) - T_{SOFC}(x)}{dx} \times L \times d_{SOFC} \quad \text{(A34)}$$

From these equations, $h_{fuel}(x+dx)$ and $h_{air}(x+dx)$, which denote the enthalpy of the outlet gases of the fuel and air channel, can be calculated. From these values and the compositions of the outlet gases, which can be calculated from the electrochemical reaction, internal reforming reaction, and water-gas shift reaction, $T_{fuel}(x+dx)$ and $T_{air}(x+dx)$, which denote the temperature of the outlet gases of the fuel and air channel, can be calculated. Meanwhile, $Q_{cond}(x+dx)$ can also be calculated from the above energy balance formulas and can be used to calculate $T_{SOFC}(x+dx)$.

C.4. Direct internal reforming and water-gas shift reaction

Although it was assumed that only H_2 participates directly in the electrochemical reaction, CH_4 and CO also participate indirectly in the electrochemical reaction through internal reforming and the WGS reaction. The internal reforming and the WGS reaction were conducted when the fuel gas of the fuel channel contacted the surface of the anode and were eventually considered to occur in the fuel channel control volume.

The internal reforming reaction was modelled as the reaction shown in equation (A35). The reforming rate was determined by calculating the reaction rate of this reaction. The formulas for calculating the reaction rate have been studied with various anode and catalyst materials.[46, 76-79] Among these, the relatively simple first-order formula expressed in equation (A36), which is often used for direct internal reforming SOFC, was selected.[76] The constants in the formula were determined as follows: activation energy E_a of 82 kJ/mol and pre-exponential constant k_0 of 4274 mol/(s m^2 bar).[46] Additionally, it was assumed that the internal reforming reaction occurs throughout the area where the fuel channel and the anode are in contact.

$$CH_4 + H_2O \longleftrightarrow CO + 3H_2 \quad \text{(A35)}$$

$$rate = k_0 P_{CH4} \exp\left(\frac{-E_a}{RT}\right) \quad \text{(A36)}$$

For the WGS reaction, the reaction can be considered to always be in equilibrium because the reaction rate of this reaction is generally very high.[46]

$$CO + H_2O \longleftrightarrow CO_2 + H_2 \quad \text{(A37)}$$

C.5. Boundary conditions

The boundary conditions established for the differential equations modelled in appendices 1 ~ 4 are as follows.

$$Fuel\ channel:\ \dot{m}_{fuel}(0) = \dot{m}_5 \quad h_{fuel}(0) = h_5 \quad X_{fuel}(0) = X_5 \quad T_{fuel}(0) = T_3$$

$$Air\ channel\ :\ \dot{m}_{air}(0) = \dot{m}_{16} \quad h_{air}(0) = h_{16} \quad X_{air}(0) = X_{16} \quad T_{air}(0) = T_{16}$$

$$SOFC\ :\ \frac{dT_{SOFC}}{dx}(0) = 0 \quad \frac{dT_{SOFC}}{dx}(L) = 0$$

As shown above, the thermodynamic states of the inlet gases of the fuel and air channels are the same as the thermodynamic states of streams 5 and 16 (in figure 4.1 of the main text), respectively, in the SOFC–HCCI engine hybrid system. Additionally, $\frac{dT_{SOFC}}{dx}$ of both ends is considered to be 0 because it was assumed that there is no heat lost to the surroundings.

References

1. O'hayre, R., et al., *Fuel cell fundamentals*. 2016: John Wiley & Sons.

2. Buonomano, A., et al., *Hybrid solid oxide fuel cells–gas turbine systems for combined heat and power: a review.* Applied Energy, 2015. **156**: p. 32-85.

3. Calise, F., et al., *Simulation and exergy analysis of a hybrid solid oxide fuel cell (SOFC)–gas turbine system.* Energy, 2006. **31**(15): p. 3278-3299.

4. Costamagna, P., L. Magistri, and A. Massardo, *Design and part-load performance of a hybrid system based on a solid oxide fuel cell reactor and a micro gas turbine.* Journal of Power Sources, 2001. **96**(2): p. 352-368.

5. Perna, A., et al., *Performance assessment of a hybrid SOFC/MGT cogeneration power plant fed by syngas from a biomass down-draft gasifier.* Applied Energy, 2017.

6. Campanari, S. *Full load and part-load performance prediction for integrated SOFC and microturbine systems*. in *ASME 1999 International Gas Turbine and Aeroengine Congress and Exhibition*. 1999. American Society of Mechanical Engineers.

7. Campanari, S., *Parametric analysis of small scale recuperated SOFC/gas turbine cycles.* ASME paper, 2004(2004-GT): p. 53933.

8. Ferrari, M.L., *Advanced control approach for hybrid systems based on solid oxide fuel cells.* Applied Energy, 2015. **145**: p. 364-373.

9. Ferrari, M.L., et al., *Hybrid system test rig: chemical composition emulation with steam injection.* Applied energy, 2012. **97**: p. 809-815.

10. Harun, N.F., D. Tucker, and T.A. Adams II, *Technical challenges in operating an SOFC in fuel flexible gas turbine hybrid systems: Coupling effects of cathode air mass flow.* Applied Energy, 2017. **190**: p. 852-867.

11. Harun, N.F., D. Tucker, and T.A. Adams, *Impact of fuel composition transients*

on SOFC performance in gas turbine hybrid systems. Applied Energy, 2016. **164**: p. 446-461.

12. Roberts, R. and J. Brouwer, *Dynamic Simulation of a Pressurized 220kW Solid Oxide Fuel-Cell–Gas-Turbine Hybrid System: Modeled Performance Compared to Measured Results.* Journal of fuel cell science and technology, 2006. **3**(1): p. 18-25.

13. Leeper, J., *220 kWe solid oxide fuel cell/microturbine generator hybrid proof of concept demonstration report, California Energy Commission*. 2001, report.

14. Lim, T.-H., et al., *Operating characteristics of a 5kW class anode-supported planar SOFC stack for a fuel cell/gas turbine hybrid system.* International Journal of Hydrogen Energy, 2008. **33**(3): p. 1076-1083.

15. Gengo, T., Y. Ando, and T. Kabata, *Development of 200 kW class SOFC combined cycle system and future view.* Technical review, Mitsubishi Heavy Industries, Ltd, 2008: p. 45.

16. Kobayashi, Y., et al., *Recent progress of SOFC combined cycle system with segmented-in-series tubular type cell stack at MHI.* ECS Transactions, 2013. **57**(1): p. 53-60.

17. Veyo, S.E., et al. *Status of pressurized SOFC/GAS turbine power system development at Siemens Westinghouse*. in *ASME Turbo Expo 2002: Power for Land, Sea, and Air*. 2002. American Society of Mechanical Engineers.

18. Cheddie, D.F., *Thermo-economic optimization of an indirectly coupled solid oxide fuel cell/gas turbine hybrid power plant.* International journal of hydrogen energy, 2011. **36**(2): p. 1702-1709.

19. Vora, S.D. *Office of Fossil Energy's Solid Oxide Fuel Cell Program Overview*. in *15th Annual SECA Workshop, July*. 2014.

20. Owens, B., *The rise of distributed power.* General Electric, 2014. **47**.

21. Ahn, K.Y., et al., *Fuel cell-engine hybrid system*. 2015, Google Patents.

22. Cheng, R., et al., *Synthesis gas combustion: fundamentals and applications*. 2009, CRC Press, Turbulent Combustion Properties of Premixed Syngas.

23. Heywood, J., *Internal combustion engine fundamentals*. 1988: McGraw-Hill Education.

24. Bhaduri, S., et al., *The effects of biomass syngas composition, moisture, tar loading and operating conditions on the combustion of a tar-tolerant HCCI (Homogeneous Charge Compression Ignition) engine.* Energy, 2015. **87**: p. 289-302.

25. Bhaduri, S., H. Jeanmart, and F. Contino, *EGR control on operation of a tar tolerant HCCI engine with simulated syngas from biomass.* Applied Energy, 2017.

26. Kozarac, D., et al., *Analysis of benefits of using internal exhaust gas recirculation in biogas-fueled HCCI engines.* Energy conversion and management, 2014. **87**: p. 1186-1194.

27. Kang, S. and K.-Y. Ahn, *Dynamic modeling of solid oxide fuel cell and engine hybrid system for distributed power generation.* Applied Energy, 2017. **195**: p. 1086-1099.

28. Lee, Y.D., *Thermodynamic, economic and environmental evaluation of solid oxide fuel cell hybrid power generation systems.* 2015.

29. Park, S.H., Y.D. Lee, and K.Y. Ahn, *Performance analysis of an SOFC/HCCI engine hybrid system: System simulation and thermo-economic comparison.* International Journal of Hydrogen Energy, 2014. **39**(4): p. 1799-1810.

30. Lee, Y.D., et al., *Exergetic and exergoeconomic evaluation of an SOFC-Engine hybrid power generation system.* Energy, 2017.

31. Bedoya, I.D., et al., *Experimental evaluation of strategies to increase the operating range of a biogas-fueled HCCI engine for power generation.* Applied energy,

2012. **97**: p. 618-629.

32. Yamasaki, Y. and S. Kaneko, *Prediction of Ignition and Combustion Development in an HCCI Engine Fueled by Syngas*. 2014, SAE Technical Paper.

33. Alger, T., et al., *Laser ignition in a pre-mixed engine: the effect of focal volume and energy density on stability and the lean operating limit*. 2005, SAE Technical Paper.

34. Alger, T., J. Gingrich, and B. Mangold, *The effect of hydrogen enrichment on EGR tolerance in spark ignited engines*. 2007, SAE Technical Paper.

35. Alkidas, A.C., *Combustion advancements in gasoline engines.* Energy Conversion and Management, 2007. **48**(11): p. 2751-2761.

36. Andreae, M.M., et al., *On HCCI engine knock*. 2007, SAE Technical Paper.

37. Caton, P.A., *Residual-effected homogeneous charge compression ignition using variable valve actuation.* 2004.

38. Plee, S., T. Ahmad, and J. Myers, *Flame temperature correlation for the effects of exhaust gas recirculation on diesel particulate and NO x emissions*. 1981, SAE Technical Paper.

39. Goodwin, D., H.K. Moffat, and R.L. Speth, *Cantera: An object-oriented software toolkit for chemical kinetics, thermodynamics, and transport processes.* Caltech, Pasadena, CA, 2009.

40. Ament, F., D.J. Patterson, and A. Mueller, *Heat Balance Provides Insight Into Modern Engine Fuel Utilization*. 1977, SAE Technical Paper.

41. Woschni, G., *A universally applicable equation for the instantaneous heat transfer coefficient in the internal combustion engine*. 1967, SAE Technical paper.

42. Stambouli, A.B. and E. Traversa, *Solid oxide fuel cells (SOFCs): a review of an environmentally clean and efficient source of energy.* Renewable and sustainable energy reviews, 2002. **6**(5): p. 433-455.

43. Bowman, C.T., *Kinetics of pollutant formation and destruction in combustion.* Progress in energy and combustion science, 1975. **1**(1): p. 33-45.

44. Aceves, S.M., et al., *A multi-zone model for prediction of HCCI combustion and emissions*. 2000, SAE Technical paper.

45. Gregory P. Smith, D.M.G., Michael Frenklach, Nigel W. Moriarty, Boris Eiteneer, Mikhail Goldenberg, C. Thomas Bowman, Ronald K. Hanson, Soonho Song, William C. Gardiner, Jr., Vitali V. Lissianski, and Zhiwei Qin, *GRI-MECH 3.0.*

46. Aguiar, P., C. Adjiman, and N.P. Brandon, *Anode-supported intermediate temperature direct internal reforming solid oxide fuel cell. I: model-based steady-state performance.* Journal of power sources, 2004. **138**(1): p. 120-136.

47. Colpan, C.O., I. Dincer, and F. Hamdullahpur, *Thermodynamic modeling of direct internal reforming solid oxide fuel cells operating with syngas.* International Journal of Hydrogen Energy, 2007. **32**(7): p. 787-795.

48. Kang, Y.-W., et al., *A reduced 1D dynamic model of a planar direct internal reforming solid oxide fuel cell for system research.* Journal of Power Sources, 2009. **188**(1): p. 170-176.

49. Shin, G., J. Yun, and S. Yu, *Thermal design of methane steam reformer with low-temperature non-reactive heat source for high efficiency engine-hybrid stationary fuel cell system.* International Journal of Hydrogen Energy, 2017. **42**(21): p. 14697-14707.

50. Yun, J., G. Shin, and S. Yu. *Study on Performance Enhancement of Low Temperature Reformer for Fuel Cell-Engine Hybrid System*. in *The Korean Hydrogen & New Energy Society*. 2016.

51. Lee, Y.D., et al. *Integration and Proof-of-concept Test Results of SOFC-Engine Hybrid Power Generation System*. in *The 9th Asian Conference on*

Electrochemical Power Sources 2017. 2017. Gyeongju, Korea.

52. Brett, D.J., et al., *Intermediate temperature solid oxide fuel cells.* Chemical Society Reviews, 2008. **37**(8): p. 1568-1578.

53. Ishihara, T., *Perovskite oxide for solid oxide fuel cells*. 2009: Springer Science & Business Media.

54. U.S.DOE. *Why SOFC Technology?*; Available from: https://energy.gov/fe/why-sofc-technology.

55. Youngjae, C., et al., *Study on Internal Reforming Characteristic of Planar Type Solid Oxide Fuel Cell Stack.* New & Renewable Energy, 2016. **12**(4): p. 98-104.

56. Lieuwen, T., V. Yang, and R. Yetter, *Synthesis gas combustion: fundamentals and applications*. 2009: CRC Press.

57. Song, H. and C. Edwards, *Understanding chemical effects in low-load-limit extension of homogeneous charge compression ignition engines via recompression reaction.* International Journal of Engine Research, 2009. **10**(4): p. 231-250.

58. *Bloom Energy*; Available from: http://www.bloomenergy.com/fuel-cell/es-5710-data-sheet/.

59. *GE power homepage*; Available from: https://www.gepower.com/gas/reciprocating-engines.

60. *Korea Gas Corporation homepage;* Available from: http://www.kogas.or.kr.

61. Oh, S. and H.H. Song, *Exergy analysis on non-catalyzed partial oxidation reforming using homogeneous charge compression ignition engine in a solid oxide fuel cell system.* International Journal of Hydrogen Energy, 2018.

62. Hanna, J., et al., *Fundamentals of electro-and thermochemistry in the anode of solid-oxide fuel cells with hydrocarbon and syngas fuels.* Progress in Energy and Combustion Science, 2014. **40**: p. 74-111.

63. Jiang, Y. and A.V. Virkar, *Fuel composition and diluent effect on gas transport and performance of anode-supported SOFCs.* Journal of The Electrochemical Society, 2003. **150**(7): p. A942-A951.

64. Calise, F., et al., *Single-level optimization of a hybrid SOFC–GT power plant.* Journal of Power Sources, 2006. **159**(2): p. 1169-1185.

65. Singhal, S.C. and K. Kendall, *High-temperature solid oxide fuel cells: fundamentals, design and applications*. 2003: Elsevier.

66. Costamagna, P. and K. Honegger, *Modeling of solid oxide heat exchanger integrated stacks and simulation at high fuel utilization.* Journal of the Electrochemical Society, 1998. **145**(11): p. 3995-4007.

67. Holtappels, P., et al., *Reaction of Hydrogen/Water Mixtures on Nickel-Zirconia Cermet Electrodes: II. AC Polarization Characteristics.* Journal of the electrochemical society, 1999. **146**(8): p. 2976-2982.

68. Jiang, S. and S. Badwal, *An electrode kinetics study of H 2 oxidation on Ni/Y 2 O 3–ZrO 2 cermet electrode of the solid oxide fuel cell.* Solid State Ionics, 1999. **123**(1): p. 209-224.

69. Massardo, A. and F. Lubelli, *Internal reforming solid oxide fuel cell-gas turbine combined cycles (IRSOFC-GT): Part a—Cell model and cycle thermodynamic analysis.* ASME J. Eng. Gas Turbines Power, 2000. **122**(1): p. 27-35.

70. Bessette, N.F., W.J. Wepfer, and J. Winnick, *A mathematical model of a solid oxide fuel cell.* Journal of the Electrochemical Society, 1995. **142**(11): p. 3792-3800.

71. Thyssenkrupp, V., *Material Data Sheet No. 4046 for Crofer 22 APU.* Jun-2006.[Online].[Accessed: 28-Feb-2011], 2010.

72. Chan, S., K. Khor, and Z. Xia, *A complete polarization model of a solid oxide fuel cell and its sensitivity to the change of cell component thickness.* Journal of Power

Sources, 2001. **93**(1): p. 130-140.

73. Bird, R.B., W.E. Stewart, and E.N. Lightfoot, *Transport phenomena*. 2007: John Wiley & Sons.

74. Palsson, J., A. Selimovic, and L. Sjunnesson, *Combined solid oxide fuel cell and gas turbine systems for efficient power and heat generation.* Journal of power sources, 2000. **86**(1): p. 442-448.

75. Bossel, U.G., *FACTS & FIGURES: Final report on SOFC data*. 1992: Swiss Federal Office of Energy, Operating Agent Task II.

76. Achenbach, E. and E. Riensche, *Methane/steam reforming kinetics for solid oxide fuel cells.* Journal of Power Sources, 1994. **52**(2): p. 283-288.

77. Ahmed, K. and K. Foger, *Kinetics of internal steam reforming of methane on Ni/YSZ-based anodes for solid oxide fuel cells.* Catalysis Today, 2000. **63**(2): p. 479-487.

78. Dicks, A., K. Pointon, and A. Siddle, *Intrinsic reaction kinetics of methane steam reforming on a nickel/zirconia anode.* Journal of power sources, 2000. **86**(1): p. 523-530.

79. Lee, A.L., R. Zabransky, and W. Huber, *Internal reforming development for solid oxide fuel cells.* Industrial & engineering chemistry research, 1990. **29**(5): p. 766-773.

국 문 초 록

SOFC 하이브리드 시스템은 SOFC와 또 다른 전력생산장치를 결합하여 효율을 증가시키는 시스템이다. 지금까지 SOFC 하이브리드 시스템으로는 SOFC–가스터빈(gas turbine) 하이브리드 시스템이 주로 연구되어왔다. 그러나 현재의 SOFC 발전용량인 수 MW 이하급의 분산발전에서는 내연기관(internal combustion engine)이 가스터빈보다 더 효율이 좋고 경제적이어서 더 많이 사용되고 있다. 이에 입각해 최근 기계연구원과 서울대학교 어드밴스드 에너지시스템 연구실에 의해 SOFC–내연기관 하이브리드 시스템 컨셉이 제시되었다. 이때 내연기관의 연소전략으로는 spark ignition (SI) 대신 homogeneous charge compression ignition (HCCI) 가 선택되었는데, 불연성분(diluent)인 H_2O와 CO_2가 과다 함유된 SOFC anode off-gas를 내연기관 내에서 잘 연소시키고 충분한 전력을 생산하기 위함이다.

SOFC–HCCI 엔진 하이브리드 시스템의 컨셉이 이렇게 제시되었음에도 불구하고, 시스템에 대한 학술적인 연구는 아직까지 많이 이루어지지 못하였다. 따라서 본 논문에서는 이러한 시스템에 대한 시뮬레이션 및 실험적 연구를 수행하여 시스템 운전의 특성을 연구하고, 이를 바탕으로 성공적인 운전을 위한 시스템 설계를 구체화하는 것을 목표로 하였다.

연구의 첫번째 단계로 SOFC anode off-gas로 운전되는 HCCI 엔진 운전에 대한 실험이 수행되었다. 우선, 단기통의 HCCI 엔진과 SOFC anode off-gas를 모사할 수 있는 실험 장비들을 구축하고, 이를 이용하여 다양한 system control parameter들(예컨대 SOFC anode off-gas의 조성과 유량에 큰 영향을 미치는 SOFC의 fuel utilization factor 등)을 변경시켜 가며 HCCI 엔진 실험을 수행하였다. 실험 결과 SOFC anode off-gas로 운전되는 HCCI 엔진은 일반적으로 안정적인 HCCI 연소(< 5% COV $IMEP_g$)를 일으키며 상당한 양의 일을 약 25 ~ 30%의 도시효율로 생산하는 동시에, 매우 낮은 NO_x 배출량(< 5 ppm

@ O_2 15%)을 갖는다는 것을 확인하였다. 실험이 작은 단기통 엔진으로 이루어진 점을 고려할 때, 이러한 실험 결과는 SOFC 의 bottoming cycle로서의 HCCI 엔진의 가능성을 충분히 보여준다. 그러나 HCCI 엔진 운전이 모든 조건에서 안정적인 것은 아니었다. 특히 엔진 로드가 매우 낮은 경우($IMEP_g$ < ~1.8 bar)는 엔진 운전의 안정성을 저해하기 때문에 피해야 하는 것을 확인하였다. 또 엔진 흡기가스안의 연료성분(H_2 와 CO)에 비해 불연성분이 일정 수준 이상으로 매우 많은 경우(fuel molar fraction < 0.125)는 엔진 배기가스 내의 불연 CO 배출량을 줄이고 CO 연소효율을 90% 이상으로 유지하기 위해서 기피하여 운전해야 함을 확인하였다.

연구의 두번째 단계로 하이브리드 시스템 내에서의 SOFC 운전과 전체 시스템의 운전에 관한 분석이 수행되었다. 전체 시스템 운전은 HCCI 엔진의 실험 결과와 나머지 시스템 구성 요소들에 대한 시뮬레이션 모델을 결합하여 분석하였다. 시뮬레이션 모델들은 정상상태로 모델링 되었으며, 모델링에는 Mathworks사의 MATLAB과 Cantera 열역학 tool box 와 GRI 3.0 메커니즘이 사용되었다. 하이브리드 시스템 내의 SOFC로는 direct internal reforming planar-type SOFC가 사용되었고, SOFC 내부에서 내부 개질 반응(internal reforming reaction)과 전기화학반응이 서로 지속적으로 영향을 주고 있는 상황을 모사하기 위하여 one-dimensional 시뮬레이션 모델이 구축되었다. 시스템 분석 결과 하이브리드 시스템 내의 SOFC는 anode 입구 가스의 온도가 비교적 낮고(예: 750 ~ 800 K), 외부 개질율이 낮은 상황(예: 30 ~ 40%)에서 운전되는 특징이 있다는 것을 확인하였다. 따라서 SOFC의 입구부분에서의 SOFC 운전 온도는 상대적으로 낮고(예: 900 K), 이 때문에 낮은 온도에서 자칫 크게 증가할 수 있는 electrolyte의 ohmic loss를 줄여줄 수 있는 anode supported type을 사용하는 것이 바람직하다는 결론을 도출할 수 있었다. 한편으로는 전체 시스템에 대한 분석을 시스템의 다양한 system control

parameter들(예: SOFC의 fuel utilization factor)을 변경시켜가면서 수행하였다. 이러한 분석을 기반으로 시스템을 안정적으로 운전할 수 있으면서도 좋은 시스템 성능을 얻을 수 있는 시스템의 운전 설계점(design point)을 선정하였다. 이러한 운전 설계점에서 SOFC는 4.97 kW를, HCCI 엔진은 0.93 kW를 생산하여 전체 시스템 효율을 58.5%를 달성하는 동시에 1 ppm 미만의 NO_x와 약 1300 ppm의 CO 를 배출하는 것을 확인하였다.

연구의 세번째 단계로 전체 하이브리드 시스템에 대한 실험적 연구가 수행되었다. 특히 시스템 운전의 실현 가능성을 직접 확인하고자 200시간 연속의 시스템 운전 실험을 최초로 수행하였다. 이때 실험은 앞서 결정한 운전 설계점을 바탕으로 진행되었다. 그 결과, 시스템이 200시간 연속운전을 안정적으로 수행할 수 있음을 확인하였다. 특히 HCCI 엔진으로 인해 생기는 흡기 쪽의 압력 진동이 SOFC와 HCCI 엔진 사이의 유로에서 많이 상쇄되어 SOFC 운전에 큰 영향을 미치지 않는 것이 확인되었다. 실험을 통하여 SOFC–HCCI 엔진 하이브리드 시스템의 실현가능성이 직접적으로 검증되었다고 할 수 있을 것이다. 그러나 한가지 염두해 두어야 할 것은, 실험 결과 시스템에서 예상보다 많은 열손실이 발생되어, 이를 보상하고 SOFC 운전의 안정성을 높이기 위해 전기 히터들과 천연가스 버너가 추가적으로 사용되었다는 점이다. 결론적으로 보다 성공적인 시스템 운전을 위해서는 시스템에서의 열손실을 최소화하는 것이 필요함을 알 수 있었다.

연구의 네번째 단계로 앞선 분석들을 통하여 파악한 시스템 운전의 3가지 주요 문제점(①CO 배출물, ②많은 열전달 양, ③SOFC의 fuel utilization factor를 증가시키지 못하는 점)을 해소하고, 시스템 성능을 향상시키기 위한 방법들에 대한 연구가 시뮬레이션을 통해 수행되었다. 세가지 방법(① catalytic oxidizer 추가, ②엔진에서의 열손실 일부 회수, ③엔진 압축비 증가)이 제시되고 분석되었다. 이러한 세가지 방법을 적용함으로써 시스템의 효

율이 약 63.8%에 달하는 동시에, 오염물질 배출량은 거의 존재하지 않는 5-kW급 SOFC–HCCI 엔진 하이브리드 시스템의 설계를 제안할 수 있었다.

SOFC–HCCI 엔진 하이브리드 시스템에 대한 연구의 마지막 단계로 앞서 결정된 시스템 설계를 유지하면서 시스템 크기가 100-kW 급으로 증가할 때의 시스템 성능에 관한 연구가 시뮬레이션을 통해 수행되었다. 시스템의 용량이 증가할 때 SOFC는 모듈화 된 스택의 숫자가 증가하고, HCCI 엔진은 실린더의 크기가 증가한다고 가정하였다. 시뮬레이션 결과 시스템 사이즈가 증가하면, 표면적-부피 비율이 감소하면서 엔진 열손실 량이 감소하고, 이에 따라 HCCI 엔진, SOFC, 그리고 전체 시스템 효율이 모두 증가함을 확인할 수 있었다. 이를 통해 시스템의 스케일업은 시스템 효율 증가에 도움을 주는 것을 확인하였으며, 특히 100-kW 급으로 시스템이 스케일업 되면 약 67.4%의 효율을 달성할 수 있음이 검증되었다. 이러한 결과는 SOFC–HCCI 엔진 하이브리드 시스템이 초고효율 발전시스템으로 사용될 수 있는 가능성을 보이는 매우 고무적인 결과라고 볼 수 있다.